NAVAL POSTGRADUATE SCHOOL

MONTEREY, CALIFORNIA

THESIS

THRUST MEASUREMENT OF A SPLIT-PATH, VALVELESS PULSE DETONATION ENGINE

by

Brady J. Bartosh

December 2007

Thesis Advisor:	Christopher M. Brophy
Second Reader:	Knox T. Millsaps

Approved for public release; distribution is unlimited

THIS PAGE INTENTIONALLY LEFT BLANK

REPORT DOCUMENTATION PAGE		*Form Approved OMB No. 0704-0188*
Public reporting burden for this collection of information is estimated to average 1 hour per response, including the time for reviewing instruction, searching existing data sources, gathering and maintaining the data needed, and completing and reviewing the collection of information. Send comments regarding this burden estimate or any other aspect of this collection of information, including suggestions for reducing this burden, to Washington headquarters Services, Directorate for Information Operations and Reports, 1215 Jefferson Davis Highway, Suite 1204, Arlington, VA 22202-4302, and to the Office of Management and Budget, Paperwork Reduction Project (0704-0188) Washington DC 20503.

1. AGENCY USE ONLY *(Leave blank)*

2. REPORT DATE
December 2007

3. REPORT TYPE AND DATES COVERED
Master's Thesis

4. TITLE AND SUBTITLE: Thrust Measurement of a Split-Path, Valveless Pulse Detonation Engine

5. FUNDING NUMBERS

6. AUTHOR(S) Brady J. Bartosh

7. PERFORMING ORGANIZATION NAME(S) AND ADDRESS(ES)
Naval Postgraduate School
Monterey, CA 93943-5000

8. PERFORMING ORGANIZATION REPORT NUMBER

9. SPONSORING /MONITORING AGENCY NAME(S) AND ADDRESS(ES)
Office of Naval Research (ONR)
Ballstone Tower One
800 N. Quincy St.
Arlington, VA 22217-5660

10. SPONSORING/MONITORING AGENCY REPORT NUMBER
N/A

11. SUPPLEMENTARY NOTES The views expressed in this thesis are those of the author and do not reflect the official policy or position of the Department of Defense or the U.S. Government.

12a. DISTRIBUTION / AVAILABILITY STATEMENT
Approved for public release; distribution is unlimited

12b. DISTRIBUTION CODE

13. ABSTRACT (maximum 200 words)

Theory predicts ideal pulse detonation technology offers significant fuel efficiency advantages over ramjet/scramjet architecture within a range from high subsonic to low hypersonic velocities. In practice, Pulse Detonation Engines (PDE) require implementation of loss-inducing techniques such as turbulence-generation devices to achieve and sustain detonation events, which effectively narrows the efficiency gap between the two technologies. Pressure losses associated with such obstacles lower system specific thrust (I_{sp}) and reduce overall system performance. Although fundamental PDE research has been ongoing at NPS for seven years, no dedicated attempt has been made to accurately measure the experimental performance. Fuel-based I_{sp} is a function of the ratio of thrust produced to fuel mass flow rate; thus, accurate computation requires precise knowledge of both thrust and input fuel. This thesis focused on creating an accurate thrust collection system incorporating an existing, uncalibrated rocket thrust stand. An in depth, axial component thrust calibration was conducted for the stand itself, then with the engine mounted in the firing configuration. As expected, harmonic responses of the stand during detonation experimentation were experienced which required creation and implementation of filtering algorithms to successfully extract useful thrust values.

14. SUBJECT TERMS Pulse Detonation Engines, PDE, Transient Plasma Ignition, TPI, Split Path, PDE Average Thrust, PDE Thrust Stand, Moving Time Average, MTA, Lowpass Filter

15. NUMBER OF PAGES
115

16. PRICE CODE

17. SECURITY CLASSIFICATION OF REPORT
Unclassified

18. SECURITY CLASSIFICATION OF THIS PAGE
Unclassified

19. SECURITY CLASSIFICATION OF ABSTRACT
Unclassified

20. LIMITATION OF ABSTRACT
UU

NSN 7540-01-280-5500

Standard Form 298 (Rev. 2-89)
Prescribed by ANSI Std. 239-18

i

THIS PAGE INTENTIONALLY LEFT BLANK

**THRUST MEASUREMENT OF A SPLIT-PATH, VALVELESS
PULSE DETONATION ENGINE**

Brady J. Bartosh
Commander, United States Navy
B.S., Rice University, 1991

Submitted in partial fulfillment of the
requirements for the degree of

MASTER OF SCIENCE IN ASTRONAUTICAL ENGINEERING

from the

**NAVAL POSTGRADUATE SCHOOL
December 2007**

Author: Brady J. Bartosh

Approved by: Christopher M. Brophy
                    Thesis Advisor

                    Knox T. Millsaps
                    Second Reader

                    Anthony J. Healey
                    Chairman, Department of Mechanical & Astronautical Engineering

THIS PAGE INTENTIONALLY LEFT BLANK

ABSTRACT

Theory predicts ideal pulse detonation technology offers significant fuel efficiency advantages over ramjet/scramjet architecture within a range from high subsonic to low hypersonic velocities. In practice, Pulse Detonation Engines (PDE) require implementation of loss-inducing techniques such as turbulence-generation devices to achieve and sustain detonation events, which effectively narrows the efficiency gap between the two technologies. Pressure losses associated with such obstacles lower system specific thrust (I_{sp}) and reduce overall system performance. Although fundamental PDE research has been ongoing at NPS for seven years, no dedicated attempt has been made to accurately measure the experimental performance. Fuel-based I_{sp} is a function of the ratio of thrust produced to fuel mass flow rate; thus, accurate computation requires precise knowledge of both thrust and input fuel. This thesis focused on creating an accurate thrust collection system incorporating an existing, uncalibrated rocket thrust stand. An in depth, axial component thrust calibration was conducted for the stand itself, then with the engine mounted in the firing configuration. As expected, harmonic responses of the stand during detonation experimentation were experienced which required creation and implementation of filtering algorithms to successfully extract useful thrust values.

THIS PAGE INTENTIONALLY LEFT BLANK

TABLE OF CONTENTS

THIS PAGE INTENTIONALLY LEFT BLANK

LIST OF FIGURES

THIS PAGE INTENTIONALLY LEFT BLANK

LIST OF TABLES

THIS PAGE INTENTIONALLY LEFT BLANK

ACKNOWLEDGMENTS

The author would like to express his sincere gratitude to Dr. Christopher Brophy for his educational support and direction provided throughout the experimentation process conducted in support of this thesis. The flexibility he showed in focusing the research deeper into areas of unexpected results allowed this project to achieve meaningful results which will significantly enhance future PDE testing. Along the same lines, Dr. Jose Sinibaldi provided technical support without which the calibration of the thrust stand and data filtering techniques may not have been completed. Additionally, a debt of gratitude is owed George Hageman for his continuous technical support ranging from rig construction to component repair.

The author would also like to express his appreciation for the invaluable assistant provided by Mr. Gregg Stuart and Mr. Clifford Baird; representatives from the thrust stand manufacturer, Force Measurement Systems, Inc. Their time spent teaching thrust stand calibration techniques and investigating post run filtering processes contributed significantly to final product provided in this report.

Finally, and most importantly, the author would like to express his heartfelt gratitude to his wife, Christina and son, Ryan for affording him the exorbitant amount of time required to complete this thesis. Without the strong support from family, this and all professional endeavors would not be possible.

THIS PAGE INTENTIONALLY LEFT BLANK

I.   INTRODUCTION

The history of Pulse Detonation Engines (PDE) can be traced back to the German engineer H. Hoffmann, who initially identified and investigated the concept of utilizing intermittent detonations as a source of propulsion [1]. It was decades later before the PD concept was applied to high-speed flight and began to demonstrate a possible alternative to existing air and spacecraft propulsion systems. The past twenty years have seen a renewed interest in this emerging field, resulting in a shift from long-term theoretical research to investigation and practical development of pulse detonation engines.

Current air and space vehicles incorporate propulsion systems selected from a limited arsenal of chemical propellant engines. Figure 1 illustrates the primary propulsion systems currently in use today, and provides a trade space demonstrating a comparison of system specific impulse (I_{sp}) versus range of Mach number, where I_{sp} is the effective thrust per fuel mass flow rate.
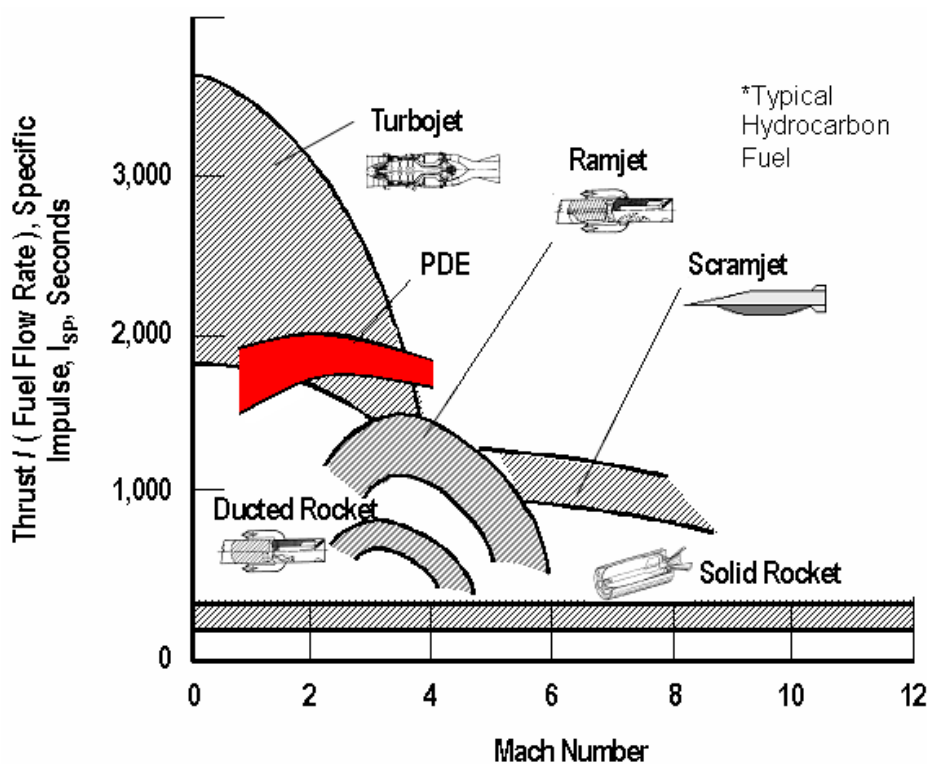
Figure 1.   Propulsion System Trade Space (From Ref. 2)

1

Included in the figure is the theoretical performance range of PDE's. This technology offers an alternative source of propulsion to turbojet and ramjet/scramjet systems, including several operational advantages. At low speeds (subsonic to low supersonic) turbojet engines provide a higher Isp; however, maximum flight velocity is effectively limited to approximately Mach 2.5- 3 due to thermodynamic and structural limitations. Additionally, turbojet engine design is quite complex, requiring many moving parts which affect cost and reliability. Ramjet and scramjet technology offer significantly higher top-end speed; however both pay significant I_{sp} penalties due to Brayton cycle limitations.

In contrast, pulse detonation engines incorporate nearly constant volume combustion vice constant pressure combustion which governs Brayton cycle operation. By utilizing detonation waves which inherently provide compression, no mechanical energy is required on turbine/compressor assembly operation and significantly higher thermodynamic efficiencies can be realized. Additionally, engine design is quite simple, requiring little or no moving parts in the combustor section and minimal in the engine as a whole [3]. A final characteristic which makes PDE technology so appealing is the capability to provide transition from subsonic to high supersonic operational velocities without additional propulsion systems or support vehicles.

PDE technology appears well-suited as a propulsion system for several critical areas of interest, most notably cruise missile propulsion and combined cycle rocket engine design. Currently, cruise missile propulsion technology is based upon long range, subsonic turbojet-powered vehicles or super/hypersonic, ram/scramjet vehicles. Subsonic cruise missiles require no boost to achieve flight velocities; however, slow top-end velocities often severely limit mission employment. Conversely, ram/scramjet-powered vehicles provide a supersonic operational capability, but require either a dedicated supersonic launch vehicle or alternate on-board propulsion system to provide minimum operational velocities prior to the transition to the primary system employment. The PDE may allow missile designers to combine the best of both systems listed above while overcoming the limitations of each.

The second area of interest which may benefit from PDE technology is a combined cycle rocket engine design. Currently rockets, by definition, carry the required supply of both fuel and oxidizer for engine operation on board. Orbital insertion is extremely expensive, requiring a very large propellant mass fraction. For every kg less of oxidizer required to achieve desired mission parameters, an equal amount of payload can then be added. The concept of a combined cycle PDE involves using ambient air as an oxidizer while within the lower region of the atmosphere, systematically increasing supplemental oxygen as levels decrease with increased altitude. The reduction of required on board oxidizer may significantly increase fuel efficiencies, potentially enhancing performance sufficiently to warrant readdressing the feasibility of a single-stage-to-orbit (SSTO) launch vehicle.

Pulse detonation engines operate by propagating a detonation wave through a tube filled with a combustible mixture, which combusts the fuel as it transits the combustor tube. This process results in a near-constant volume combustion which produces high pressures resulting from the leading shock wave. In contrast, Brayton cycle combustion process which governs turbojet and ramjet operation is defined by a constant pressure combustion cycle. As a result, the PDE combustion cycle not only produces a slightly higher temperature increase than a Brayton cycle system, it also creates significantly higher pressure. This additional increase in total enthalpy results in thermodynamic efficiency increases of 25-35% over that of Brayton cycle systems [4]. Each detonation cycle provides a discrete impulse as the combustion wave traverses the tube. To be an effective source of propulsion, a rapid series of detonation impulses must be achieved. Theoretically, sufficiently high frequency operation can produce an almost constant thrust level, and dampen longitudinal engine vibration caused by individual detonation impulses. PDE's incorporating ethylene-air mixtures have achieved 80 Hz in experimental testing.

Achieving precise performance measurements for pulse detonation engines has historically been quite difficult [5]. The industry standard for system performance measurement is system specific impulse, or more specifically, the fuel-based specific impulse, since only the fuel is actually carried on the air-breathing engine.

3

$$I_{spf} = F/m_f g_o \qquad\qquad \text{Equation (1)}$$

Specific thrust calculations require determination of both thrust (F) and fuel mass flow rate with a high degree of accuracy. Accurate measurement of both parameters provides challenges more difficult to overcome than intuition might suggest. For fuel mass flow rate, two problematic issues must be overcome before values may be computed with reasonable fidelity: mass of fuel injected per cycle and percent of fuel burned per cycle. In previous experiments, fuel injection profiles have been assumed to be uniform and, thus, predictable. Techniques involving time accurate spectroscopy via optical transmission have recently been incorporated to investigate actual fuel injection profiles within PDE combustors. Results have shown the fuel injection profiles to be non-uniform and irregular, which effectively decreases levels of accuracy of computed performance. Of equal complexity is obtaining an accurate computation of percentage of fuel combusted within the combustor per cycle. A complete PDE cycle consists of filling the combustion chamber with a reactive mixture of fuel and air, igniting/combusting the mixture, purging of combustion products, then commencing the next cycle. At high frequency operations, purge air refreshes the chamber at high velocities and fuel fill times are on the order of milliseconds. If all fuel in the chamber is not consumed prior to refresh or exits the tube before being consumed, a performance penalty results due to fuel being injected , but no utilized. Conversely, if insufficient fuel is introduced to optimally fill the chamber (partial fill), all the fuel may be combusted; however, a reduction in total thrust will occur but with a higher fuel-based specific impulse [6].

The issues associated with force data collection from a PDE result from the impulse nature of the cycle. The primary experimental methods applied to this problem include exhaust velocity measurements and spring/damper thrust stands. An effective exhaust velocity measurement system was developed at Stanford which injected minute liquid metal droplets into the exhaust stream and measured velocities with high speed optical sensors [7]. This system was limited by the quantity of liquid metal and difficulty of introducing droplets into the tube, and was well-suited for single-shot research only. As an alternative method, thrust stands are ideally suited as a data collection platform for constant thrust engines, such as turbojet or rocket. The reaction of a stand when exposed

to a series of impulses from a PDE is often unknown, but it is suspected that detonation impulses fired at a rate near thrust stand natural frequencies may produce responses which will preclude accurate thrust data extraction.

The objective of this thesis was to identify an accurate method for of thrust measurement utilizing a 500-lb class thrust stand. The task included calibration of the stand, investigation into engine mounting techniques, creation of data collection software, construction of data filtering methods for thrust data extraction, and identification of a data export method conducive to simple integration with mass flow rate data to compute desired performance values.

THIS PAGE INTENTIONALLY LEFT BLANK

II.   BACKGROUND

A.   COMBUSTION THEORY

1.   Combustion

Prior to conducting an evaluation of PDE performance characteristics, combustion principles and definitions should be reviewed. A critical phenomenon associated with the combustion process is that of explosion. Explosion is defined as a rapid energy release produced when a fuel source is ignited. This energy release may take the form of temperature increase, pressure rise, or both. While a critical element, all explosions do not lead to a combustive reaction. To achieve combustion, the mixture ratio of fuel to oxidizer must be within the flammability limits of the explosive gas, and the process physically contained to allow the formation and propagation of a flame front (combustion wave) [8].

2.   Detonation versus Deflagration Combustion

Combustion is further divided into two categories characterized by the speed of the combustion wave. A deflagration is a subsonic combustion wave, or flame, sustained by a chemical reaction in the combustible medium and occurs at near constant pressure. Alternately, a detonation is defined as a supersonic shock wave sustained by a chemical reaction in the highly compressed medium and occurs at nearly constant volume. Historically, if reference is made to a combustion process, the user is generally assumed to imply deflagration.
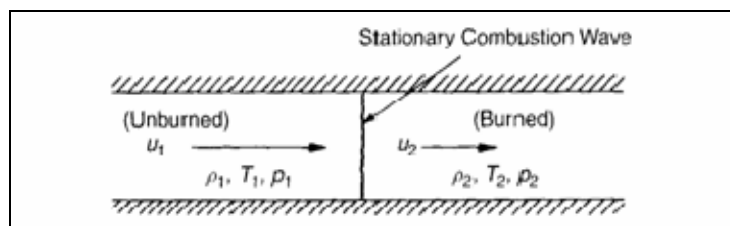
Figure 2.   Schematic Diagram of a Stationary 1-D Combustion Wave (From Ref. 4)

The initial explanation of combustion wave form dynamics is simpler if limited to one-dimensional (1-D) planar waves. Figure 2 shows a 1-D combustion wave within a long, constant cross-section duct. The more likely real world scenario of the system illustrated above would see a combustion wave traveling through unburned gasses from right to left with velocity V_w (wave velocity), and leaving burned gasses in its wake as it passes. This discussion will instead assume a stationary wave reference frame, with unburned gasses traveling left to right into the wave at velocity u_1 and burned gasses traveling left to right away from the wave at velocity u_2.

The distinction between deflagration and detonation is of extreme importance, as the thermodynamic properties of each mode possess very unique characteristics. Table 1 compares the physical properties of the two modes of combustion. Several of these rows highlight the most significant differences. The first row (u_1/c_1) compares wave velocity with acoustic velocity in the unburned gas and provides the Mach number of the wave. As shown, detonations produce wave Mach numbers two to three orders of magnitude higher than deflagration. Additionally, while temperature increases are slightly higher in a detonation, velocity ratio (u_2/u_1) and pressure ratio (P_2/P_1) between the burned and unburned gasses both show ratios with approximately one order of magnitude difference as well. As can be seen, detonation events contain higher total enthalpy than deflagration, which is the enabling characteristic that makes PDE theory so appealing [4].

Table 1.   Detonation/ Deflagration Differences in Gasses (After Ref. 4)

Ratio	Magnitude of	Ratio
	Detonation	Deflagration
u_1/c_1	5-10	0.0001-0.03
u_2/u_1	0.4-0.7 (decel)	4-16 (accel)
P_2/P_1	13-55 (comp)	0.98-0.976
T_2/T_1	8-21 (heat addition)	4-16 (heat addition)
ρ_2/ρ_1	1.4-2.6	0.06-0.25

3.   Hugoniot Curve

A convenient method to obtain a more in depth understanding of wave dynamics is to investigate the theory and construction of the Hugoniot Curve. Simply stated, given pre-combustion pressure and density of a mixture, the Hugoniot Curve is a graphical representation of post-combustion pressure plotted against the inverse of the fuel density, resulting in a curve showing all theoretically possible combustion product states of the specific system. As will be shown, not all solutions provided by the curve are physically possible; however, all actual combustion events generally fall very near the predictive curve.

The Hugoniot Curve is derived from the conservation equations which govern one-dimensional flow in a constant cross section combustor. This derivation assumes no external heat change and no body forces. The three governing equations are:

Continuity:
$$\frac{d(\rho u)}{dx} = 0$$
Equation (2)

Momentum:
$$\rho u \frac{du}{dx} = -\frac{dp}{dx} + \frac{d}{dx}[(\frac{4}{3}\mu + \mu')\frac{du}{dx}]$$
Equation (3)

Energy:
$$\rho u[\frac{d}{dx}(h + \frac{u^2}{2})] = -\frac{d}{dx}q_{cond} + \frac{d}{dx}[u(\frac{4}{3}\mu + \mu')\frac{du}{dx}]$$
Equation (4)

where
$$q_{cond} = -\lambda \frac{dT}{dx}$$
Equation (5)

and
$$h = C_p T + h^o$$
Equation (6)

The bulk viscosity (μ') is generally very small and will be neglected, and du/dx and dT/dx are zero for both the burned and unburned gasses. Lambda (λ) represents the

thermal conductivity of the mixture and h^o documents initial system enthalpy. When these simplifications are applied to the original conservation equations and Equations (5) and (6) are substituted, Equations (2) to (4) reduce to the following:

Continuity: $$\rho_1 u_1 = \rho_2 u_2 = \dot{m} \qquad\qquad \text{Equation (7)}$$

Momentum: $$p_1 + \rho_1 u_1^2 = p_2 + \rho_2 u_2^2 \qquad\qquad \text{Equation (8)}$$

Energy: $$h_1 + \frac{1}{2} u_1^2 = h_2 + \frac{1}{2} u_2^2 \qquad\qquad \text{Equation (9)}$$

Equation of State: $$p_2 = \rho_2 R_2 T_2 \qquad\qquad \text{Equation (10)}$$

As shown by Kuo [4], these four equations can be combined into a single equation with only two unknowns: p_2 and ρ_2. Reducing the first two equations produces a version of the formula known as the Rayleigh-line relation:

$$\rho_1^2 u_1^2 = \frac{p_2 - p_1}{\dfrac{1}{\rho_1} - \dfrac{1}{\rho_2}} = \dot{m}^2 \qquad\qquad \text{Equation (11)}$$

Finally, by completing several additional substitutions for Mach number and specific heat, the Hugoniot relation is obtained:

$$\frac{\gamma}{\gamma - 1}\left(\frac{p_2}{\rho_2} - \frac{p_1}{\rho_1}\right) - \frac{1}{2}(p_2 - p_1)\left(\frac{1}{\rho_1} + \frac{1}{\rho_2}\right) = q \qquad\qquad \text{Equation (12)}$$

As can be seen, this formula eliminates most independent variables and allows for a meaningful comparison between pre- and post-combustion pressures and densities. For a given mixture (constant thermal conductivity, λ), p_1 and $\dfrac{1}{\rho_1}$, fixing a constant heat per unit mass, q, allows for direct comparison of p_2 versus $\dfrac{1}{\rho_2}$. The following figure is the Hugoniot curve for an arbitrary fuel mixture.
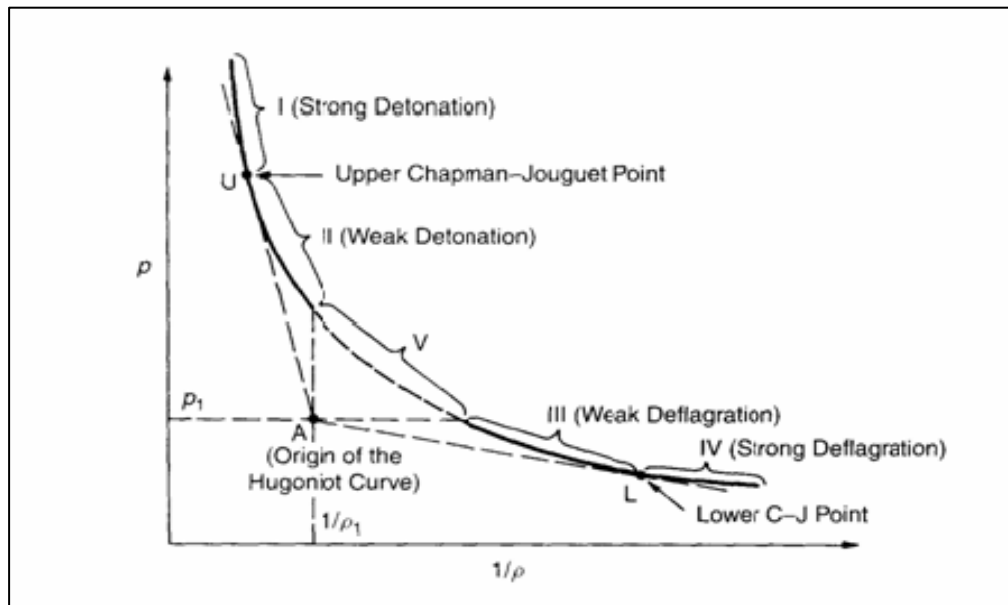
Figure 3.   Hugoniot curve on p-versus-$\dfrac{1}{\rho}$ (From Ref. 4)

Construction of the curve centers on the Origin (Point A), which is the plotted reference values of p_1 and $\dfrac{1}{\rho_1}$. The possible combustion regions are segmented by the lines tangent to the curve through the Origin and the intersection of the horizontal and vertical lines extending from the Origin. The intersections of the tangent lines to the curve are known as the Upper and Lower Chapman-Jouguet Points, and are often referred to as the Upper and Lower C-J points. All told, each curve contains five regions, denoted by Roman numerals I-V. As mentioned previously, the curve represents all possible

11

wave form solutions for a specific system; however, not all solutions are physically possible. Further examination of each region provides a limit to the number of possible solutions and focuses areas for experimental investigation.

The simplest region to analyze lies between the intersections of the horizontal and vertical lines through the Origin, region V. Physical interpretation of the curve shows both p_2 versus $\dfrac{1}{\rho_2}$ are greater than p_1 and $\dfrac{1}{\rho_1}$. Inserting any of these ratios into equation (11) results in a negative value for u_1^2. This solution implies u_1 is imaginary; thus, not a physically achievable solution. As a result, region V of the curve is included as a dotted line, which indicates a region of no possible solutions.

Next we must interpret the significance of the C-J points. Equation (12), utilizing a fixed value q, is differentiated with respect to $\dfrac{1}{\rho_2}$. Through several equation manipulations and substitutions, Kuo obtains the desired formula:

$$|u^2| = c^2 \qquad \text{Equation (13)}$$

which demonstrates that at each C-J point, $M_2=1$.

Regions I and II represent the detonation branch of the curve, and are separated by the Upper C-J point. At this point, detonation wave velocity is the theoretical minimum. In these regions, $\dfrac{1}{\rho_2}$ is less than $\dfrac{1}{\rho_1}$ which implies:

$$u_1>u_2 \qquad \text{Equation (14)}$$

Again, physical interpretation and algebraic manipulation reveal several important characteristics of the combustion wave in these regions. First, gas velocities experience a

12

deceleration after the passing of a wave front. Second, combustion waves in these regions are always supersonic. Region I is called the strong-detonation region and is characterized by wave forms where p_2 is greater than p_U (pressure at the Upper C-J point). Within this region, pressure increases drastically after the passing of the detonation wave, and the velocity of the burned gasses, while still traveling in the same direction as the wave, experiences a significant deceleration to a subsonic value. Kuo notes strong detonations characterized by region I are seldom realized, as structural concerns are difficult to overcome in the laboratory environment. In contrast, region II represents the weak-detonation region and is defined by a relationship where p_2 is less than p_U. In this environment, pressure rise and velocity decelerations are also experienced as a detonation wave passes; however, the differences in magnitudes are lower and u_2 remains supersonic. Again, weak detonation waves are rarely experienced in experimental research as requirements call for fuel with extremely fast chemical reaction properties, which are not easily obtained or operationally practical. Therefore, most experimental detonations achieved are from the solution region found at the Upper C-J point.

Regions III and IV represent the deflagration regions and are separated by the Lower C-J point. This point represents the maximum flame velocity for all deflagration events. Region III is known as the weak-deflagration region and is characterized by the relationship where p_1 is greater or equal to p_2. Manipulation of Equations (7) and (8) when coupled with the density ratios in this region produce a response characterized by an increase in u_2 from a subsonic velocity to a higher subsonic velocity. Additionally, the slight pressure drop across the wave front, when compared to the significant pressure increase across a detonation wave, is a defining characteristic which makes detonation research so appealing. Weak-deflagration waves described by Region III are often produced in the laboratory environment and, as will be shown, are the only physically viable solutions within the deflagration regions of the Hugoniot curve. Last to be described is the strong-deflagration portion of the curve, region IV. This portion is also characterized by slight pressure drop across a wave. The difference from Region III lies in the acceleration experienced as a deflagration wave passes. The passing of a strong

13

wave requires acceleration from subsonic to supersonic velocity. Gas dynamics theory rules out the possibility of accelerating a subsonic flow to supersonic through a constant cross-section vessel. As a result, region IV then becomes a portion of the curve with no physically possible solutions.

In summary, the Hugoniot curve displays thermodynamic states of all theoretically possible wave solutions for a particular system. In reality, combustion product conditions described by regions I, II, IV and V have been shown to be either extremely difficult or physically impossible to obtain. The practical solutions for detonation waves are found at the Upper C-J point and the physically feasible solutions for deflagration waves are found in the weak-deflagration portion of the curve, region III.

B.   DETONATION WAVE STRUCTURE

With combustion now defined, attention will now be focused largely on detonation waves. A brief summary of classic one dimensional wave structure theory, dating back to the 1940's, is necessary to understand the highly dynamic environment of a detonation. A detonation wave consists of a thin leading shock front traveling at the detonation velocity, followed by a thicker region where the actual chemical reaction occurs (Figure 4). The leading shock wave increases temperature and pressure of the reactants such that reactions behind the shock take place at rates sufficient for the ensuing deflagration to propagate as fast as the shock wave. (In reality, the leading shock wave transverses in a spherical front, which produces lateral shock waves that interact until a self-sustaining detonation wave forms.)

The Detonation Wave

Unburned Region
(Uniform Properties)

Burned Region
Uniform Pressure & Velocity

Background :   Mach Stem Structure in a Reactive Gas

ramp

Slipstream

Reflected
Shock
(R)

(M)
Mach - stem
Shock

Streamlines

T (Triple Point)

Incident Shock
(I)
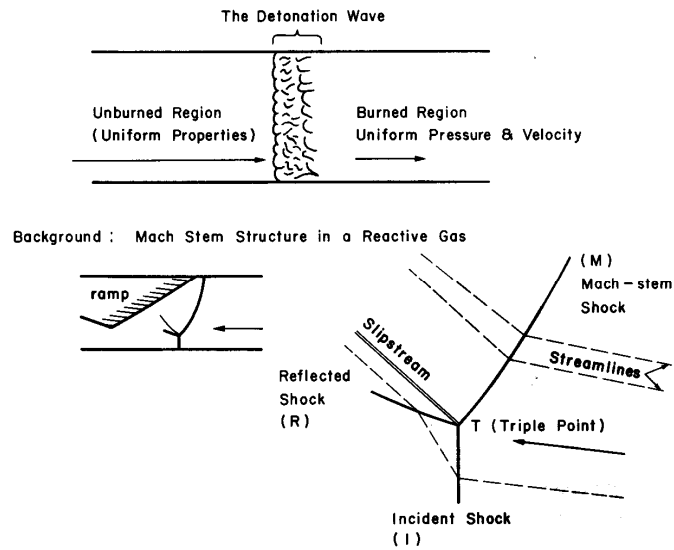
Figure 4.   Shock-wave Structure and Triple Point (From Ref. 2)

Classic C-J theory was advanced by Zel'dovich, von Neumann, and Doring create when a one-dimensional, steady-state wave model was proposed, known as the ZND one-dimensional wave structure [4].   This one-dimensional model provides a simplified graphic representation of physical wave characteristics during the detonation process (Figure 5).
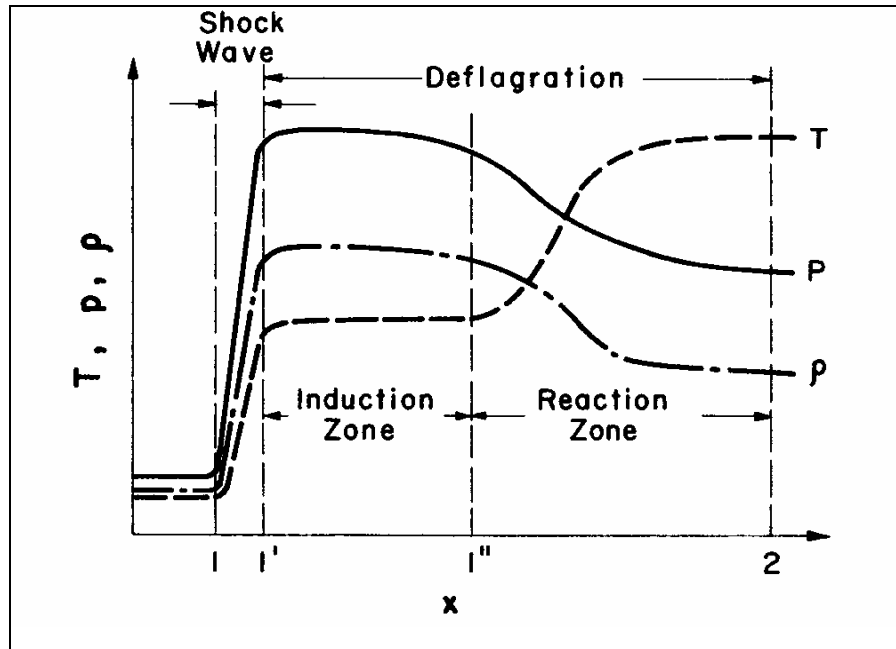
Figure 5.   Variation of Properties through a ZND Detonation Wave (From Ref. 2)

Investigation of one-dimensional wave structure is helpful in understating theory; however, detonation waves are multi-dimensional. In 3-D structure, the leading shock wave is actually curved due to laterally propagating waves behind the leading shock, which produces shock reflection from the detonation containment structure (Figure 6).
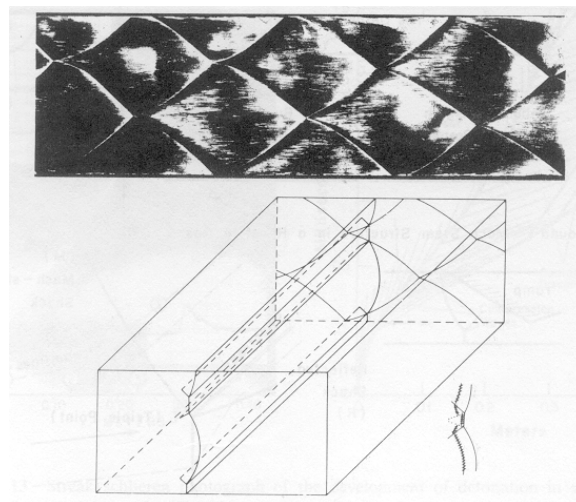
Figure 6.   Smoke-foiled Record and Diagram of Planar Interaction (From Ref. 4)

16

The most significant difference when addressing multi-dimensional waves stems from the interaction of the normal, non-planar shock fronts with reflected lateral shock waves. These shock waves combine to form triple points (Figure 4). Triple points are physical locations of extremely high pressure and are found to trace a "fish-scale" pattern on the walls of the containment structure and can be seen when the walls have been properly prepared with a thin layer of soot. The "scales" have characteristics associated with the specific fuel/air mixture used for the detonation. Figure 6 (upper) illustrates the passing of a detonation wave using a "smoke-foil" method within the containment structure to record cell structure and size [4].

Cell size is of extreme interest in fuel selection for PDE research. Size is a direct indicator of the detonation sensitivity of a particular fuel. Glassman states that highly sensitive fuels are easily-detonable and produce smaller cell sizes [8]. In addition to providing physical evidence for fuel suitability for a PDE, cell size imposes an important limit on PDE operations. Cell size limits the minimum diameter of the containment tube which can sustain detonation. This phenomenon is known as quenching diameter and must be considered when selecting fuel types for a specific PDE or when designing an engine to detonate a specific fuel type.

Practical implications of fuel selection are obvious. The Office of Naval Research (ONR) has financially supported PDE development for over a decade, with the desire to advance technologies to a point such that these engines may offer an improved propulsion alternative for high-velocity cruise missiles and other projects. Military acquisitions organizations have decided against higher performance gaseous fuel sources such as Ethylene and desire operation based on standard liquid military fuel types such as JP-10. The resulting challenge becomes finding a common liquid fuel with sufficiently high performance (small cell size) that may be detonated within an engine small enough to be incorporated onto a cruise missile.

C.   DETONATION INITIATION

Of critical importance in continued PDE research is the development of an efficient process with which to produce reliable, repeatable detonation waves. The

minimum diameter and distance within a combustor required for detonation initiation are fundamentally limiting factors which influence both size of the engine and operating frequency range. Additionally, the carriage of onboard oxidizer will effectively negate performance gains offered by the use of PDE technology. Research continues into techniques which reduce initiation time and initiation distance. The most common techniques in the research community are direct initiation, shock focusing, and Deflagration-to-Detonation Transition (DDT).

1. Direct Initiation

Direct initiation is defined by Frolov as a near-instantaneous application of energy into a fuel mixture which generates a blast wave of sufficient strength and intensity to decay into a self-sustained detonation [10]. Application of this technique would require the use of high explosives (not practical for PDE) or electrical initiation sources such as lasers or sparks. Energy levels on the order of 100-1000 kJ applied on a cyclic basis would be necessary and at this time are not feasible. This technique has the potential to offer the shortest detonation time and lengths, and remains and area of active research; however, limitations listed above require current PDE research to incorporate self-initiation techniques or those with low net power requirements.

2. Shock Focusing

Shock focusing techniques use geometric designs to focus a shock wave or multiple shock waves to create regions of high temperatures and pressures which results in the local ignition of a reactive mixture. Research conducted by Channel found that multiple methods can be used to achieve focusing of these waves such as combustor geometry, turbulence devices or injection jets [9]. In a reactive mixture, these regions of high temperature can produce violent explosions, and eventually detonations. This technique is strongly dependent on both engine geometry and the initial creation of moderate shock waves, and has proven to be of limited value within the dynamic constraints of PDE research.

3. Deflagration-to-Detonation Transition

DDT has become the initiation technique most suitable to PDE operation at this stage of research. This method is capable of providing reliable detonation initiation using ignition energy levels and geometric configurations compatible with small size engines.

Kuo provides and excellent description of the DDT process [4]. This process occurs within a closed-end tube and begins with an ignition source providing a flame kernel which grows as a laminar flame within the reactants. Compression waves are generated and travel ahead of the accelerating laminar flame. At this stage, the laminar flame front is wrinkled (Figure 7).
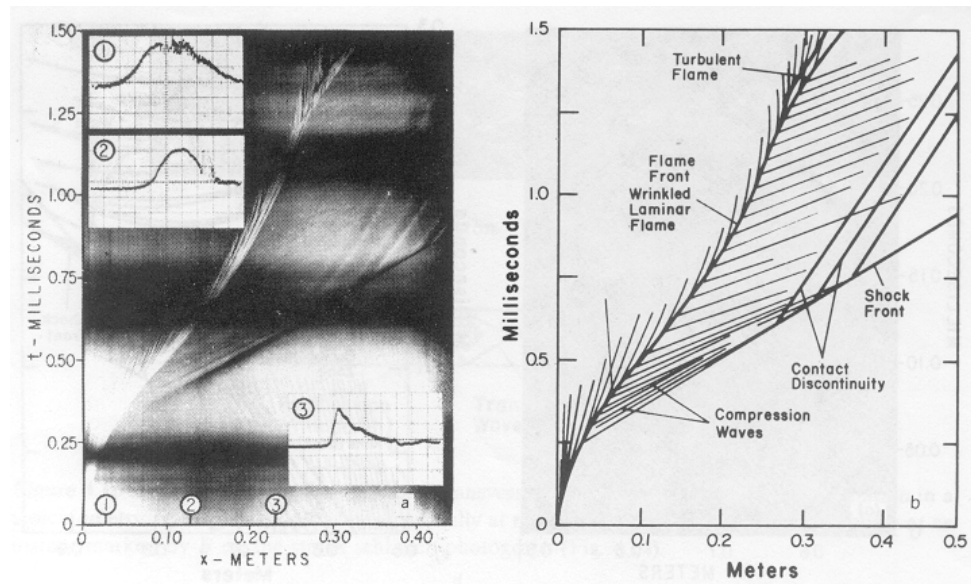
Figure 7.   Detonation Wave Development (From Ref. 2)

The compression waves coalesce into a shock front, which induces movement of the gasses which cause the flame to break into a turbulent brush. The wrinkled flame front and turbulent brush act to increase the flame surface area which enables the onset of an "explosion in an explosion" within the turbulent reaction zone. The explosion produces two strong shock waves, one which travels forward into the unburned gasses

(superdetonation wave), and one which travels backward into the combustion products (retonation wave, Figure 8). Additionally, a spherical shock wave is generated during the explosion and travels outward from the area near the boundary layer (Figure 9).
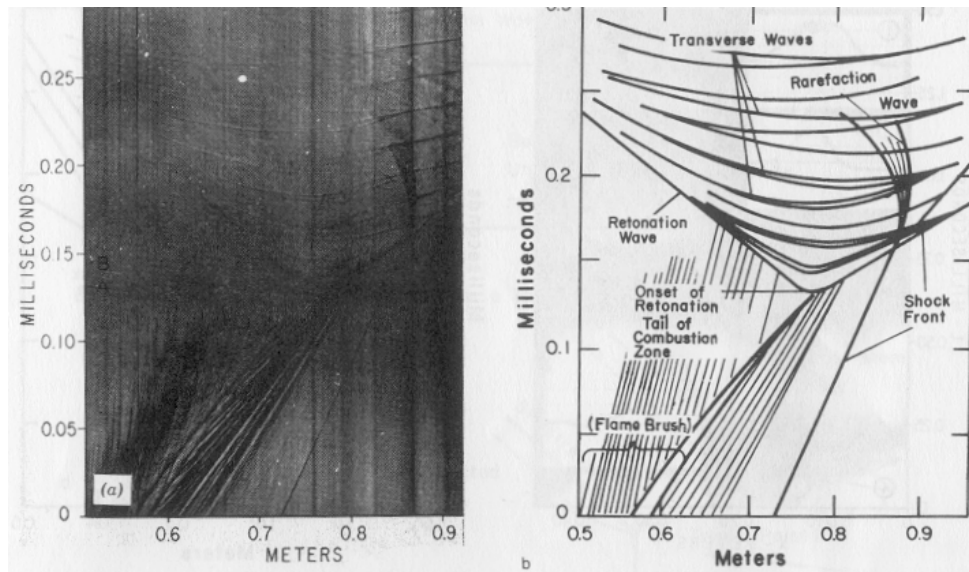
Figure 8.   Streak Schlieren Photograph of Onset of Retonation (From Ref. 2)
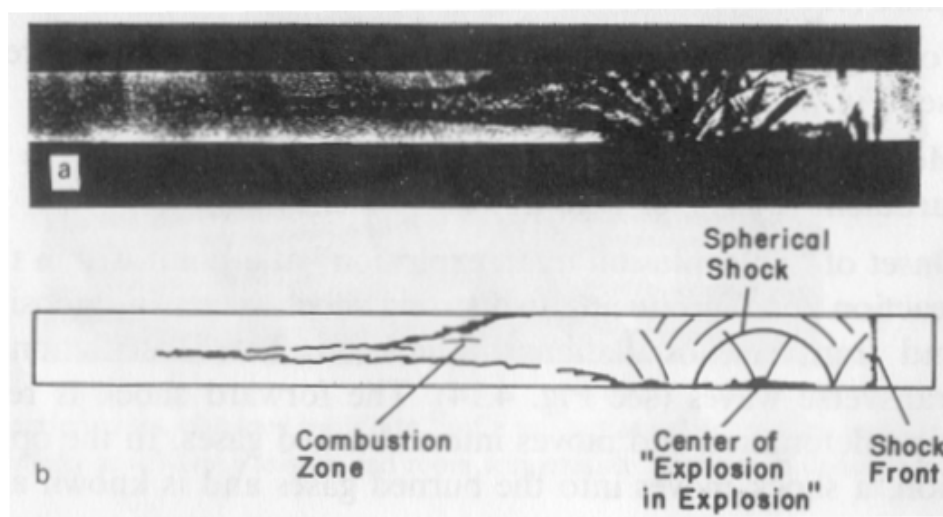
Figure 9.   Flash Schlieren Photograph of Onset of Retonation (From Ref. 2)

20

Finally, the interaction of the transverse waves with the shock front, retonation wave and reaction zone create a final, steady-state detonation wave.

Research has found that use of obstacles within the detonation chamber can significantly increase flame propagation speeds and reduce distances required to complete the DDT process. Work by Laffite, Chapman and Wheeler dating as far back as the 1920s has studied the role of obstacles and the tube wall roughness on turbulent flame acceleration [10]. Current understanding of this phenomenon indicates detonation initiation is accelerated as a result of increased turbulent shear mixing caused by the creation of both vortices and transverse shock waves in the wake of the obstacles. Experimentally, obstacles of various shapes and sizes have been incorporated into rectangular and circular cross-section area combustors. In circular shaped combustors, the most efficient turbulence-generation devices tend to be spiral structures mounted to the inside wall which transverse the length of the tube. Spiral-type obstacles with average blocking ratios up to 40% have been shown to allow for orders of magnitude reductions in the length scale required for DDT.

While turbulence-generation devices offer several advantages well suited to PDE detonation initiation operations, they also create a performance penalty in the form of a total pressure loss which detracts from the theoretic efficiency advantages PDE's maintain over Brayton Cycle engines. Pressure losses result as flow crosses the obstacles which reduce system efficiencies, and increase as blockage ratio and length of obstacles increase. To limit pressure losses and efficiency reductions, research into optimally designed turbulence-generation devices continues.

4.   Transient Plasma Ignition for PDE Operation

Operation of a PDE becomes increasingly more difficult as operational frequency increases. Each cycle requires completion of the four-step process of fuel fill, ignite, detonate, and purge before the following cycle can begin. As operational frequency increases, time available to complete the four-step process decreases. For example, a frequency of 50 Hz allows only 20 msec to complete a cycle. Thus, operational frequency is limited to a finite value based on minimum time required to complete each

phase of the cycle. Until recently, Capacitive Discharge (CD) ignition systems have been used as ignition sources for PDE operation. Relatively slow ignition and initiation processes led researchers at NPS to investigate new ignition sources which could produce lower ignition time. One critical new technology which has enabled researchers to solve both issues is Transient Plasma Ignition (TPI) [11]. Transient Plasma Ignition systems provide a pseudo-spark (corona) discharge in a nano-second timeframe to the fuel/air mixture. The corona sparks with many streamers, each of which provides relatively uniform energy transfer (Figure 10). In comparison, heritage CD systems provide a single electric arc.
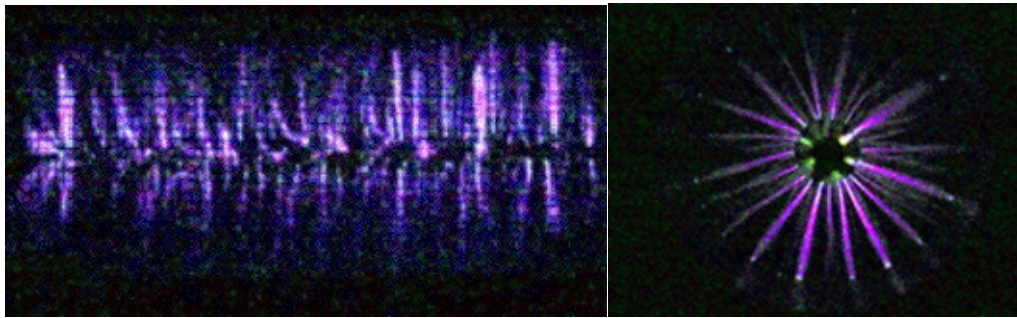
Figure 10.   Transient Plasma Ignition Coronal Discharge (From Ref. 9)

Although a similar amount of energy is applied to the fuel/air mixture as CD equipment, the energy is distributed over a much larger area and occurs at much shorter durations, resulting in significantly higher power levels. As shown in Figure 11, a typical coronal discharge imparts 100 kV to the mixture at approximately 500 Amps.
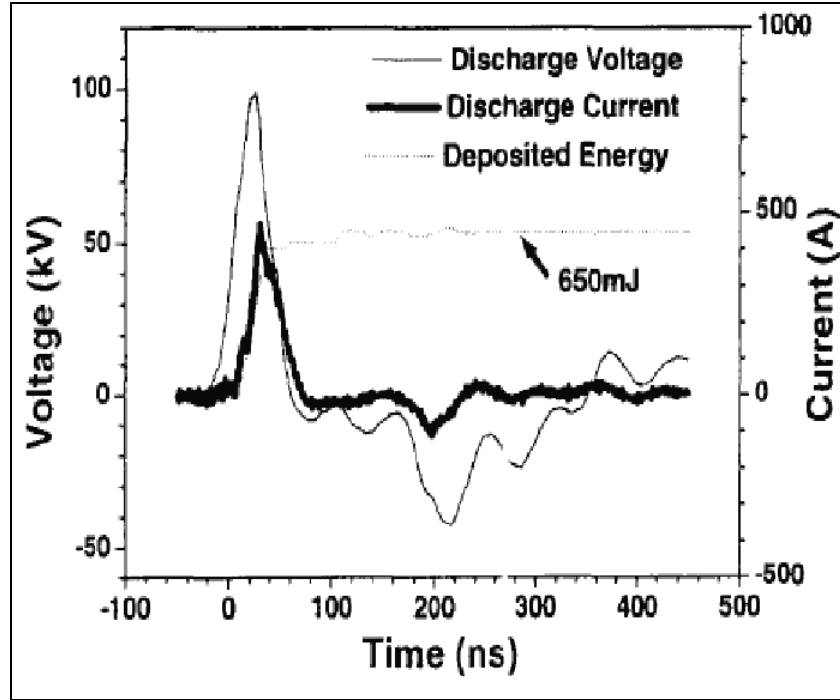
Figure 11.   Typical Energy of Corona Discharge (From Ref. 9)

The combination of increased power density and larger discharge volume has led to an ignition delay decrease on the order of 2.5-3 times lower than capacitive discharge techniques [11]. This reduction in ignition delay translates directly into shorter cycle time requirements and the capability to operate at higher frequencies.

D.   DETONATION DIFFRACTION

Another area of importance to PDE researchers is detonation diffraction. If a detonation can be sustained through a confinement tube with an instantaneous increase in cross-sectional area, smaller tubes could be used to initiate detonations in larger, main combustors. The significance within practical PDE design is quite important, as it enables practical detonation initiation techniques such as DDT to be produced on a small scale, and still provide effective detonation initiation on a larger, more operationally practical scale.

As a review, a self-sustaining detonation wave exists as a result of the symbiotic relationship between the leading shock wave and the chemical reaction within the trailing reaction zone. The leading shock generates a suitable thermodynamic condition which enables sufficiently strong chemical reaction to create compression waves which in turn coalesce with the leading shock wave and perpetuate the detonation. As a detonation wave leaves the confinement tube, a core planar shock wave continues through the medium, while the trailing combustion wave diffracts spherically outward until it reaches the walls of the larger confinement tube. At the intersection of the combustion wave and the walls, triple points are reestablished and the process described in the DDT section occurs. Here, one of two physical states are produced: sufficient energy exists within the combustion reaction to reinforce the shock wave and detonation is successfully transmitted, or insufficient energy exists which causes the shock front and reaction zone to decouple and the detonation fails.

Experimental thesis research conducted at NPS by Tousse produced Shadowgraph images of the expansion process for both a successful and failed detonation diffraction [12]. The pictures displayed were obtained experimentally using ethylene-nitrogen-oxygen mixtures within the initiator and ethylene-air within the combustor. Ratios of nitrogen were increased during the experiment to match the stoichiometric ratio found in air to investigate the sensitivity associated with using only an ethylene-air mixture within the initiator. Figure 12 shows a series of photos which capture successful detonation transmission through an abrupt 4:1 area expansion [12]. The first photo shows a vertical wave front where the leading shock wave transits the fuel medium within the combustor. The rapidly curving upper portion of the wave is indication of shock wave weakening. The three successive photographs show a marble-like, bright pattern within the dark areas immediately following the shock front. This discoloration is indication of intense chemical reactions within the reaction zone, and shows the combustion wave remaining attached to the leading shock.

55 µs   65 µs   75 µs

80 µs
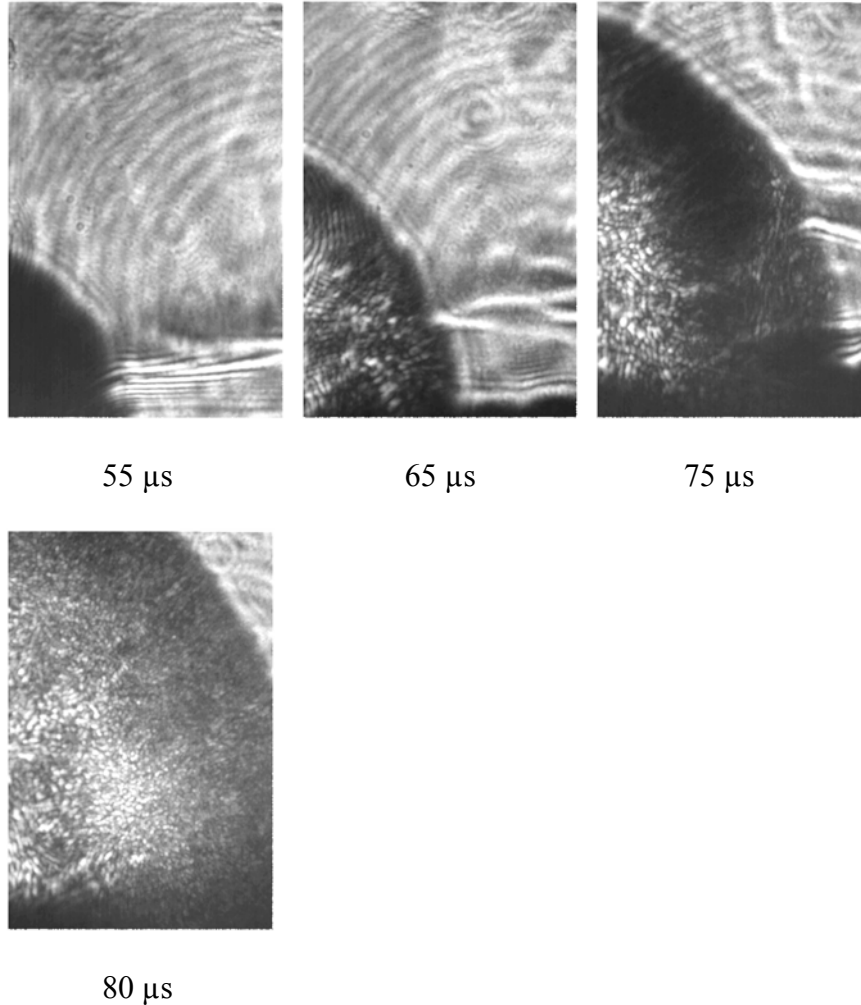
Figure 12.   Shadowgraph Images of Successful Detonation Transmission

Figure 13 shows a series of photographs which capture the failure of a detonation wave to transmit through a 4:1 area expansion [12]. In this experiment, nitrogen levels were increased within the initiator fuel mixture to levels higher than normally found in air. The first photo shows a less defined planar shock front, which indicates a breakdown of the core shock wave. The second and third photographs recorded clear areas behind the wave front, which shows the reaction zone has detached from the shock wave causing the detonation wave to decay and fail. The final photograph shows a more irregular marble-like pattern than in the successful wave, which was most likely a result of transitory chemical reactions ignited by reflected compression waves.

55 μs   65 μs   75 μs

80 μs
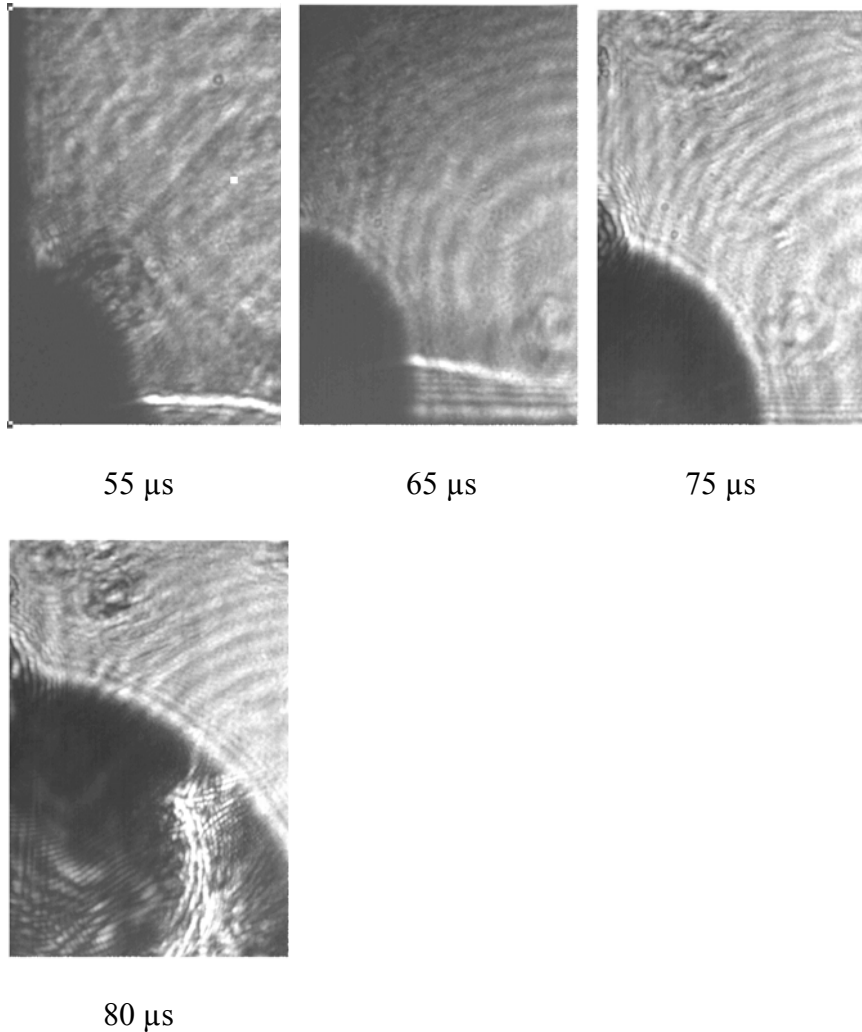
Figure 13.   Shadowgraph Images of Unsuccessful Detonation Transmission

Successful detonation diffraction is dependent on several critical factors: fuel mixture composition, initial thermodynamic state, and geometry of the confinement. The mixture composition inherently possesses a characteristic cell size. Cell size has been experimentally found to limit the minimum diameter of the initiator tube. In his doctoral research, Schultz concludes that for successful expansion into an infinite fuel medium-filled area, the initiator tube diameter must be no smaller than 13 times the cell size of the fuel mixture [13]. This is known as critical diameter, d_c. As the expansion area becomes finite and decreases in size, d_c also decreases to a lesser requirement of approximately 4 to 5 times cell size.

E.   THERMODYNAMIC CYCLE COMPARISON

To understand the rational behind PDE research, an investigation into the theoretical benefits over existing technologies must first be conducted.   The most compelling arguments for continued PDE research can be made when comparing the thermodynamics of the Brayton cycle (turbojet, ramjet) with that of the PDE cycle. To attempt a meaningful comparison, several assumptions must first be made. The cycles of each process will first be treated as ideal, assuming optimal isentropic expansion. Additionally, while closed-loop Brayton cycle can be considered steady-state, PDE cycle is at best quasi-steady-state. For this comparison, it will be assumed that both are steady-state processes, and losses due to non-ideal characteristics will be addressed in a later section.

To review, Brayton cycle engines mechanically (free-stream deceleration or dedicated compressor) compress a fuel-air mixture, combust (deflagrate) this mixture under near-constant pressure conditions, and then expand the flow to free-stream static pressure.   Figure 12 shows a nominal Brayton cycle engine with important stages numbered for follow-on reference.
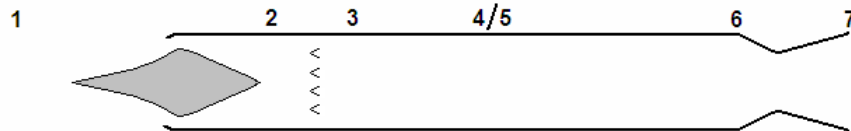
Figure 14.   Nominal Brayton Cycle Engine (From Ref. 2)

Similar to Brayton cycle engines, PDE cycle engines also compress (free-stream deceleration) and expand the flow to free-stream static pressure; however, the combustion process is vastly different and is the source of the theoretical performance improvements. As described in Section A, PDE technology incorporates detonation, vice deflagration during the combustion phase of the cycle.   Regardless of the detonation initiation technique, the wave consists of two components: a leading edge shock wave, followed by

27

a combustion wave. The shock wave gas dynamically compresses the fuel mixture which is then combusted by the following combustion wave. This process occurs non-isentropically, which results in not only a temperature increase but a large pressure increase as well. This and the benefit of the inherent compression by the combustion wave lead to the theoretical increased energy released, and subsequent superior performance realized by the PDE cycle. A more detailed discussion and analysis can be found in the referenced article by Heiser and Pratt [5]. Figure 15 shows a nominal PDE cycle engine with important stages numbered for follow-on reference.
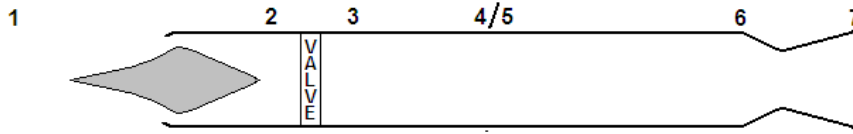
Figure 15.   Nominal PDE Cycle Engine (From Ref. 2)

In his thesis dated December 2006, Hutcheson modeled a single-scenario simulation comparing Brayton cycle and PDE cycle using chemical equilibrium software called CEQUEL [2]. This Excel-based software applies solvers and optimization routines for chemical equilibrium-based analysis. The scenario presented comparison of a PDE with a ramjet applying identical parameters such as inlet losses (MIL-SPEC) over a range of flight Mach numbers from 0 to 4. Cycle performance comparisons are conveniently displayed on temperature-entropy (T-s) diagrams and simulated results of properties at each numbered stage are used to calculate specific impulse, work and entropy change.

The ramjet engine shown in Figure 14 has labeled the position of the important flow parameters to be evaluated post-simulation. These locations are: 1- the ambient flow prior to compression, 2- compressed flow prior to entry into the combustor, 6- combusted flow prior to expansion, and 7- expanded flow. The PDE shown in figure 15 highlights 1- the ambient flow prior to compression, 3- compressed flow prior to entry into the combustor, 6- combusted flow prior to expansion, and 7- expanded flow. Results of Hutcheson's simulation are presented in Figures 16 and 17 [2].
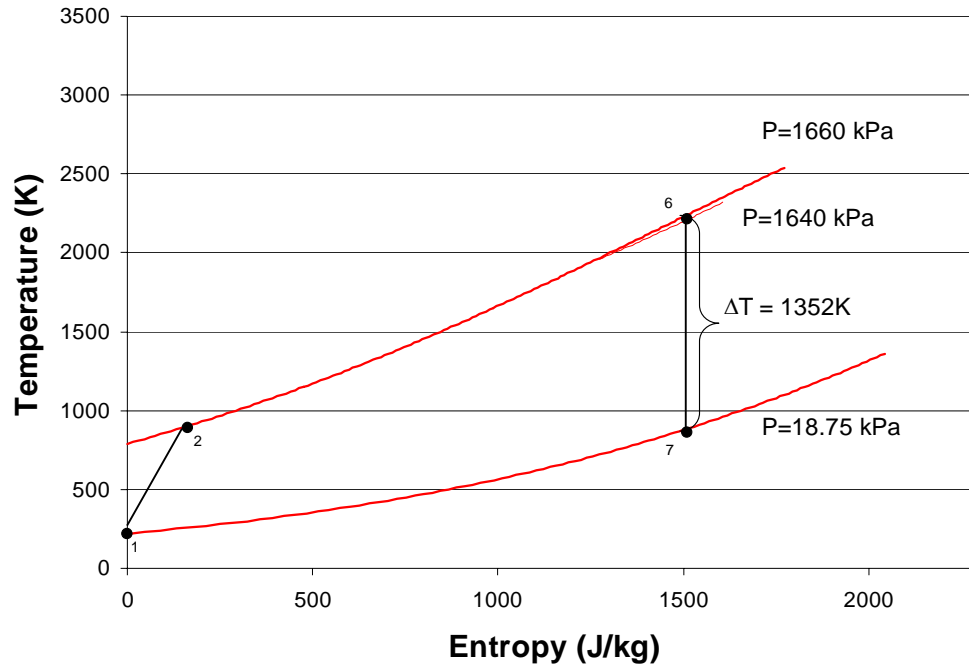
Figure 16.   Temperature-Entropy Diagram for a Generic Ramjet at M=4
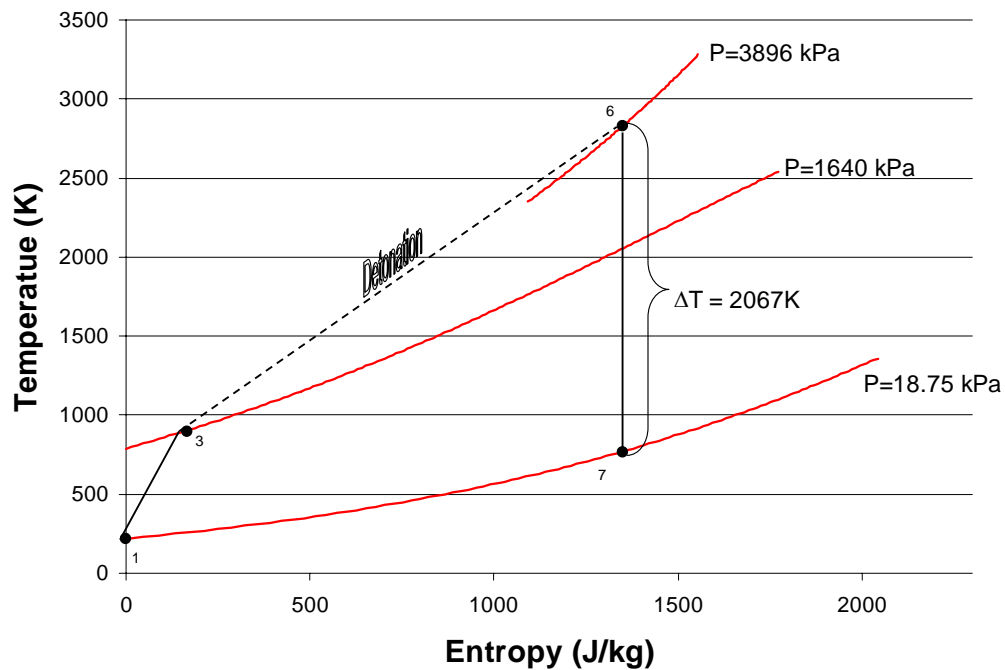
Figure 17.   Temperature-Entropy Diagram for a Generic PDE at M=4

The differences in results from the simulation show a significantly higher change in both pressure and temperature was produced within the PDE model. Not quite as obvious, but of importance with respect to performance was the smaller rise in entropy also produced by the PDE.

Table 2.　　　　Performance Comparison of Ramjet and PDE (From Ref. 2)

	Entropy Change (kJ/kg)	Net Work (kJ/kg)	Specific Impulse Isp (s)
PDE	1.350	1803	1772
Ramjet	1.511	1092	1319

Heiser and Pratt show the detailed formulation required to convert flow parameter values at the various locations into useful performance data. The results in table 2 show for the specific scenario modeled, an entropy reduction of 11%, net work increase of 39%, and specific impulse increase of 26% were obtained by the PDE versus the ramjet. This simulation was conducted with conditions modeled to incorporate losses evenly to both systems. Heiser and Pratt conclude in their article that during REAL thermodynamic analysis (vice IDEAL conditions), as Mach numbers increase, losses affect efficiencies of the PDE more significantly than Brayton cycle engines. It will be interesting to see if theoretical efficiency advantages remain as real-world operating considerations are applied to experimental research.

III. EXPERIMENTAL SETUP

This section provides information specific to the equipment and techniques used to complete the experimentation performed in support of this thesis. All testing associated with this project occurred in the NPS Rocket Laboratory located at an off-campus site. An engine capable of burning both ethylene/air and JP-10/air mixture was required to complete the desired research. A PDE designed and used for previous experimentation was used as the baseline engine for this project [9]. Prior to initial experimentation, numerous modifications were made to the engine and test cell to improve on the previous design and enable switching between fuel types with minimum impact. New fuel supply systems were constructed, a thrust stand was incorporated to measure axial thrust data, and new data acquisition software created for high-speed data capture.

A. PULSE DETONATION ENGINE

A single tube, "valveless" PDE was constructed over five years of continuous research by previous graduate students conducting thesis research. The engine consisted of a combustion tube, fuel injector system, and ignition system. Since the initial design, modifications made by current research students to fuel injector scheme, flow choke sizing, fuel/air inlet geometry, spiral dimensions and mounting technique, tube diameter, and combustion chamber volume have been implemented to facilitate performance improvements throughout continuous experimentation. Specific engine parameters and systems used during experimentation in support of this research are discussed below and a photograph of the test rig is included in Figure 18.
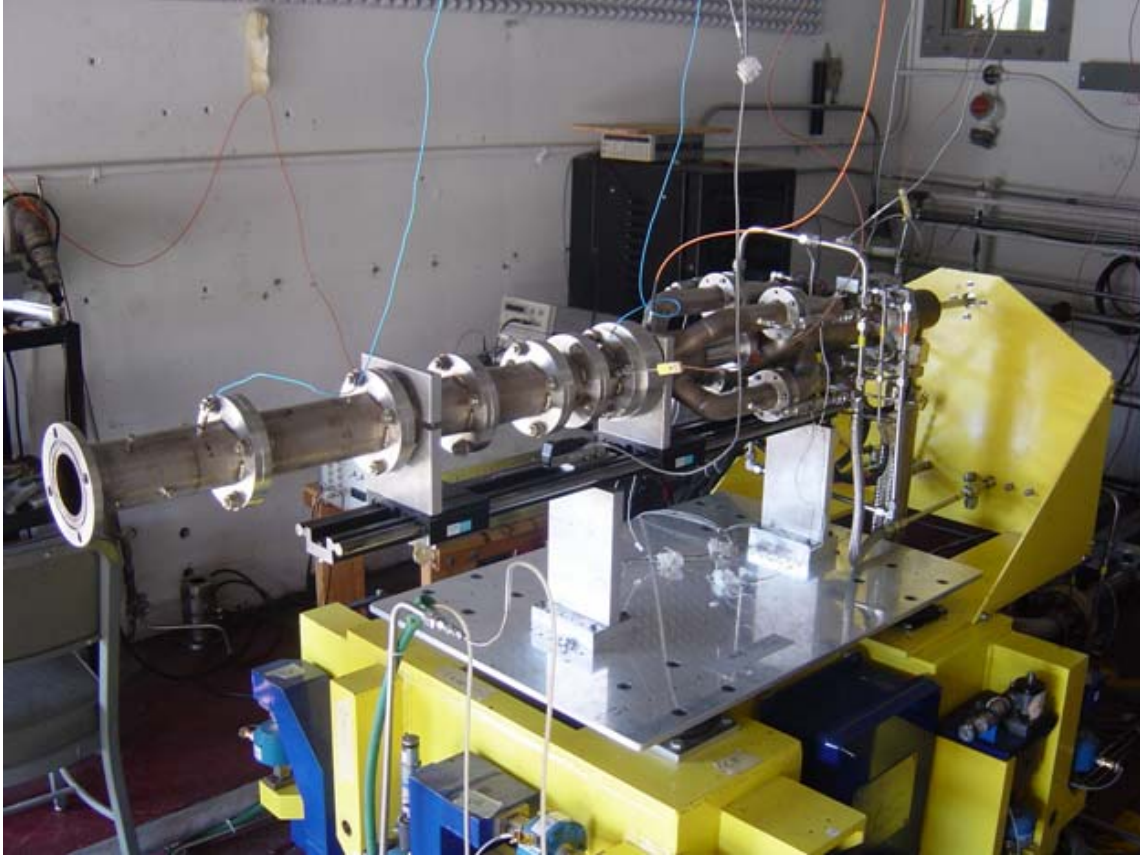
Figure 18.   Pulse Detonation Engine

1.   Fuel Injection/Air Delivery

The fuel injection/air delivery system was designed to provide control of the stoichiometry of the fuel/air mixture supplied to the combustor. Supply air delivery incorporated a valveless design in that a constant flow of supply air was provided to the engine. Control of the fuel mixture was achieved by varying the pressure of injected fuel. Fuel pressure changes altered the mass flow rate ratio of fuel to supply air, which is defined as the equivalency ratio (φ). The mathematical expression for equivalence ratio is given by

$$\varphi = [(F/A)/(F/A)_{ST}]$$
 Equation (15)

where (F/A) is the mass ratio of fuel to air for the experimental mixture and $(F/A)_{ST}$ is the mass ratio of fuel to air for the stoichiometric mixture. Performance varied with changing equivalency (φ) ratio, so accurate measurement and control of fuel injection was critical. Theoretically, an equivalence ratio near one provides the fuel/air mixture which optimizes both thrust and I_{sp}. An equivalence ratio of $\varphi > 1$ implies more fuel exists than can be combusted with existing oxidizer, leaving unburned fuel. While still theoretically maximizing thrust for a given oxidizer, wasted fuel results in a lower I_{sp} value due to increased fuel mass flow rate while producing the same thrust values. Conversely, insufficient fuel ($\varphi < 1$) indicates the system was capable of burning more fuel, which results in less than maximum thrust values, but may produce advantageous performance values.

a. Air Delivery

Supply air was delivered from the vitiator (Section 3) at mass flow rates up to 1.25 kg/sec via a 2" diameter tube. Once in the forward section of the engine, flow was split into four-1 ½" diameter fueling arms in which fuel was added. Supply air chokes were installed within each of the fueling arms to condition the flow prior to entry into the combustion chamber and isolate the vitiator from downstream pressure oscillations. The split flow design allowed for fuel/supply air mixing prior to and a more uniform fuel/air injection into the combustion chamber.

b. Ethylene Injection

An independent quad injector system was designed and constructed to supply ethylene into the four fuel arms described above. Four electrically-controlled high frequency Valvetech (PN#15060-2) solenoid valve injectors were joined by a common feed manifold and mounted to the fuel arms downstream of the flow chokes. The gaseous fuel mixed with supply air prior to entry into the combustion chamber.

c. JP-10 Injection

A separate independent quad injector system was designed and constructed to supply JP-10 into the four fuel arms described above. Four hydraulic-controlled valve injectors were joined by a common feed manifold and inserted upstream of the air chokes. The injectors vaporize liquid JP-10 prior to insertion into the fuel arms.

Mixture with supply air and further vaporization occurred as the fuel passed through the chokes, providing a detonable mixture into the combustor.

A photograph of the fuel injection/ air delivery system is provided in Figure 19. .
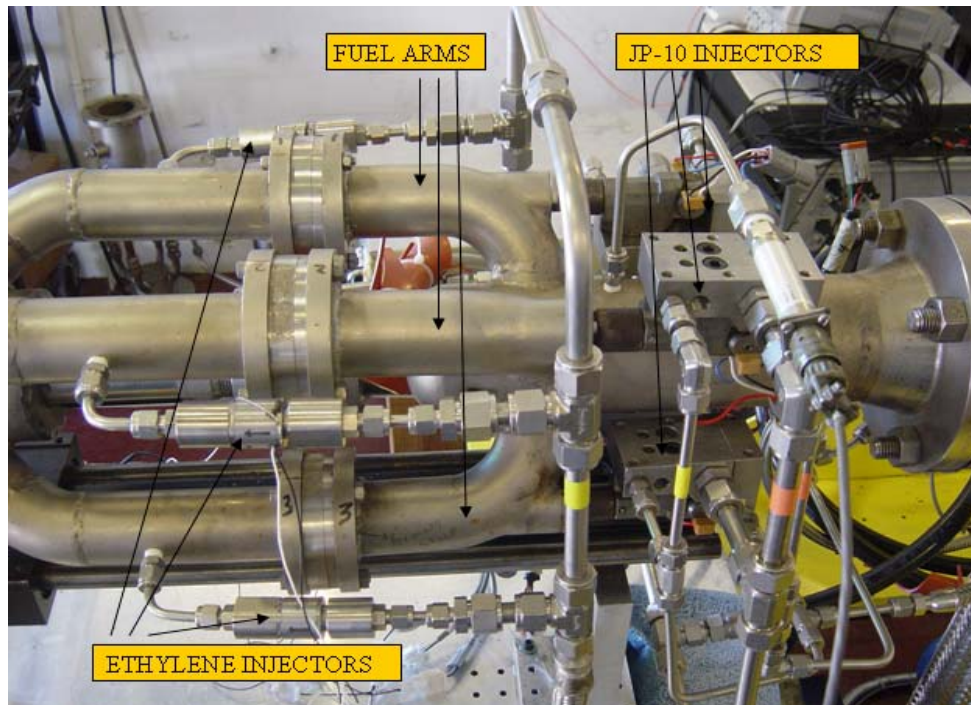
Figure 19.   Fuel Injector and Air Delivery System

2.   Ignition System

The merits of several types of PDE ignition systems were discussed in Chapter II-C-4, and the advantages offered by Transient Plasma Ignition led to its selection for use during this project. Professor Gunderson and his team of researchers at University of Southern California designed and constructed a unique, small-scale TPI system which met the size and performance requirements for operation within the NPS engine. Interface between the TPI unit and the combustion chamber was accomplished by inserting a steel probe through a machined orifice directly into the combustion chamber. The probe was 7" long with the first 4 ¾" shielded by a cylindrical Macor (ceramic) tube to prevent premature arcing to the engine wall. An optical port was included on the

combustor for concurrent thesis research by LCDR Hackard to study the timing characteristics of corona discharge and associated ignition delay within the engine. Research techniques designed by Hackard provided visual confirmation of successful corona discharge, discharge timing, and ignition delay within the engine during experimental engine runs [14].

### 3.	Combustion Tube

The combustion tube was a 38" long segmented stainless steel tube with 3" inner diameter. Segments were initially designed to allow for installation of a variety of turbulence-generation devices, which result in shorter DDT within the combustion chamber. A 30" long spiral was installed for this purpose, with one end mounted flush with the upstream end of the tube. Sensor ports were drilled into the tube to allow for internal measurements during hot-fire testing. Six pressure ports allowed measurements which provided not only confirmation of detonations, but isolation of location of detonation initiation as well. This information is of significant importance when sizing an initiator tube within a main combustor. Additionally, pressure information will be used to provide an alternate method to wave speed. Also, two temperature ports were installed, one near each end of the tube. These ports allow for measurement of temperature rises within the detonation cycle and provide a means to perform repeatable experimentation. Finally, several optical ports were installed to provide a capability for spectroscopic interrogation of a detonation cycle. A photograph of the combustion tube is provided in Figure 20.
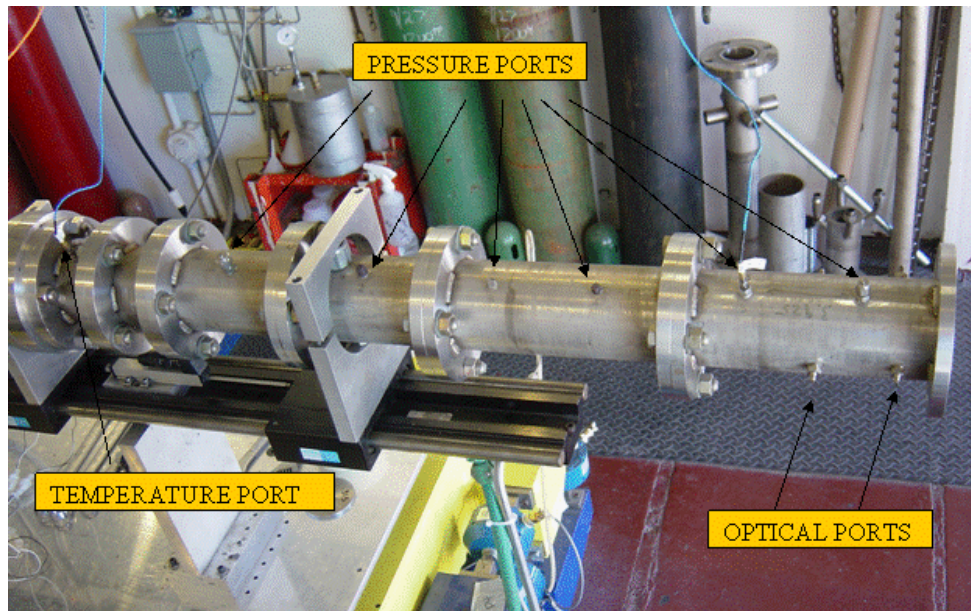
Figure 20.   Combustion Tube

B.   THRUST STAND

A multi-component Thrust Measuring System (TMS) designed and constructed by Force Measurement Systems of Fullerton, CA was used as the primary method of force determination during experimentation. The TMS was designed to measure both force and bending moment data in all three primary axes. Research for this project required thrust measurements in the axial direction exclusively and utilized only one of the six stand measurement capabilities. The physical dimensions of the stand were approximately 60" long by 60' wide by 36" high, weighing more than 1700 lbs without the engine and engine support structure, and was made up primarily of two large sections, the live bed and the ground frame. Data ranges of the stand for the axial component force was zero to 500 lbf (2225 N) and the thrust stand was capable of supporting up to 750 lbs of engine/engine adapter hardware. The baseline TMS design provided a 40" by 27" horizontal aluminum base plate to serve as the interface between the live bed and the engine. Additionally, calibration algorithms and an in-frame calibration system were provided based on anticipation of an engine mounted with centerline 18" above the base plate. A photograph of the thrust stand with engine mounted is shown in Figure 18.

1.   Primary Structure

The live bed was the active portion of the stand which "floated" independent of external mechanical forces, and isolated and resolved forces produced by the engine. The ground frame was a robust structure used as an interface between the live bed and the floor of the test cell. The manufacturer provided an aluminum horizontal base plate which rested on the live bed for engine mounting. In an effort to provide an alternative force transmission path during engine firing, a three eights inch thick vertical steel plate was mounted at the head of the live bed. This plate was 24" tall, traversed the width of the stand, affixed with triangular steel webbing, and was mounted to the front and side of the live bed with 12 3/8" by 1" steel bolts. A more detailed discussion of the vertical plate is provided below.

2.   Load Cell

The physical force measurement hardware which bridged the gaps between the live bed and the ground frame were load strings. Each string consisted of a series of individual load cells which, when combined, provided measurements required to isolate and compute thrust for each primary axis. In all, 18 load cells were mounted on the thrust stand, 10 for data collection and eight for thrust stand calibration. Each load cell was a shear beam construction, double bridge foil strain gauge which output changes in strain by varying voltage signals, with full-scale output of 2mV/V. Each load cell was joined with the live bed and ground frame via Universal flexures. Flexures were designed to provide a single point of articulation, prevent free play or hysteresis, and allow for a high degree of accuracy [15]. A photograph showing a load cell and connecting flexures is provided in Figure 21.

Figure 21.   Load Cell and Flexures

3.   Data Collection Hardware

Each of the 18 individual load cells were linked to the data acquisition system via 3/16" shielded wiring. The acquisition system consisted of three eight-channel cards mounted within a National Instruments Signal Conditioning Extensions for Instrumentation-1520 (NI SCXI-1520) module located on the lower, right side of the thrust stand. This module routed data through an SCXI-1000 Chassis to a PXI 6221 Chassis Communicator which was accessible by a PC located in the control room. The wiring was completed by a previous thesis research student; however, one load cell was not yet installed. The missing load cell was subsequently added to the stand and data acquisition channel assignments to the SCXI-1520 were created prior to calibration. Thrust stand load cell data acquisition assignments have been documented in Table 3.

Table 3.   Thrust Stand Load Cell Data Acquisition Assignments

Thrust Stand	PXI slot 7
SCXI 1520	
Slot 1 ACH0	Load Cell C8
ACH 1	Load Cell D9
ACH 2	Load Cell D4
ACH 3	Load Cell D3
ACH 4	Load Cell D8
ACH 5	Load Cell C5
ACH 6	Load Cell D1
ACH 7	Load Cell C2
Slot 2 ACH0	Load Cell C7
ACH 1	Load Cell D10
ACH 2	Load Cell D6
ACH 3	Load Cell D7
ACH 4	Load Cell C4
ACH 5	Load Cell C6
ACH 6	Load Cell C1
ACH 7	Load Cell D2
Slot 3 ACH0	Load Cell D5
ACH 1	Load Cell C3
ACH 2	blank
ACH 3	blank
ACH 4	blank

4.   Engine/Thrust Stand Interface

The thrust stand was designed to host constant thrust rocket or turbojet engines and originally incorporated only the single horizontal mounting plate for engine/thrust stand interface described above. Constant thrust engines have historically been mounted to the base plate via multiple vertical supports. The cyclic nature of pulse detonation and the existing air delivery system design led the research team to conclude losses due to excessive vertical support bending and non-linear stiffness produced by the air delivery tubing would introduce excessive measurement inaccuracies. The front vertical steel plate described in Section B-1 was designed and mounted to provide a support platform in the axial direction. The engine was mounted directly to a horizontal slide rail, which

in turn was supported by two vertical support braces rigidly mounted to the horizontal base plate. The forward end of the engine was attached to the front vertical support plate via a rigid six inch long, 1/2" diameter steel rod which transmitted the entire axial load to the thrust stand when fired. An alternate support method which incorporated a spring in place of the rigid rod was designed and built; however, the anticipated difficulty with data collection efforts when capturing thrust data exposed to the non-linear stiffness air delivery tubing made this a less attractive alternative. A photograph of the thrust stand which includes all described components is provided in Figure 22.
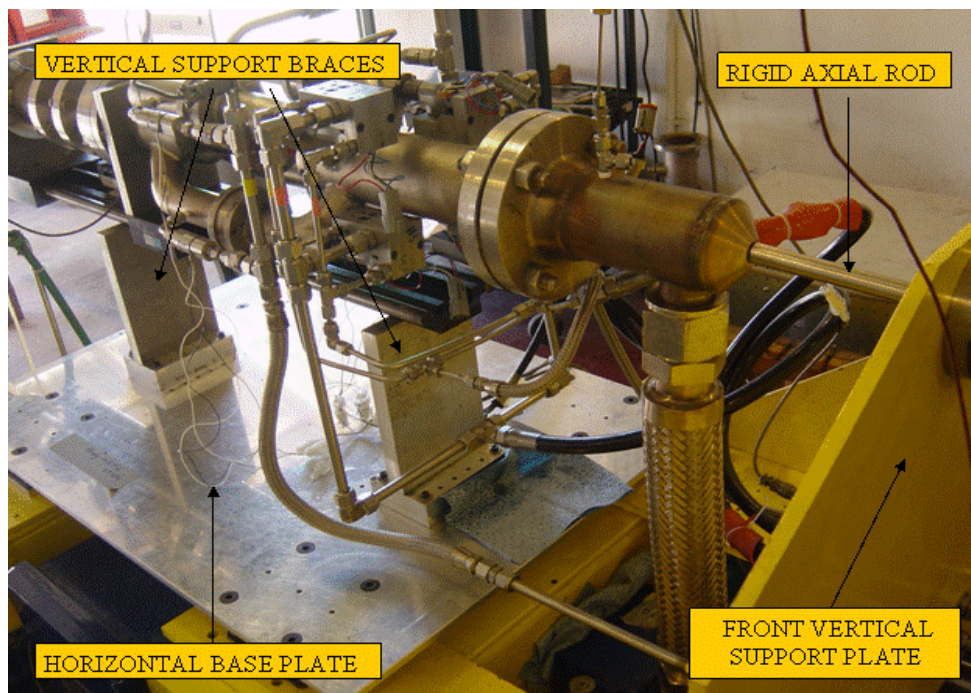

Figure 22.   Engine/Thrust Stand Interface

5.   General Vibration Model of Thrust Stand

As in all systems which contain mass and elasticity, the thrust stand was assumed to be capable of free vibration, as well as forced vibration at the excitation frequency which PDE testing would occur. Vibration analysis identifies the primary physical

characteristics which govern system response as mass, damping and stiffness. In the presence of light (assumed here) or no damping, the system will vibrate very near the natural frequency defined by

$$\omega_n = (k/m)^{1/2} \hspace{3cm} \text{Equation (16)}$$

where k is system stiffness and m represents system mass [16]. The TMS manufacturer included in the statement of work an estimate of 1700 lbs for the live bed and description of the flexures which indicates a short, stiff construction. Based on previous test stands constructed and tested by FMS, the likely range of natural frequency of this stand was 10 to 35 Hz. The stand incorporated for these experiments contained the lowest mass produced by the manufacturer, which will most likely result in a natural frequency at the higher end of the estimated range. Additional modes may have also been introduced by the modification to the support structure and the mounting design of the air delivery system.

6. Thrust Stand Calibration

The stand described above was subjected to a calibration process which resulted output thrust measurements in pounds force (lbf). The calibration process involved three phases, the first of which required manufacturer assistance and specialized hardware. Prior to calibration, computer software using National Instruments VI block-type programming was created which output data streams from all 18 load cells to the PC within the control room.

a. Channel Calibration/ Voltage-to-Thrust Conversion

The first phase of the process consisted of calibration of the individual channels which transfer load cell data to the data collection system and convert voltage data to force units. Small imperfections in cable manufacturing, varying length of supply cable per channel, and other factors lead to small variances during the data transmission process which must be normalized to eliminate constant sources of bias error. This process was completed in conjunction with manufacturer representatives, with no load on the thrust stand and support pins installed. The first step was to install a load cell simulator in place of actual load cells, and apply excitation voltages at known excitation

ranges. Output voltages were recorded for each channel at both a no load condition (0 mV/V) and an input condition of 2 mV/V. The load cell simulator was switched to a force simulation mode and again input to each channel at an excitation voltage of 2 mV/V. Data was again recorded at a no load condition (0 mV/V) and an input condition of 2 mV/V. From this data, the voltage-to-thrust coefficient (K_t) was calculated for each channel with the following equation.

$$K_t = [Force(2\ mV/V)\text{-}Force(no\ load)]/[Volts(2\ mV/V)\text{-}Volts(0\ mV/V)]$$

Equation (17)

The programming VI was then modified to multiply the load cell voltage data by K_t which then output data streams in units of force, vice voltage [15].

b.   **Empty Stand Calibration**

The second step of the calibration process was to calibrate the thrust stand with no engine or support structures mounted. The support pins were removed and mass distribution of the stand was transmitted to the load cells. A function was included into the control program which allowed the channels to be zeroed, thereby eliminating from the output data force and moment components caused by the physical properties of the stand itself. The stand was designed to host an engine mounted 18" above the horizontal support plate. Loads applied by an engine on any axis will produce not only forces within the TMS, but moments as well. A calibration system controlled by the Thrust Stand Calibration Control unit located in the control room was utilized to experimentally determine a force coefficient (K_f) specific to each thrust axis which acted as a normalizing constant to correlate induced moments and orthogonal vectors. This process essentially decoupled bending moments from the thrust axes and isolated the desired thrust components. Technical difficulties inhibited continuous reading of data from all 18 load cells and prevented a complete calibration of the stand. Research for this thesis required only axial thrust measurements and all load cells for axial load measurement functioned properly; thus, a successful calibration of the portion of the stand which measures thrust oriented in the axial direction was completed. The procedures for

operating the calibration control and computing K_f values is described in detail in the thrust stand Operations and Maintenance Manual [15], located in the control room of building 217. The control VI was first modified to display pre-calibration axial thrust data by summing load cell data from D1 and D2, and assigned the variable Dx. The force coefficient, experimentally determined to be $K_f = 1.00046$, was then multiplied by Dx which output the desired, calibrated axial thrust, X.

c.   Stand Calibration with Engine

Once an accurate calibration of the stand was verified, the engine was mounted and all supporting hardware (gas lines, fuel injectors, support devices) were installed. Due to mass and stiffness differences caused by this added structure, both the residual forces and force coefficients were expected to change. The calibration process described above was repeated and the new axial coefficient was calculated to be $K_f = 1.00024$. This new value was inserted into the control software which now outputs calibrated axial thrust specific to this engine/ engine mounting configuration.

C.   VITIATOR

A vitiator was incorporated into the main air supply line to heat air flowing into the engine and simulates different flight condition flow profiles at the combustor inlet. Hydrogen was injected into the main air flow and ignited with a hydrogen/air torch lit off by a spark plug. Once heated, main air below the vitiator was injected with make-up oxygen to replace that burned in the heating process and return the oxygen molar fraction to that of normal air. Hydrogen supply pressures were varied to adjust combustor inlet temperatures and make-up oxygen pressures trended with hydrogen to maintain normal concentrations. Temperatures up to 800 K at the vitiator inlet were possible without damage to the unit, which resulted in temperatures up to 500 K at the combustor inlet. This air delivery system/vitiator combination was capable of providing high speed heated air into the combustor which simulated flow conditions of Mach 4 or higher. A photograph of the vitiator is provided in Figure 23.
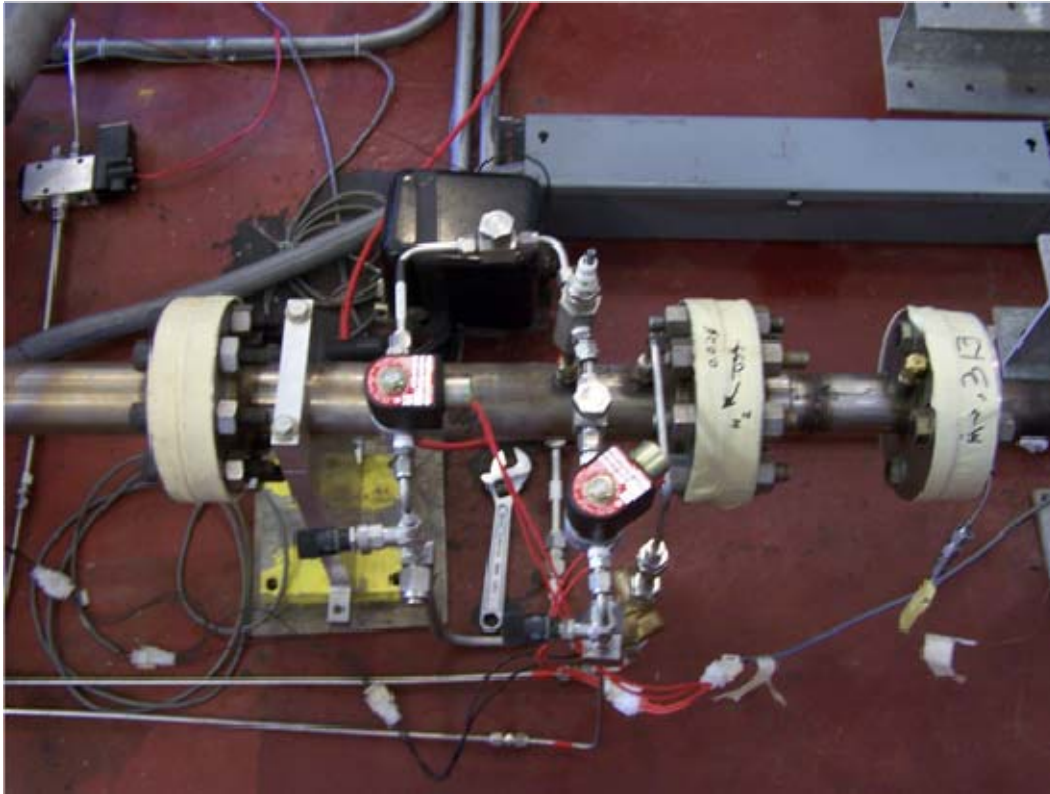
Figure 23.   Hydrogen/Oxygen Vitiator (From Ref. 2)

D.   TEST CELL/ PDE CONTROL

The engine and support equipment in test cell #2 was controlled by a National Instruments (NI) Real-Time VI software program installed on a personal computer (PC) in the control room. The PC was linked to a NI PXI-1000B controller in the test cell through an internet connection to the PXI IP address. The program controlled engine operation by managing engine supply gas operation via ball valves located in the test cell. A BNC pulse generator also located in the control room controlled timing of trigger signals sent to both the fuel injectors and TPI via electrical relays located within the test cell. Also located within the control room were 28 VDC and 110 VAC master power switches, and an emergency shutoff button. The electrical switches controlled electrical power within the cell for engine control and instrumentation equipment, such as temperature and pressure transducers. The emergency shutoff button was provided as a safety feature and would disable test cell #2 by closing all supply gas ball valves and

interrupt fuel injection and ignition trigger signals. A more in-depth description and pertinent illustrations of control elements within the test cell can be obtained from Hutcheson's thesis [2].

E.   DATA ACQUISITION

Data acquisition was controlled via the PC in the control room. The PC was linked to the PXI-1000B controller mounted on the wall in the test cell, which in turn was linked to three NI data acquisition devices (DAQ) located on the engine stand. The PXI-6031E was a 16 channel, 16 bit card which collected operational parameters such as various engine temperatures and pressures, and supply gas pressures, at a rate of 1 kHz. A data file path designated on the control program directed data in the form of an excel spreadsheet to a selected location. A second DAQ, SCXI-1520, was a series of 3 8-channel, 16 bit cards that was used to collect data from the 18 load cells within the thrust stand. These data streams were used to calibrate the stand prior to the commencement of testing, and record thrust data during engine operation. Data collection rates varied from 0.1 to 1 kHz. A second file path designated on the control panel directed thrust data in the form of an excel spreadsheet to a selected location. Additionally, thrust data was streamed to the control program GUI for real-time monitoring. Finally, the PXI-6115 was a four channel, 12 bit DAQ installed to collect high-speed pressure data from pressure transducers periodically installed near the exhaust end of the tube. The system was created to record data at rates as high as 500 kHz. Although this third data acquisition system was not used, the capability was available and provided an additional tool in support of this research. A photograph of the control VI GUI showing control interfaces, data path windows and thrust data displays is provided in Figure 24.
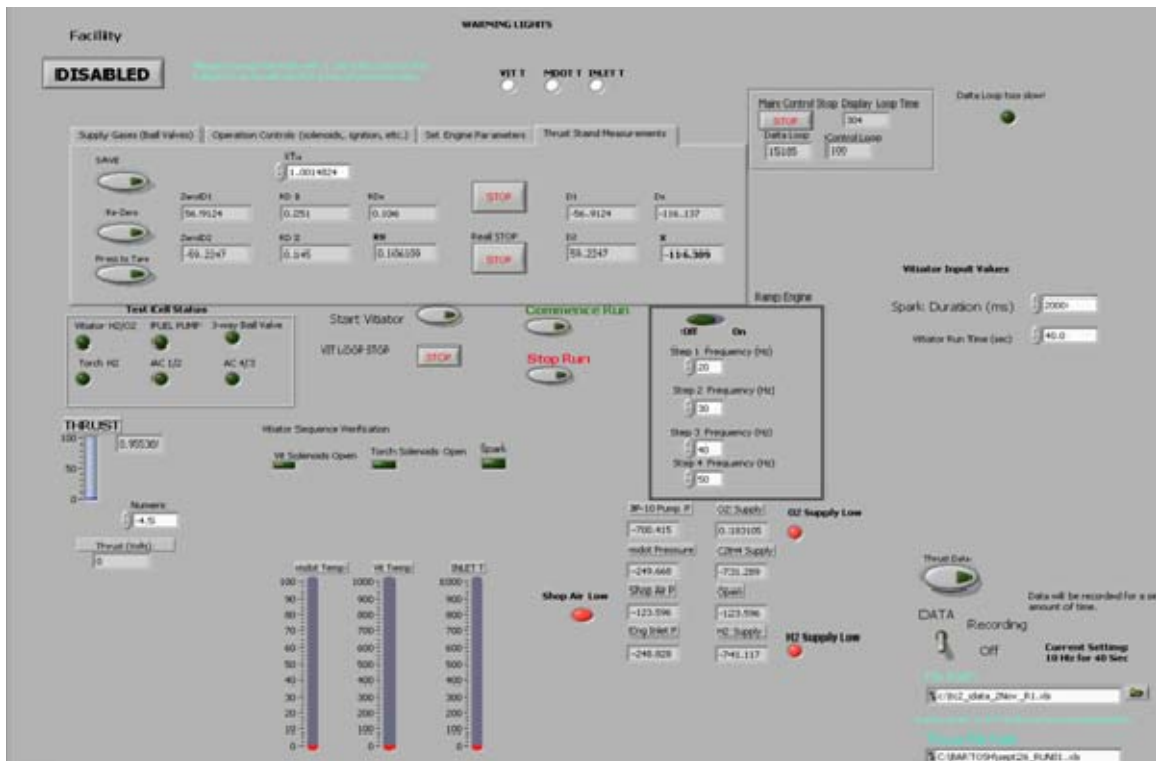
Figure 24.   Labview Control VI GUI

IV. RESULTS

The initial objectives of research conducted in support of this thesis were to experimentally measure the thrust profile of a PDE combusting both Ethylene and JP-10 and incorporate an experimentally verified fuel mass flow rate to compute specific impulse values for both fuels at various firing rates. A significant effort was made to understand how to operate the engine and understand fueling, timing and ignition effects on engine operation. Several months were spent conducting familiarization runs in preparation for data collection events, during which time suitable fuel/timing event profiles were established. The practical implications of possessing the TMS described in previous sections dictated it as being the thrust measurement system of choice for this research. As thrust measurement data was collected, it became apparent that the challenge of meeting the stated objectives would lie in understanding the physical characteristics of the TMS and developing a method to accurately extract thrust values from the measured data. As test firings began, it became immediately obvious that harmonics of the thrust stand were excited by combustion events and masked the true thrust profile. At this point, the objectives of this thesis evolved into designing an analysis system capable of filtering undesired thrust stand responses and returning accurate detonation thrust information. Additionally, system response varied with engine mounting techniques, which lead to an investigation into determining the optimal engine mounting design. Finally, the main air supply system introduced an unexpected negative thrust component as vitiated air was ported through the engine and thermal expansion effects became obvious. A final objective of this research was to understand this phenomenon and assess its impact on the stand's capability to accurately measure PDE thrust data.

A. FREQUENCY SENSITIVITIES OF THE TMS

In an effort to understand natural frequency effects of the thrust stand on data collection, a series of combustion events was conducted at operational frequencies ranging from 10Hz to 55Hz, increasing in five Hz increments. With the exception of

combustion frequency, these firing runs all utilized the same engine operation parameters, which produced a full-tube fill condition and, based on detonation theory, were expected to produce very similar impulse thrust values per firing event. A complete table of fuel, timing, pressures and ignition parameters for each run is included in Appendix A.

Plots showing raw thrust data versus time for selected frequency test firings are provided in Figures 25-30.
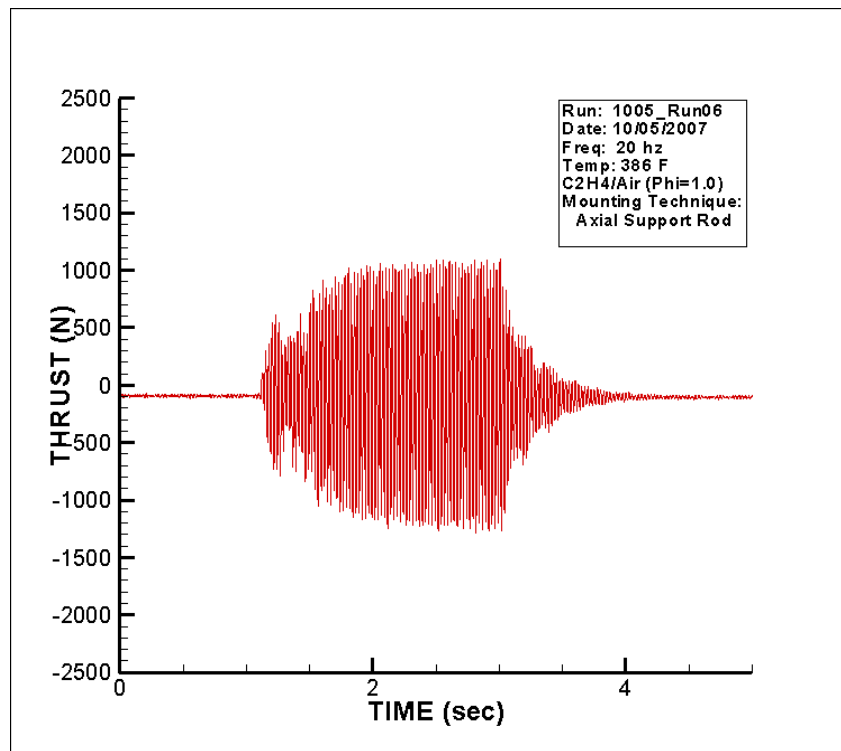

Figure 25.   20 Hz Raw Data (Abs. Unc. +/-0.452%)

While all firing events appeared to achieve quasi-consistent detonations, the temporal thrust values measured were quite varied. Amplitudes were significantly larger near 40Hz, which indicated a likely natural frequency of the stand in this range. Additionally, 20Hz response appeared resonant (sub-harmonic), and amplitudes were greater than those produced at 25, 45, and 55Hz runs. Maximum peak forces cycled between magnitudes approaching +/-2,200 N at 40Hz, +/-1,600 N at 35Hz, and +/-1,300 N at 20Hz, while achieving values of only +/-500 N at other firing frequencies. The

varying amplitude and cyclic behavior supported expectations that thrust stand harmonic responses may mask actual thrust data and make accurate data extraction difficult or impossible.
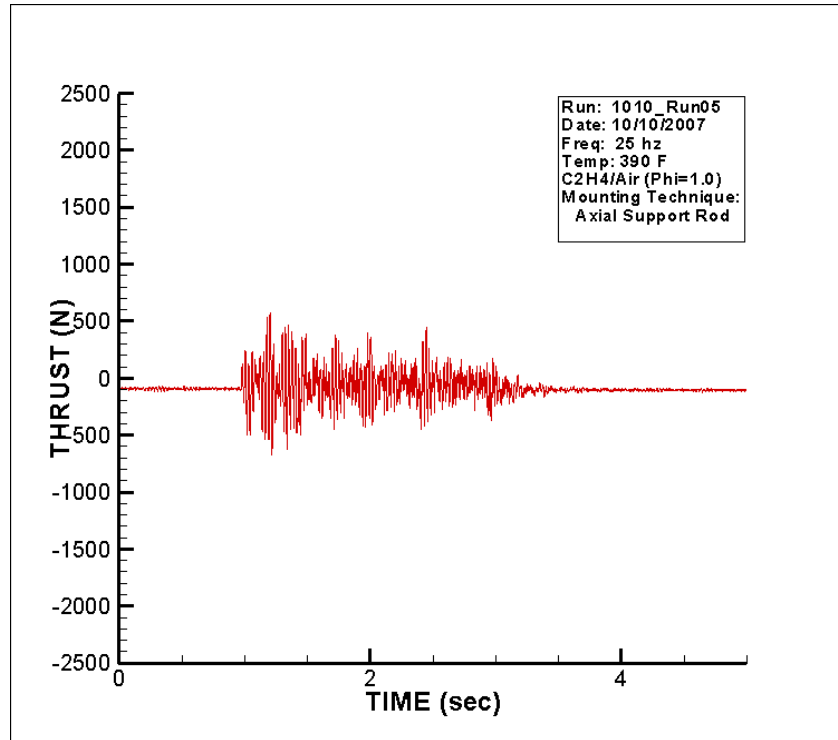

Figure 26.   25 Hz Raw Data (Abs. Unc. +/-0.452%)
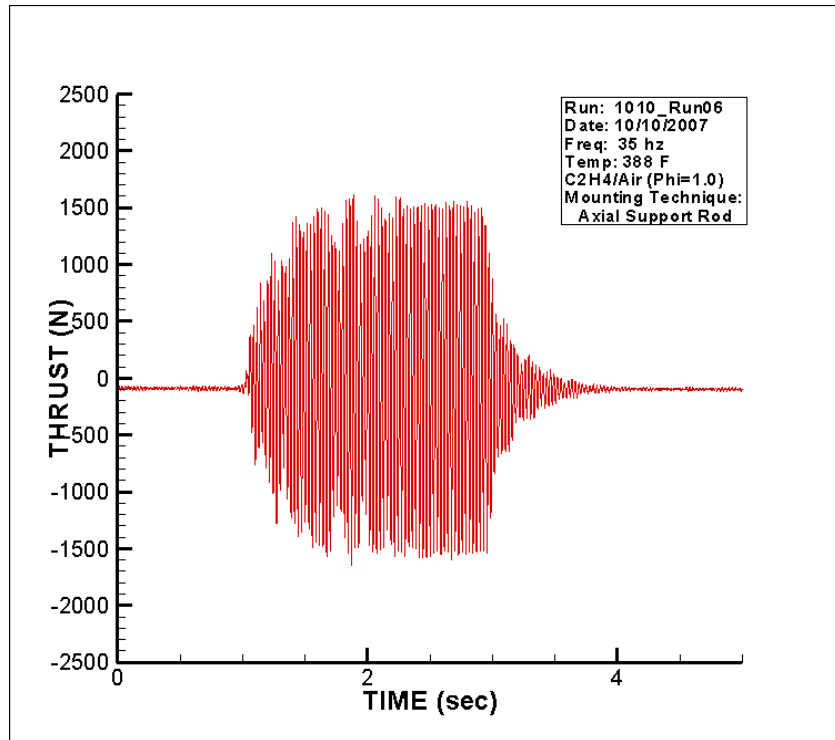
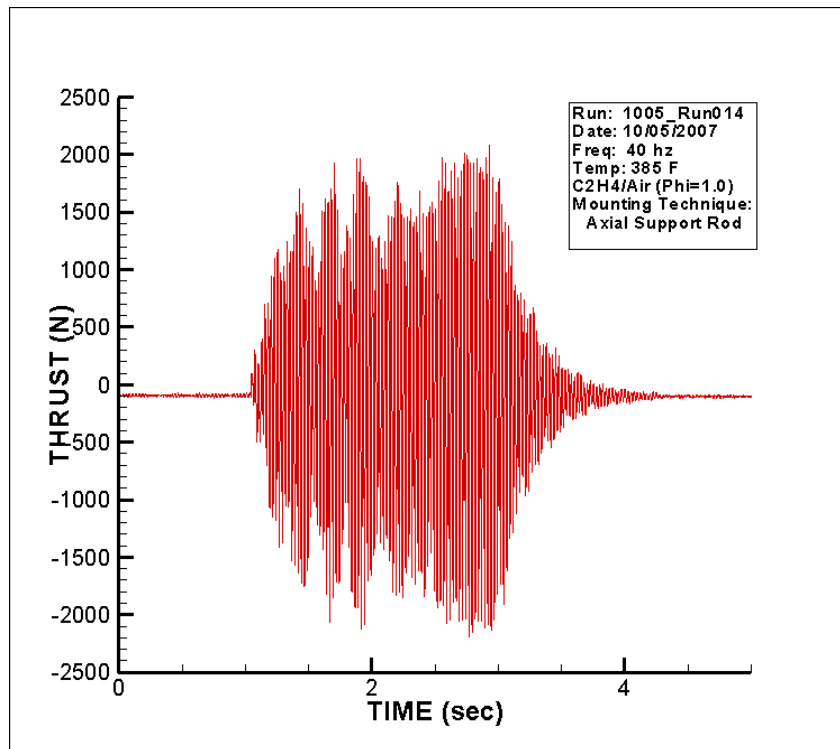Figure 27.   35 Hz Raw Data (Abs. Unc. +/-0.452%)
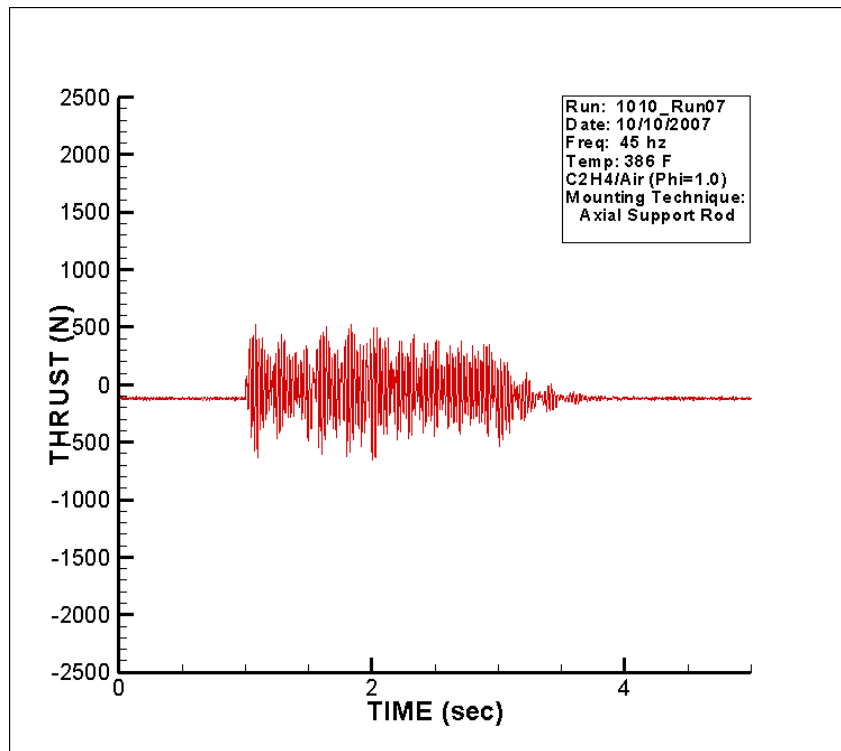

Figure 28.   40 Hz Raw Data (Abs. Unc. +/-0.452%)

50
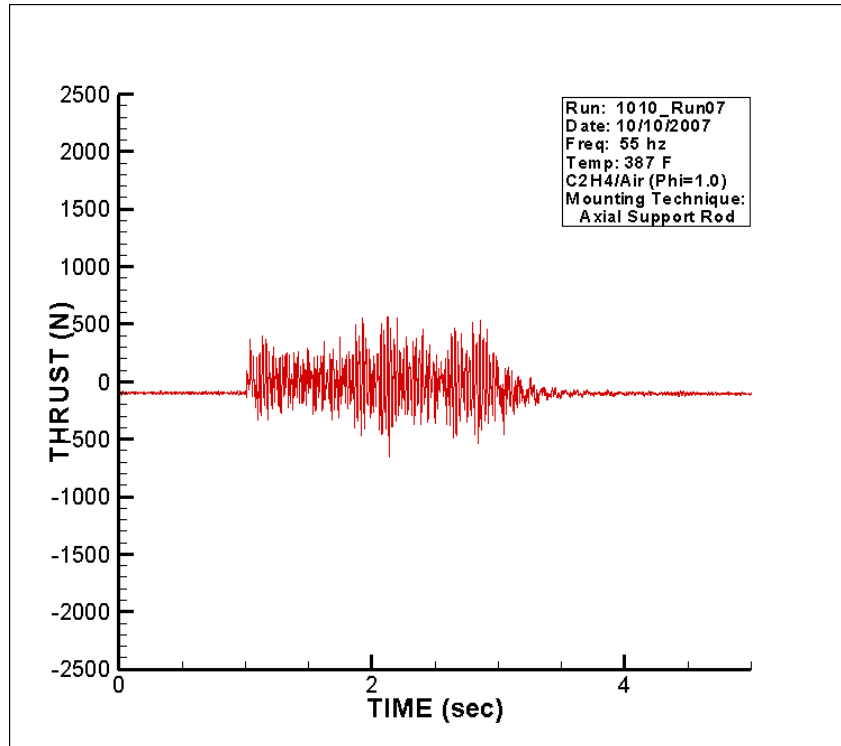
Figure 29.   45 Hz Raw Data (Abs. Unc. +/-0.452%)

Figure 30.   55 Hz Raw Data (Abs. Unc. +/-0.452%)

The first step taken to extract actual engine thrust from the raw data was to isolate natural frequencies of the TMS. Each of the data sets listed above were subjected to a Fast Fourier Transform (FFT) algorithm contained in MATLAB. This process converted the time response data shown in Figures 25-30 into frequency response data. This new data was further subjected to a Power Spectral Density (PSD) algorithm, which plotted energy within the data set versus frequency. It was expected that the natural frequencies of the thrust stand would produce the most energetic responses. Figures 31-34 illustrate the results of the experimental firings presented in the frequency domain. Analysis of data taken from the five test runs shows common, intense frequency responses in the 35-40Hz range. Additional less energetic responses were found in the 11-13Hz range for all five runs. Important to note, the only apparent differences in frequency response between these runs was the appearance of a low-energy response at the specific operational firing frequency of the engine for each individual firing event, and a more energetic response at 40 Hz when the engine was operated at 20 Hz (sub-harmonic) or 40 Hz (harmonic).
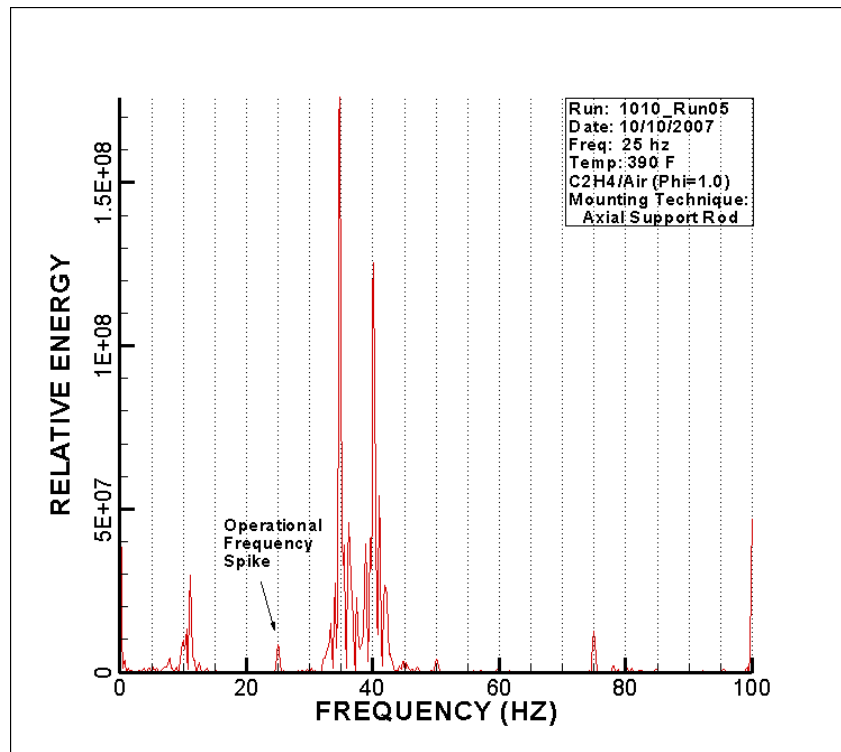

Figure 31.   Power Spectral Density (25 Hz)
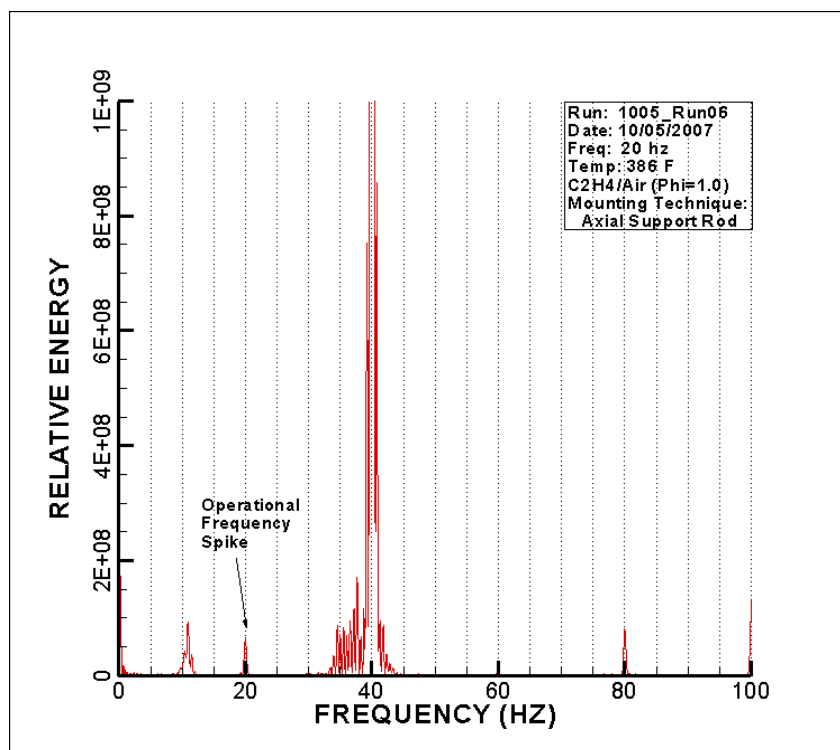
Figure 32.   Power Spectral Density (20 Hz)
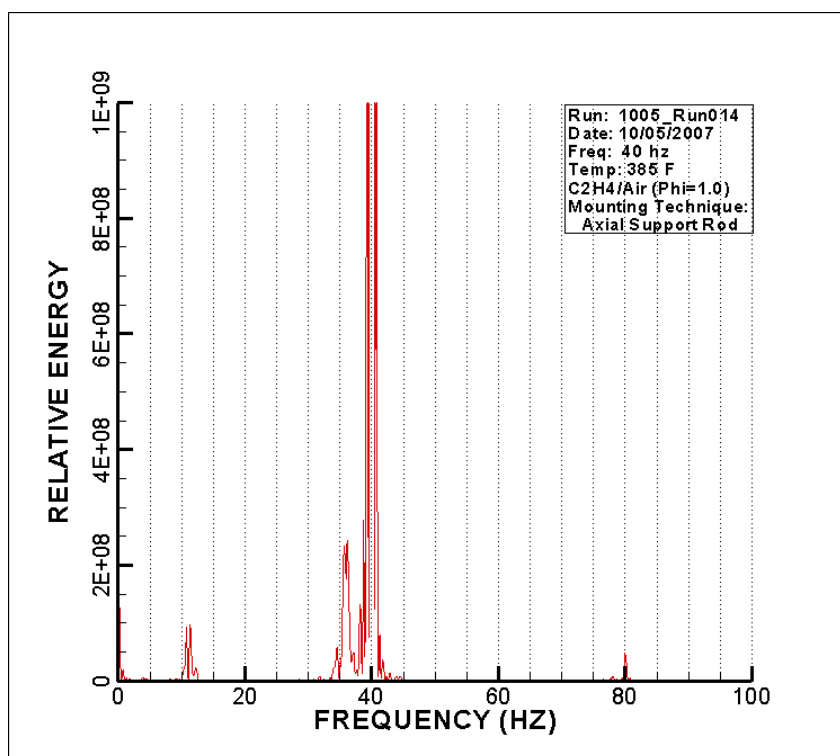
Figure 33.   Power Spectral Density (40 Hz)

53

Additionally, a single-combustion event experiment was conducted in order to apply an impulse to the stand to obtain a free response frequency sweep of the TMS. Figure 34 shows the free response exhibited virtually identical results to those found in the operational runs. In total, this data implied that the thrust stand may significantly amplify the response of forces input near the 40Hz range and to a lesser magnitude at several additional frequencies.
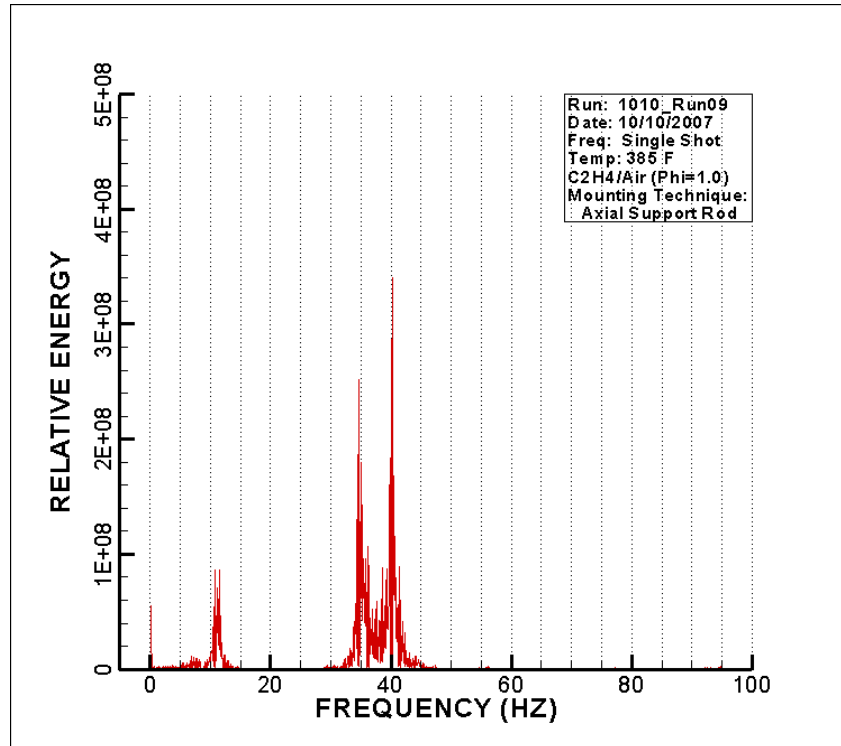
Figure 34.   Power Spectral Density (Single Detonation)

B.   DATA EXTRACTION

Raw data from the experimental runs listed above displayed a largely sinusoidal output. Actual thrust profiles from a nominal PDE should display a series of impulse thrust spikes of positive forces at the operational frequency of the engine. An average thrust profile would then be obtained by integrating the area under the thrust curve. Although this stand was designed to measure constant thrust engines, the TMS manufacturer was contacted to inquire if data reduction techniques were currently

available for this stand when incorporating impulse-type engines. As this was the first such engine encountered by the contractor, raw data from several runs were provided to their engineering staff for analysis. Subsequently, teams from Force Measurement Systems and the NPS rocket laboratory independently designed filtering techniques to extract average thrust values from the raw data.

1.   Moving Time Average/ Notch Filter

Engineers from the manufacturer incorporated a quasi-filtering technique known as Moving Time Averaging (MTA). This method required manual data interpretation to identify the period of the prominent sinusoidal wave. The data set was averaged incrementally over the individual periods, and then saved as a new data set. The process was repeated several times after identifying the remaining sine waves within the 'filtered' data set. Figures 35-36 show average thrust data for 20Hz and 40Hz runs after being filtered three times using the MTA technique.
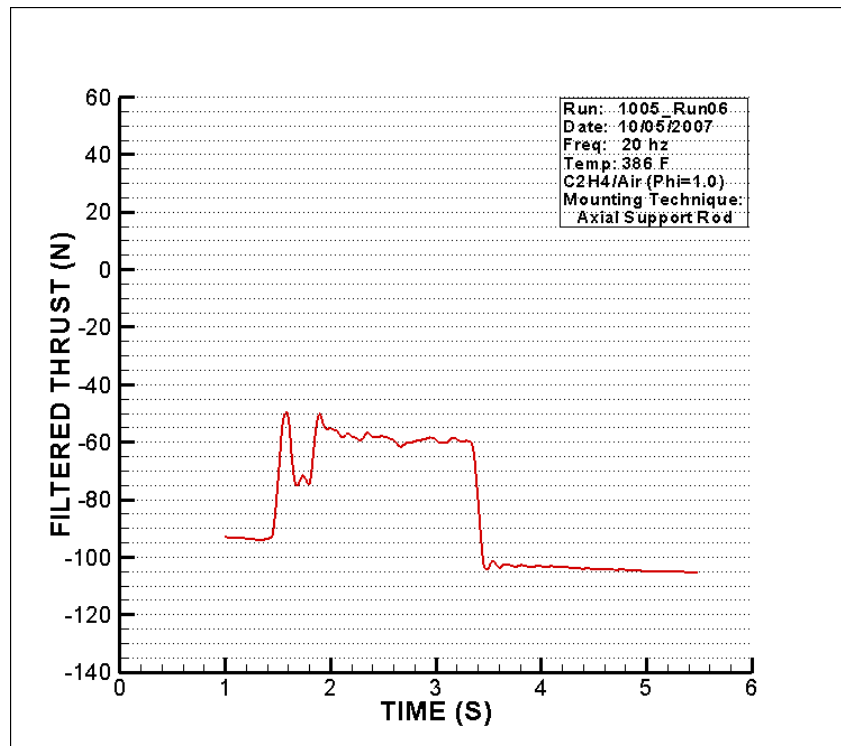
Figure 35.   MTA Filtered 20 Hz Average Thrust (Abs. Unc. +/-0.452%)
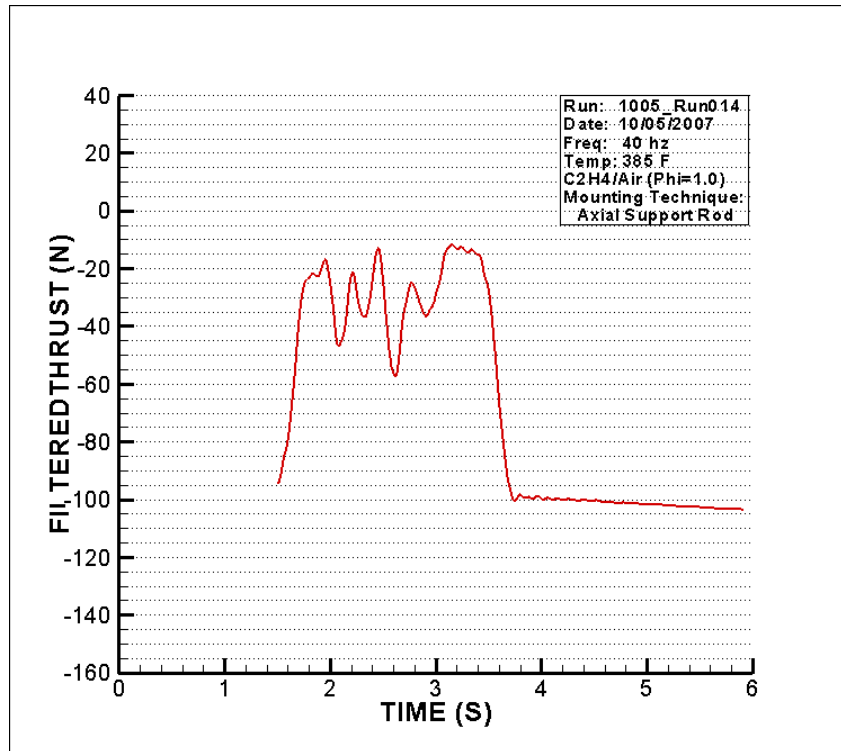
Figure 36.   MTA Filtered 40 Hz Average Thrust (Abs. Unc. +/-0.452%)

The theory behind this technique mirrored that of a notch filter. Averaging data over specific periods eliminated the resonant effects of the associated frequency, leaving only the thrust component in the data. Not surprisingly, the three periods (frequencies) filtered by the contractors closely matched the three most energetic frequency responses identified by the PSD analysis (not provided to the contractor). A specific advantage of MTA was the capability to mould data output near the end points of the firing runs based on expected curve shape, increasing validity of the computed thrust values over the ranges near the end points.

The capability of this system to provide customized data manipulation also led to the major disadvantage of incorporating this technique. MTA could not be completed using a traditional filtering method and required significant operator data interpretation and manipulation to first identify the major sinusoidal data reaction periods, then apply averaging algorithms until a thrust solution could be extracted. While thrust data computed with MTA appeared quite consistent with expected results and was tentatively considered a successful method for data extraction, the excessive data manipulation

required by the operator to compute a final average thrust profile made this technique cumbersome, and led to continued research for other more user-friendly techniques.

The same data set used for MTA analysis was also subjected to notch filters using Labview software, and produced almost identical results. The three major response frequencies were identified using a PSD profile, and applied to filtering software. As with MTA, prior knowledge of response frequencies (periods) was required which increased complexity of the data extraction process. While proving to be an accurate method of thrust data extraction, incorporation of a notch filter was not selected for the same reason as the MTA technique as the primary choice of thrust data reduction techniques.

2. Lowpass Filter

Once a successful data reduction technique was identified, the goal became to create another which required little or no user data interpretation or manipulation. By studying the PSD graphs created for each firing run, it became apparent that TMS consistently responded at frequencies in the ranges of 11-13Hz, 35-40Hz, as well as the operational firing frequency. Additionally, a DC component of data was identified on each graph by a spike at the 0Hz position (Figures 31-34.) Based on graph interpretation, the most logical choice was to incorporate a lowpass filter with a minimum cutoff frequency between the DC data frequency and the lowest consistent TMS response frequency of 11-13Hz. A lowpass filtering algorithm provided in Labview was manipulated to receive raw data from firing runs, and minimum cutoff frequency and data smoothing order values were varied to identify the optimum filter profile. Utilizing a 4Hz minimum cutoff frequency and 5th order smoothing value, data extraction graphs almost mirrored those produced by MTA techniques. Figure 37 shows the lowpass filtered average thrust data for the 20Hz firing run.
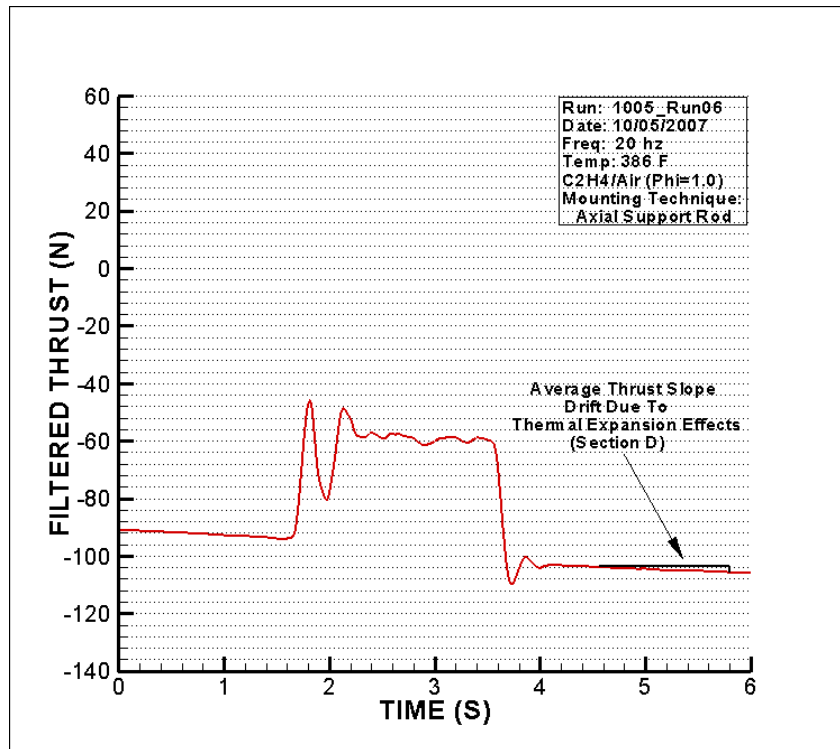
Figure 37.   Filtered 20 Hz Average Thrust (Abs. Unc. +/-0.452%)

The notable differences between the two techniques were at the endpoints of the thrust data curves. The MTA technique provided a more accurate shape of the data curve at the transition zones between engine firing and not firing. This was a direct result of operator manipulation by applying expected thrust profile reaction near these points. While accuracy was higher at these end points, operator action and data manipulation was required. Conversely, the lowpass filter returned a more sinusoidal response at the endpoints. These results are a less accurate representation of the true thrust profile of a firing run in these specific regions. This inaccurate projection results from the 5th order smoothing value applied to the system. Without user manipulation of the filtering technique, the lowpass filter required approximately 0.5 seconds for the oscillatory responses to settle and present an accurate thrust profile. After the settling period, the thrust profile of both systems converged to near-identical values.

Theory predicts that as firing frequency increases, average thrust output will increase as well. Raw data from the various runs did not support this expectation, as maximum thrust values did not trend with frequency changes. Additional verification

58

that the lowpass filter data reduction system was suitable for PDE performance measurement was obtained with analysis of the six filtered plots produced from the runs plotted above. Although raw data maximum values appeared more affected by TMS natural frequency responses than firing rates, the filtered responses all trended higher as firing frequencies increased, as theory predicted. Figures 38-42 show the filtered average thrust output of the remaining runs documented in Section A above.
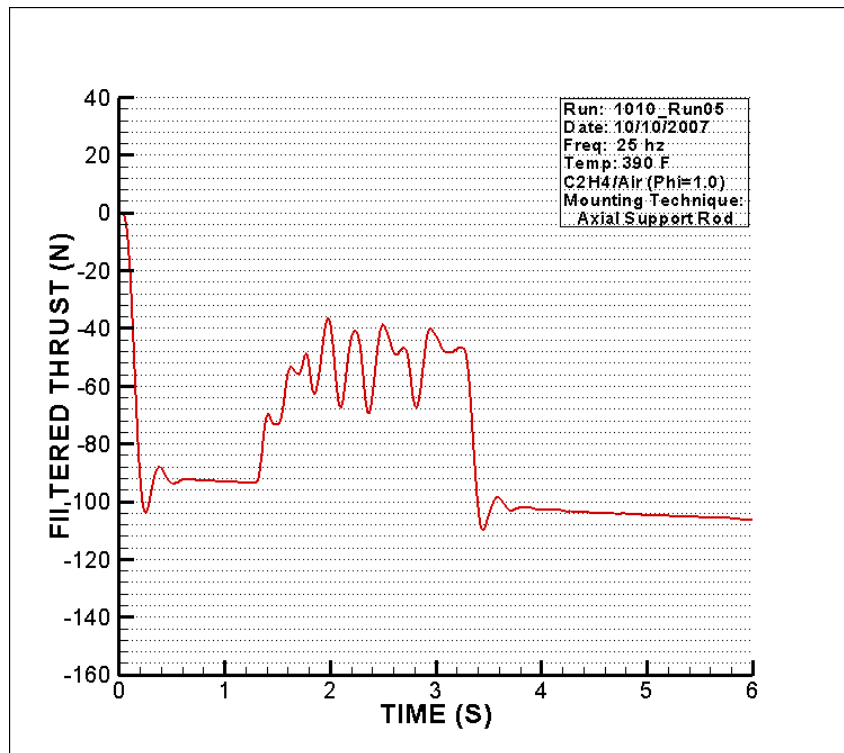

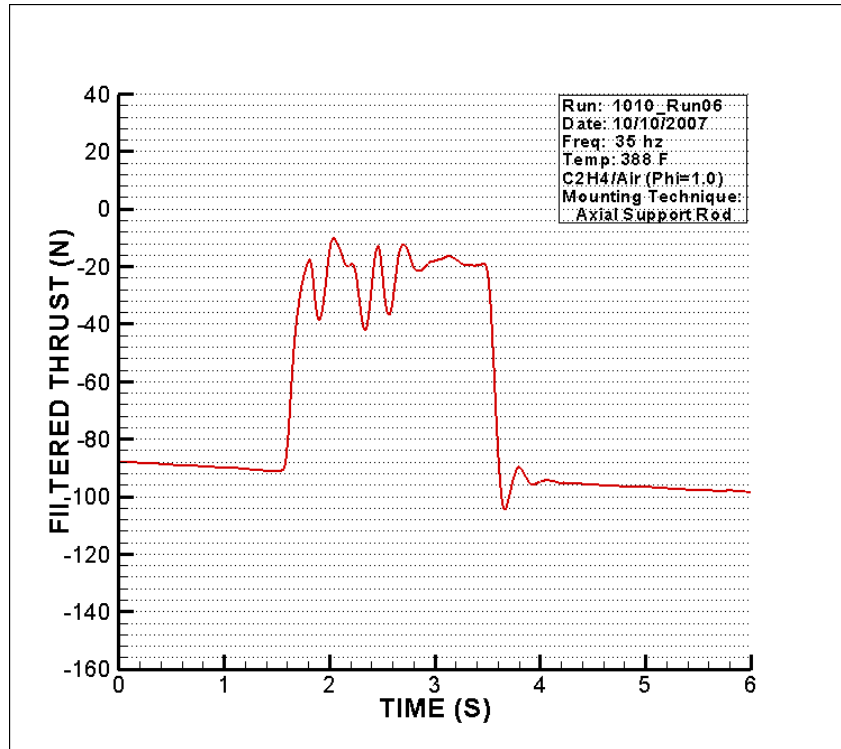Figure 38.　　　Filtered 25 Hz Average Thrust (Abs. Unc. +/-0.452%)

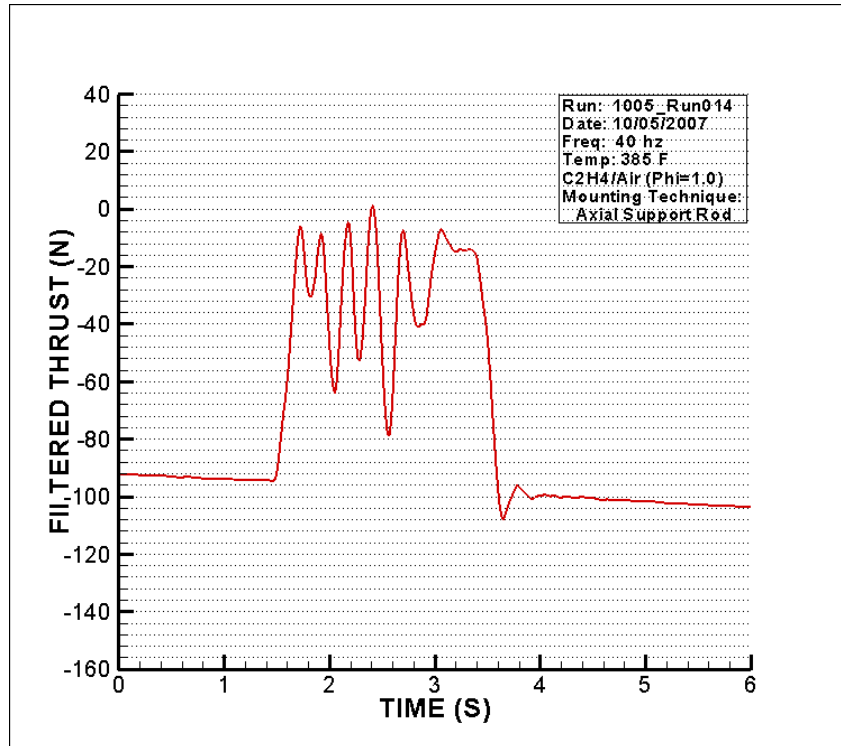Figure 39. Filtered 35 Hz Average Thrust (Abs. Unc. +/-0.452%)

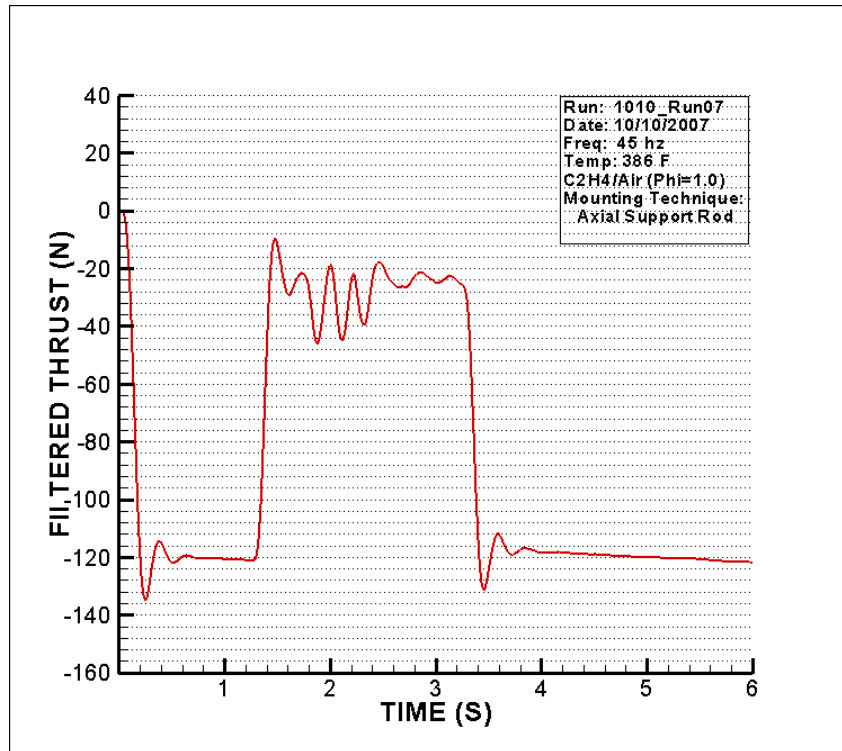Figure 40. Filtered 40 Hz Average Thrust (Abs. Unc. +/-0.452%)

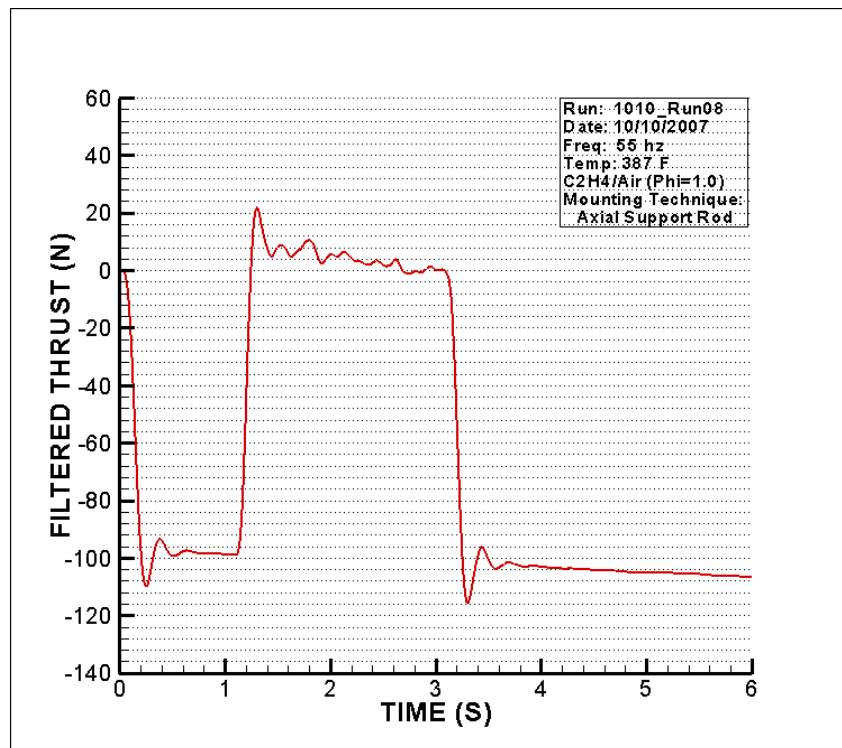Figure 41. Filtered 45 Hz Average Thrust (Abs. Unc. +/-0.452%)

Figure 42. Filtered 55 Hz Average Thrust (Abs. Unc. +/-0.452%)

61

Analysis of the lowpass filter system showed that it was effective in achieving all desired performance criteria for a thrust data extraction technique for this TMS. First, while it was not as accurate at the endpoints as MTA, the true thrust data profile for the majority of a firing experiment could be accurately obtained. All experimental firing runs utilized two second detonation bursts, which provided sufficient data for the lowpass filter to dampen the oscillatory responses and converge to the average thrust value. Functional operation of a PDE will require combustion events on a more continuous operating mode similar to a turbojet of ramjet engine. As longer experimental runs are conducted, the inaccuracies at the end points become even less relevant. More importantly, no manual data manipulation was required to achieve average thrust values. Raw data was subjected to the filter system, which returned the true thrust data into a spreadsheet for simple analysis. Most importantly, near real-time feedback of engine system performance could be obtained. A Labview VI can be constructed to filter real-time raw data from experimental firing runs and display filtered results in graphical form on the engine control GUI.

3.   Signal Simulator

Verification of intended operation of the lowpass filter system was completed by applying a known signal to the filter and analyzing the filtered response. A simulated signal was generated with the Labview Wave Generation function by convolving a 40Hz, 10Hz and 1Hz (20% duty cycle) wave, to simulate the known system responses of the TMS when subjected to a two second detonation event. The 1Hz signal and 10Hz signal were relatively low 220 N amplitude inputs, designed to be buried within the larger amplitude responses of the higher frequency waves. The 40Hz wave incorporated a 660 N amplitude response and the convolved waveform closely resembled the raw data collected from experimental firing events (Figure 43.)
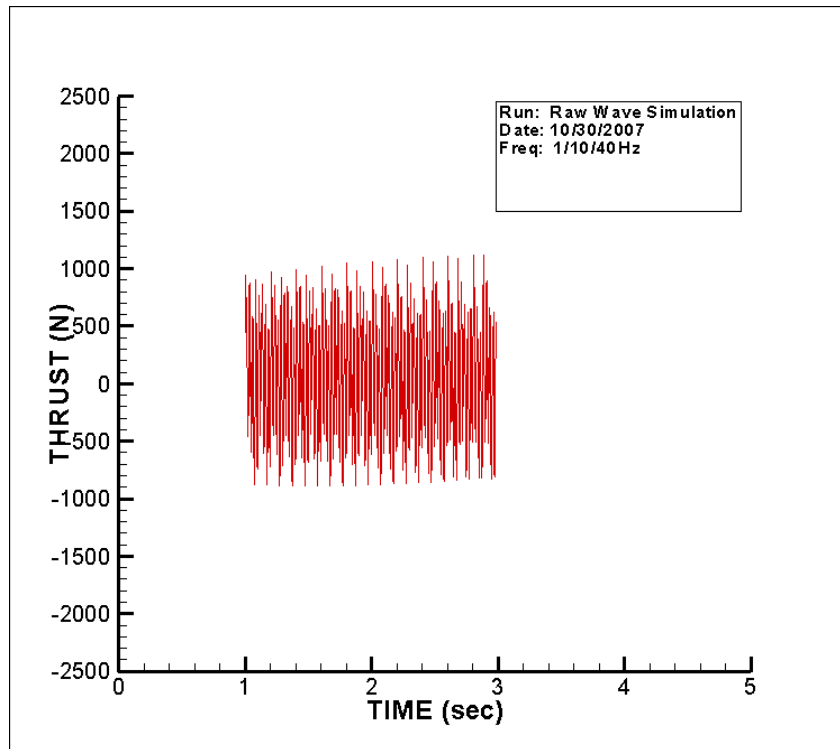
Figure 43.   Simulated Three Frequency Wave Raw Data

Figure 44 shows the lowpass filtered response of the simulated signal when using the same 4Hz minimum cutoff frequency and 5th order smoothing value. As can be seen, the filtered data shows approximately a 0.5 second interval required to achieve a near steady-state average value, and converges plus or minus two Newton to an expected average value of 44 N. This simulation partially verified the lowpass filter functioned as intended and provided validation that this method could successfully extract low frequency data from high frequency noise introduced by the TMS.
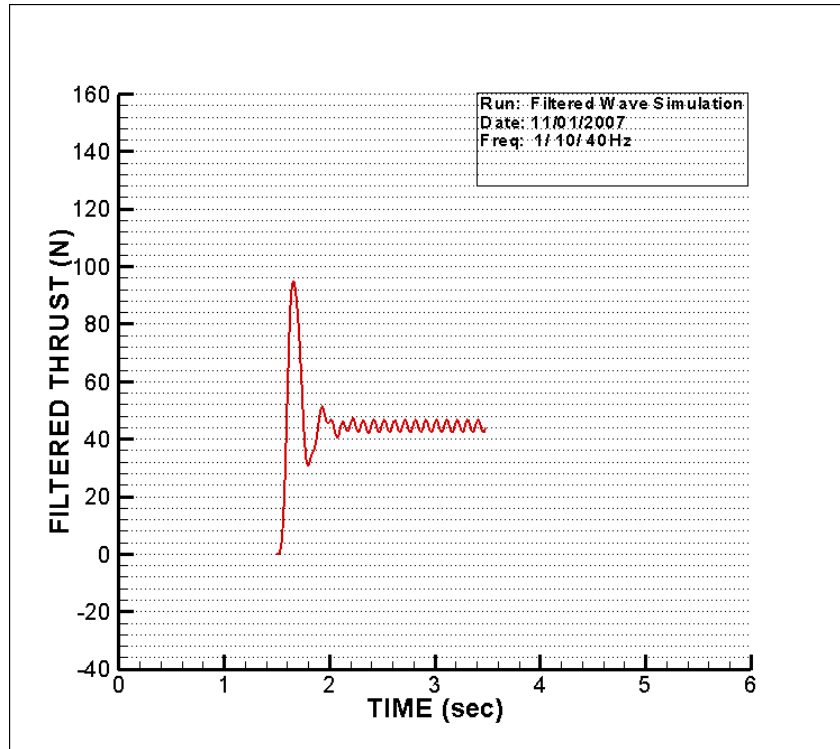
Figure 44.   Filtered Simulated Wave

4.   Data Accuracy

Data accuracy for the TMS/lowpass filter system described above was computed using the root mean square function. The two major sources of error were introduced by the data acquisition hardware (NI DAQ) and calibration/strain gauge fidelity of the TMS. National Instruments lists on their website detailed accuracy analysis of all supported DAQ equipment. For the hardware installed on this rig, the company cites offset, system noise and temperature drift as the predominant error sources, and reports a system absolute accuracy of +/- 0.377%. The TMS Operations and Maintenance Manual [15] lists an absolute system data accuracy of +/- 0.250 %, citing non-linearity, hysteresis, and non-repeatability as the major sources of error. Combined, the absolute system accuracy was +/- 0.452%. This value was based on data not affected by the lowpass filtering process; therefore, the computed data accuracy is valid for both raw and filtered thrust data.

C.   ENGINE MOUNTING TECHNIQUES

Analysis of raw data from firing runs at a mass flow rate of 0.3125 kg/s showed an increased sensitivity in thrust response at the TMS harmonic and sub-harmonic frequencies of 40Hz and 20Hz, respectively. Raw data impulse measurements of 2,200 N were obtained during 40Hz experiments, while only 500-700 N were recorded at non-harmonic operational frequencies. Peak impulse thrust values for each experimental operational frequency should theoretically be very similar, thus, the TMS experienced significantly larger force responses at selected frequencies due to resonance effects. Although the thrust stand in the axial direction is rated for 2,225 N (500 lbf), the two flexures in the thrust stand in the axial direction which combine to share the axial load are rated for 1,335 N (300 lbf) each, which provides a rating of 2,670 N (600 lbf) with no factor of safety. Testing conducted produced forces which matched the maximum thrust stand rating and were within 14% of predicted failure values. Additionally, the flexures do not share the loads evenly; thus, one flexure likely came closer to failure than the 14% listed above. At 40Hz and the current mass flow rate, average detonation thrust is approximately a relatively low 100 N (22 lbf). It was surprising to find that such a low average thrust would produce a response so close to the maximum ratings of the TMS. Based on experimental data, in this configuration the stand will not provide sufficient strength to support experimental detonations in this frequency range with higher mass flow rates. The test rig used for this thesis will eventually target PDE operations with a mass flow rate of 1.25 kg/s; thus, the engine/TMS in its original configuration would be unacceptable for future intended uses.

It was suspected that the method in which the engine was mounted to the TMS resulted in the high force sensitivity at 40 Hz. As described in Section III-B, the TMS was originally designed to support engines by incorporating two vertical mounts attached directly to the horizontal base plate. To provide additional structural rigidity, the forward vertical support plate was added to the TMS and a third engine support rod added in the axial direction. A series of experimental test firings were conducted to isolate the various response frequencies associated with different mounting techniques.   Tests were conducted first using single detonation events, followed by 40 Hz runs up to 2 seconds

with the engine mounted first in its current configuration, then without the axial support rod, and finally with the axial support rod replaced with a spring assembly. Figure 45 shows the original mounting configuration which included the axial support rod. Figure 46 illustrates the mounting technique which had the axial support rod removed. Note, the engine/slide rail assembly was clamped to the fixed base to prevent all axial engine motion. The spring assembly is not presented, and was inserted into the original mounting configuration in place of the axial rod.
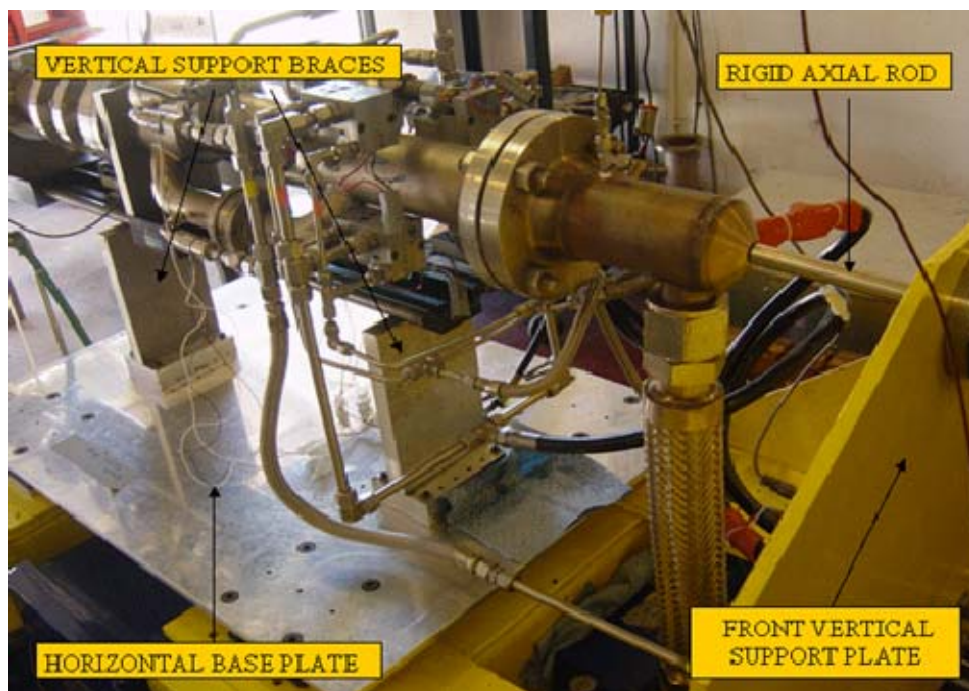
Figure 45.   Axial Support Rod Mounting Configuration
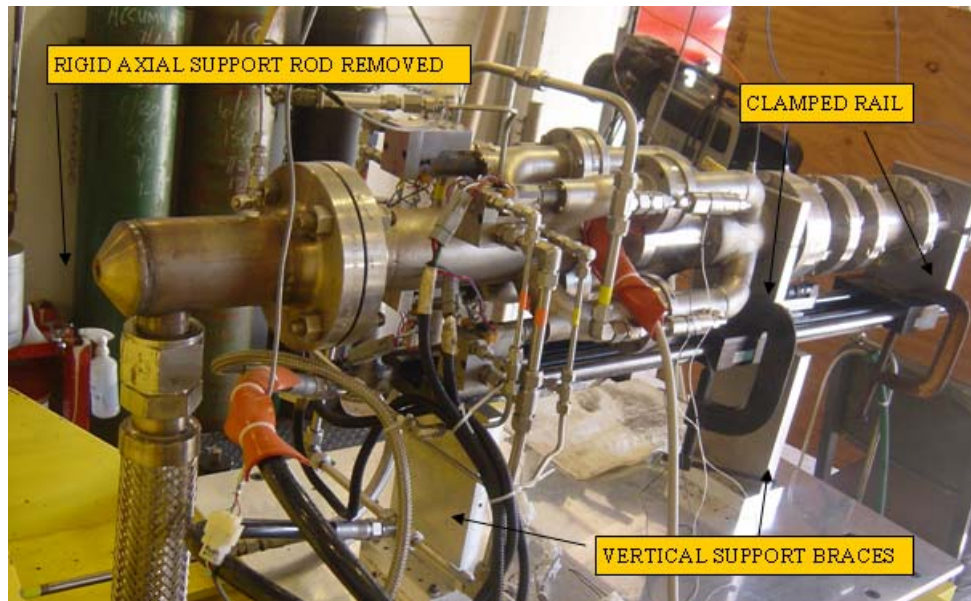
Figure 46.   Clamped Rail / Axial Support Rod Removed

1.   Single Shot Experiment

All three engine mounting configurations were subjected to single detonation events. Figures 47-49 show the raw data and Figures 50-51 illustrate the respective PSD plots for two methods. The most obvious result was the significantly larger magnitude of the raw data response measured in the current configuration. Both spring assembly and no-rod configurations showed force responses 40-60% less than that of the three point support method. This result in itself was not conclusive, as no truth data confirming detonations occurred for each event was available; however, it did indicate further inspection was warranted.
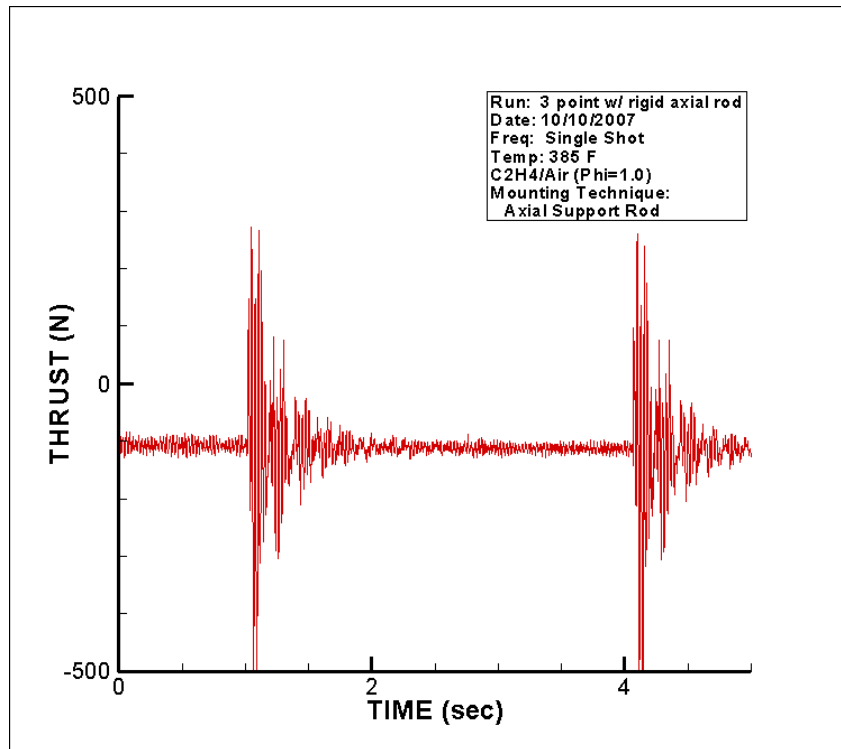
Figure 47. Raw Data With Axial Rod (Abs. Unc. +/-0.452%)
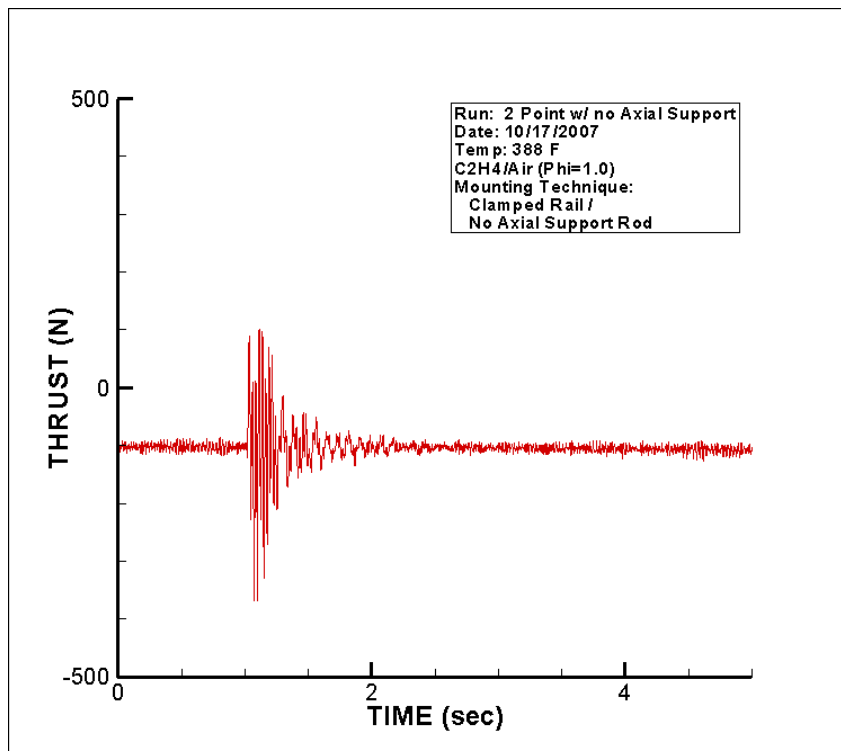
Figure 48. Raw Data Without Axial Rod (Abs. Unc. +/-0.452%)
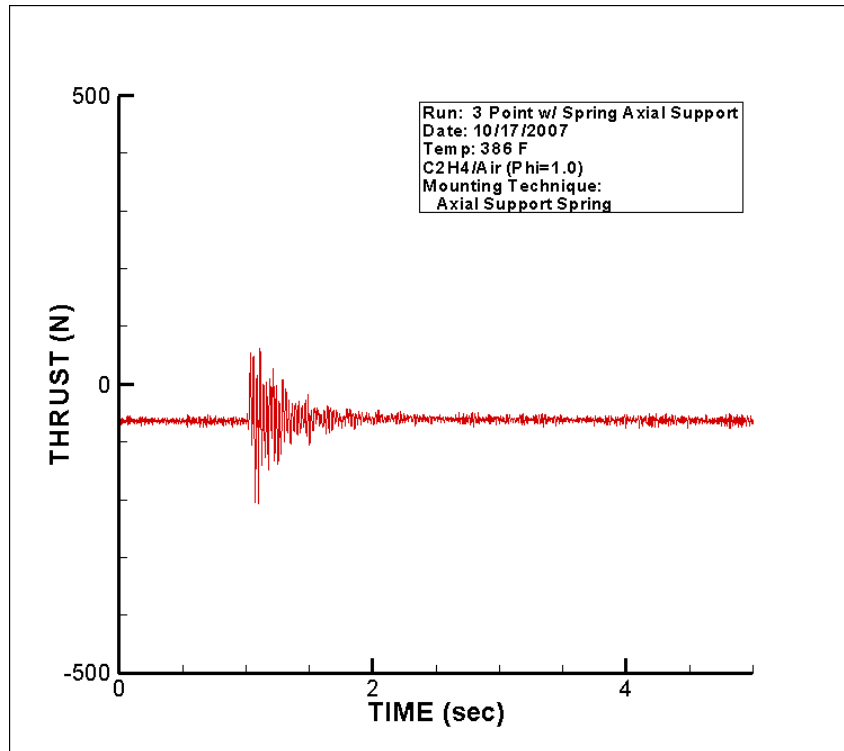
Figure 49.   Raw Data With Axial Spring Support (Abs. Unc. +/-0.452%)

Next, the PSD plots of two support methods were compared for the relative strength of response at each frequency. Most interestingly, the no-rod configuration contained most of the response energy in the DC (0Hz) range, while the original configuration focused most in the 40Hz range. The spring-mounted assembly was not analyzed further as it was deemed less suitable for this rig than the other two support methods. Analysis of both sets of figures suggested that during multi-shot experimentation, the no-rod configuration would not experience severe force amplification on the scale of the current configuration, and may provide an acceptable system response which will enable testing at higher mass flow rates. Preliminary results indicated continuous detonation experimentation was warranted.
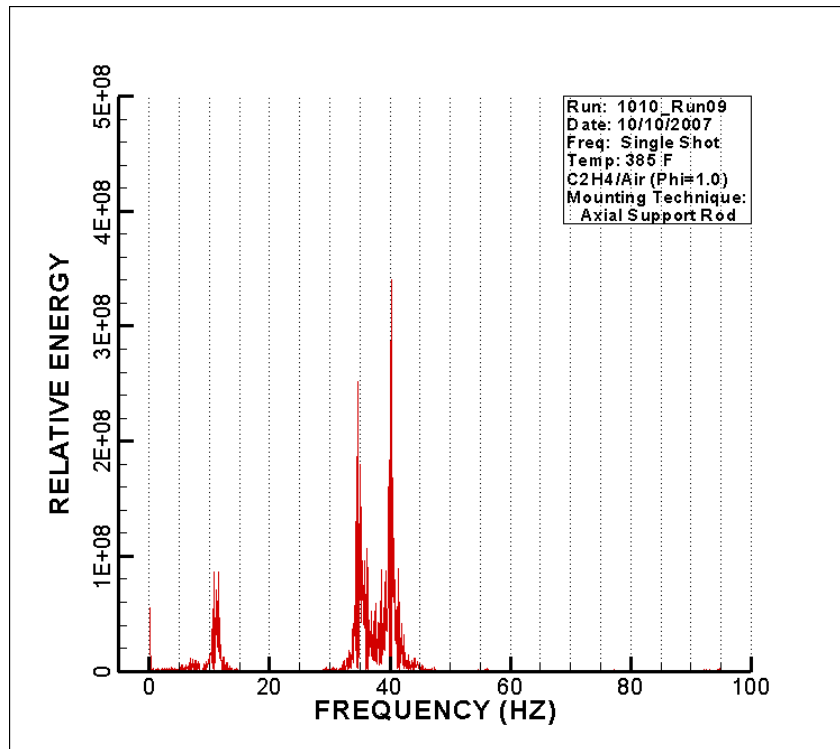
Figure 50.   Power Spectral Density With Axial Support Rod
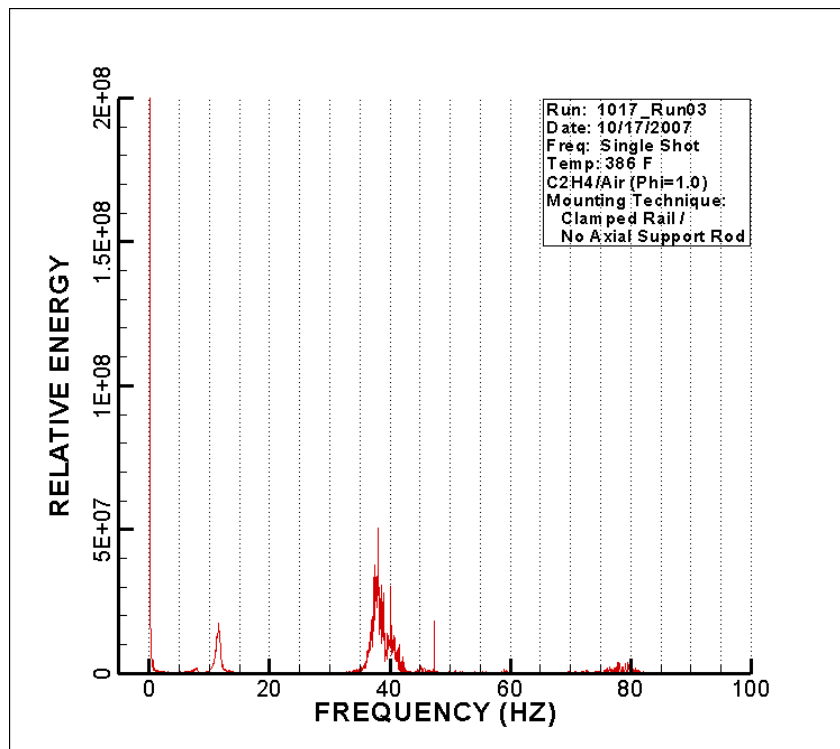
Figure 51.   Power Spectral Density Without Axial Rod

70

2.   Multi-Cycle Detonation Experiment

Dedicated detonation experiments were performed to document the variation in TMS response based on engine support method. Two-second firing runs were conducted at the maximum system response frequency of 40 Hz, one with the axial support rod installed and one without. Prior to the experiment, a diffuser cage was installed into the combustion chamber of the engine to support experimentation for separate thesis research. The overall effect of this cage on average thrust was not known; however, as the two firing runs were conducted for direct comparison, it was determined that this change to the engine would not invalidate the comparison. Several preliminary firing runs were conducted to establish optimal fuel parameters for the 0.3125 kg/s runs. Prior to thrust analysis, it was determined that both runs resulted in very similar, solid combustion events and would be suitable for comparison. Figures 52-53 show the raw data collected for each firing run.
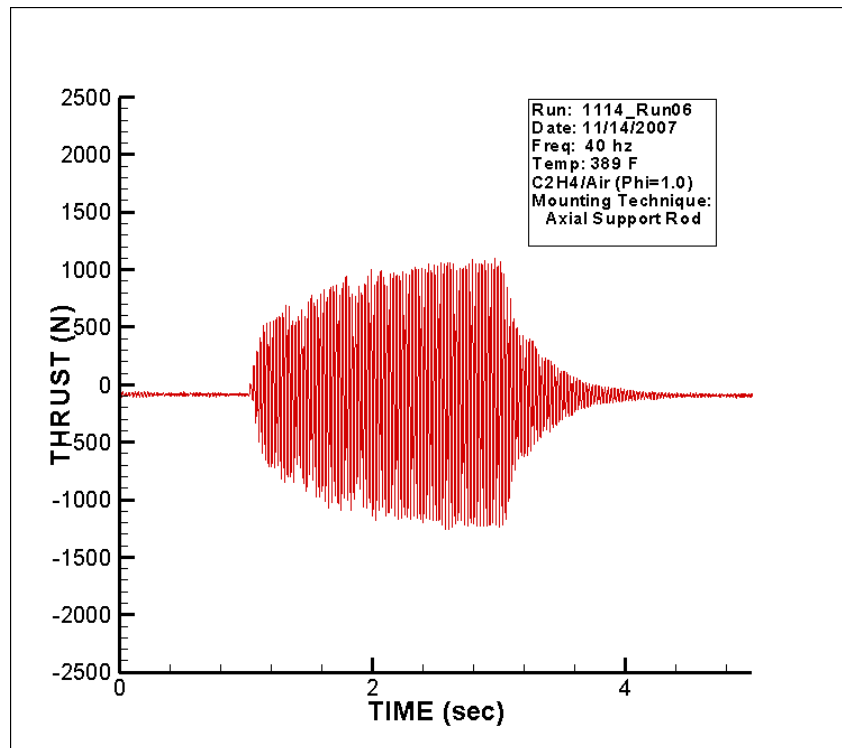
Figure 52.   Raw Data With Axial Support Rod (Abs. Unc. +/-0.452%)
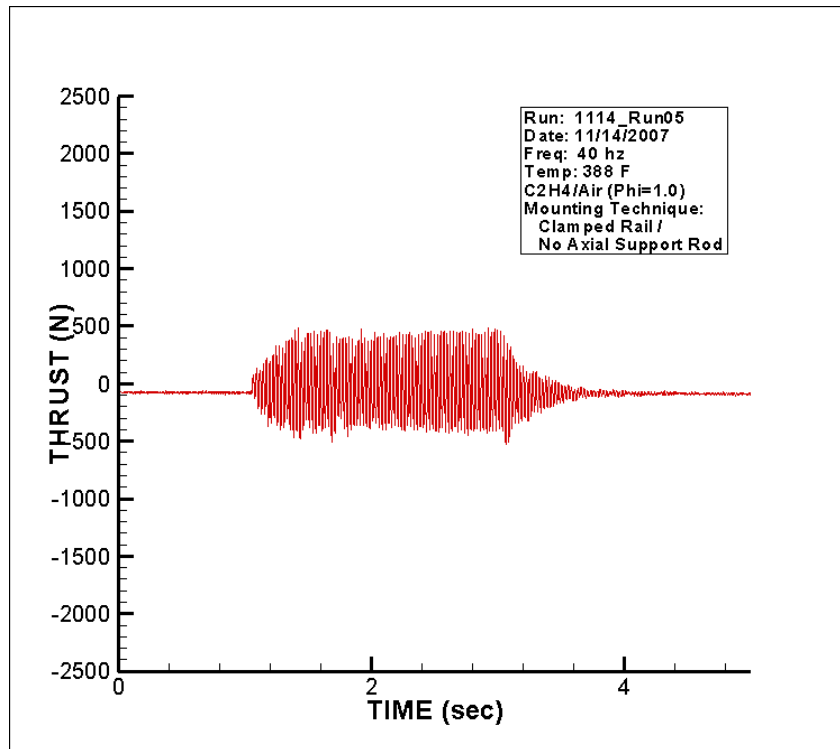
Figure 53.   Raw Data Without Axial Support Rod (Abs. Unc. +/-0.452%)

As with the single shot experimental runs conducted above, the TMS responded with a much higher indicated force output for the axial rod mounting technique than without. The axial rod being installed led to a maximum force response of approximately 1300 N, while the run with it removed resulted in a maximum force response of only 500 N. This experiment indicated that at the TMS maximum response frequency, incorporating a simpler engine support design reduced the force experienced by the TMS by approximately 62%.
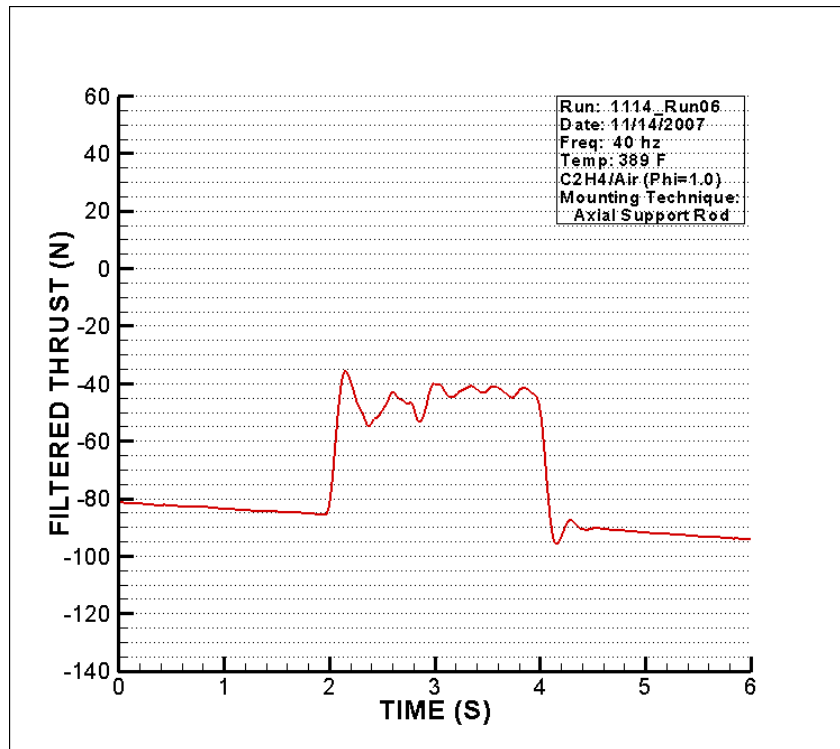
Figure 54.   Filtered Average Thrust W/ Axial Support Rod (Abs. Unc. +/-0.452%)
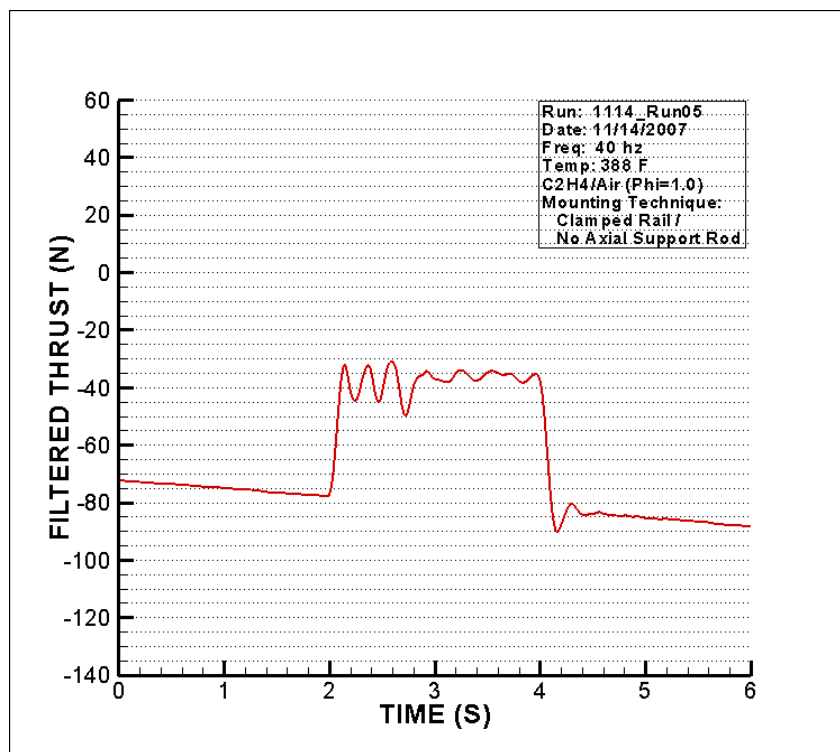
Figure 55.   Filtered Average Thrust W/O Axial Support Rod (Abs. Unc. +/-0.452%)

Figures 54-55 show the filtered average thrust response of both firing runs. Although the raw data was quite different, the average thrust profiles of both runs were very similar, with average thrust values within +/- 2 N. The similarities of the two profiles indicate that the filtering algorithm was capable of returning accurate thrust profiles for both engine mounting techniques. As a result, the incorporation of an engine mounting technique which does not include a rigid axial support rod will enable testing to be conducted at much higher thrust values at all operational frequencies attainable by the PDE evaluated. Still, thrust stand axial load limitations will most likely be a factor as mass flow rates increase. As higher mass flow rate conditions are evaluated, raw data should be monitored to ensure the trend identified in this thesis continues to hold.

D.   EFFECTS OF MAIN SUPPLY AIR ON THRUST

Prior to commencing a detonation sequence, vitiated air was supplied to the engine at the mass flow rates listed above to achieve a particular temperature. The engine has no openings other than at the exhaust end of the combustion tube; thus, approximately 40-60 N of positive momentum thrust was expected to be produced as the heated main supply air was delivered to the engine. Experimental data for all recorded firing runs showed an unexpected and repeatable result. As the heated main supply air was introduced into the engine, the TMS immediately measured an approximate 60 N **negative** thrust value, which slowly and steadily increased in magnitude throughout each run until the vitiator stopped delivering heated air into the engine main air supply system. Initially, it was suspected that the two load cells responsible for axial thrust monitoring were either inadvertently mislabeled or signs in the load calculation equations were reversed. A review of the techniques used to calibrate the TMS showed the load cells were correctly identified and a simple experiment confirmed the proper sense and functionality of the axial component within the TMS. Next, a dedicated extended vitiator-only run was conducted to allow the engine to receive heated air for 40 seconds, and then continue to receive non-heated main air for an additional 80 seconds. The results of the experiment are included in Figure 56.

74
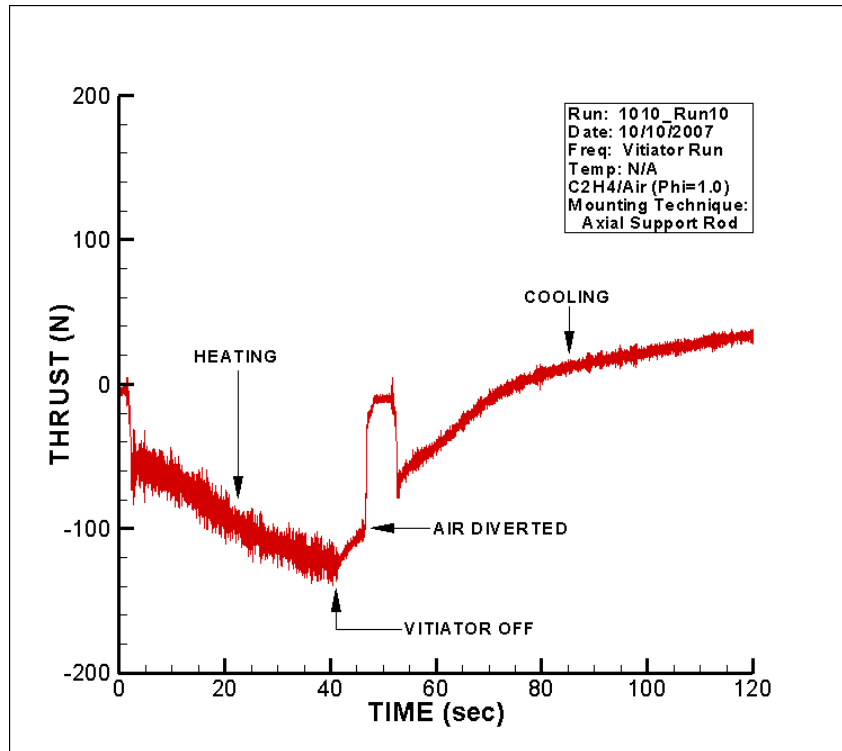
Figure 56.   Extended Vitiator Run (Abs. Unc. +/-0.452%)

The data shows the characteristic immediate 60 N negative thrust component, followed by the gradual increase in magnitude until the vitiator timed out (40 seconds). At this time, the thrust value began to decrease at a moderate rate and eventually became a positive value which then continued to slowly increase and plateau at a value of approximately positive 40 N. The sudden decrease in negative thrust several seconds after the vitiator timed out was the result of main supply air automatically being diverted away from the engine (normal operating procedure), and was then manually redirected back into the engine which produced the subsequent negative thrust increase.

Analysis of the plot shown in Figure 56 led the research team to conclude that the negative thrust component was the result of thermal expansion within the flexible aluminum main air supply tube which was mounted directly to and extended vertically below the front end of the engine (Figure 45). It was discovered that all data runs had been precluded by vitiator-only runs to "preheat" supply tubing and engine components, which allowed for shorter time intervals to achieve desired firing temperatures for the

75

subsequent detonation events. The combination of very hot metal and high pressure supply air resulted in thermal expansion and an increased stiffness within the flexible delivery tube which produced the immediate negative thrust value measured at the onset of each run. As the vitiator run continued, internal temperature continued to steadily increase, which produced a slow rise in the indicated thrust until the vitiator timed out. The main air system then continued to supply relatively cold air into the tube and engine, and rapidly cooled the surrounding metal, gradually removing the loads caused by thermal expansion. As cooling continued, the negative thrust values decreased and eventually became positive. After a significant cooling period, thrust values for the non-heated supply air approached positive values similar with those expected from momentum thrust. With the negative thrust phenomenon understood, the value can be subtracted from the computed average thrust profile with no adverse effect on data accuracy.

V.   SUMMARY/CONCLUSIONS

Research showed thrust measurements of a Pulse Detonation Engine could be measured utilizing the Thrust Measurement System installed at the Naval Postgraduate School Rocket Laboratory. The thrust stand was calibrated for the no-load configuration with the assistance of the manufacturer, and then recalibrated by the test team with the engine installed and supporting equipment attached. Programming logic was written to import thrust data and incorporated into the main engine control program to allow real-time monitoring from the control room. Testing produced largely sinusoidal force responses, which indicated resonance properties of the thrust stand were coupling into the desired thrust responses. Power Spectral Density analysis highlighted a strong, harmonic frequency at 40 Hz, and lesser reactions at 11-13 Hz as well as the engine operational firing frequency. A lowpass filter which filtered frequencies above four Hz was applied to the data sets and found to effectively eliminate unwanted resonance effects, while returning an accurate average thrust profile.

Testing also indicated sensitivity to the mounting technique used to secure the engine to the thrust stand. Experimentation at 40 Hz produced uncharacteristically large force responses from the stand, and identified a potential to overstress force measuring hardware components. Single shot testing events were conducted with various engine-mounting configurations and again subjected to PSD analysis. A comparison between the original mounting configuration (vertical support braces and axial support rod) and an alternative method which fixed the engine to the slide rail and removed the axial support rod showed a shift of the major thrust stand response frequency from 40 Hz to the DC component at 0 Hz. Multi-cycle experimentation was then conducted utilizing the same two mounting configurations. The sensitivities found in the original configuration were not experienced with the new mounting technique. Force responses produced during 40 Hz testing were reduced by 60%, which indicated a new mounting technique will enable higher thrust testing with a much reduced potential for hardware overstress. Analysis of thrust profiles produced by filtering data from the two above scenarios showed almost

77

identical average thrust profiles, which provided an additional level of verification of the capability of the TMS to extract average thrust profile from a highly dynamic data set.

VI.   FUTURE WORK

Experimental testing was conducted using a precisely known axial fuel distribution profile to support desired performance calculations. This profile was used in conjunction with experimentally obtained thrust measurements, resulting in the capability to compute I_{sp} values with high fidelity. In retrospect, it was concluded that the fuel profiles utilized did not always represent the optimum stoichiometry for ideal engine operation, which resulted in uncertainty as to whether each firing run produced a solid series of detonations, or lesser thrust-generating deflagration events. In order to calculate the appropriate performance values, an alternative method must be incorporated to verify creation of detonation events prior to calculation of I_{sp} values.

Additionally, current production of average thrust data is cumbersome and requires multiple iterations of data manipulation by the operator. Raw data is first collected by the data acquisition system described in Chapter III and saved on a remote hard drive. It is next imported as an excel file, manually sent to the filtering VI, and exported again as an excel file. Only then can the data be viewed in graphical format. Fortunately, coding has been included in the overall engine control VI which reads raw thrust data on a real-time basis. Additionally, the filtering algorithm is embedded in a self-contained VI. With slight modification to the existing control VI, the filtering software could be incorporated and a filtered average thrust output graph added to the control GUI for near real-time thrust feedback. This capability would prove invaluable for experimentation requiring thrust information and would provide an additional method for detonation verification.

Finally, results indicate that incorporating an engine mounting architecture which provides no front axial support rod will drastically reduce TMS resonance responses and allow for much higher thrust levels at all operational frequencies. The configuration tested which produced these results incorporated a temporary solution, which initially found the engine mounted to a slide rail. The test configuration saw the slide rail clamped to the support structure to prevent slippage, but was not considered a permanent

solution. A new mounting method should be constructed and tested which achieves two objectives. First, the vertical support towers which currently support the slide rail should be redesigned and relocated to effectively provide sole support of the engine. Second, a support structure which eliminates the slide rail should be designed which allows for the engine to be mounted directly to the vertical support towers.

PULSE DETONATION ENGINE RUN SHEET

DATE: 5-Oct

MAIN AIR CHOKE: 0.235 H₂ CHOKE: ____ 0.035 MAKEUP O₂ CHOKE: ____ 0.052 TIMING (MSEC)

INITIAL VIT TEMP: ____   TORCH AIR / NODE#4: 220 PSI   700

RUN#	FREQ	MASS FLOW	NODE #1 MAIN AIR	NODE#20 VIT H₂	NODE#21 VIT O₂	NODE#22 FUEL	FUEL	IGNITION	DET TEMP	DET%	COMMENTS
4	20/40	0.3125	660	412	570	350	10	10			
5	20/40						10	9			
6	20/40						11	10			
7	20/40						13	12			
8	20/40						15	14			
9	20/40						17	16			
10	20/40						9	8			
11	20/40						7	7			
12	20/40						7	6			
13	30/60						11	10			
14	40/80						11	10			
15	50/100						11	10			
16	10/20						11	10			
17	20/40						10	9			

Figure 57.	05 October Experimental Run Sheet

DATE: 10-Oct

INITIAL VIT TEMP: 700
TORCH AIR / NODE#4: 220 PSI

MAIN AIR CHOKE: 0.235 H₂ CHOKE: 0.035 MAKEUP O₂ CHOKE: 0.052

RUN#	FREQ	MASS FLOW	NODE #1 MAIN AIR	NODE#20 VIT H₂	NODE#21 VIT O₂	NODE#22 FUEL	TIMING (MSEC) FUEL	IGNITION	DET TEMP	DET%	COMMENTS
1	15/15	0.3125	660	412	570	350	11	10			
2	15/30						11	10			
3	15/30						11	10			
4	15/30						11	10			
5	25/50						11	10			
6	35/70						11	10			
7	45/90						11	10			
8	55/110						11	10			single shot
9	20/1						16	15			vit run
10							16	15			

Figure 58.   10 October Experimental Run Sheet

PULSE DETONATION ENGINE RUN SHEET

DATE: 17-Oct

INITIAL VIT TEMP: 700

MAIN AIR CHOKE: 0.235 H₂ CHOKE: 0.035 MAKEUP O₂ CHOKE: 0.052

TORCH AIR / NODE#4: 220 PSI

MAIN AIR CHOKE: 0.235 H$_2$ CHOKE: 0.035 MAKEUP O$_2$ CHOKE:

RUN#	FREQ	MASS FLOW	NODE #1 MAIN AIR	NODE#20 VIT H$_2$	NODE#21 VIT O$_2$	NODE#22 FUEL	TIMING (MSEC) FUEL	IGNITION	DET TEMP	DET%	COMMENTS
1	20/1	0.3125	660	412	570	350	16	15			clamped rail/ axial rod 100hz
2	20/1						16	15			clamped rail/axial rod 1000hz
3	20/1						16	15			clamped rail/ no axial rod
4	20/1						16	15			spring only
	14-Nov										
5	40/80					400	11	10			clamped rail/ no axial rod
6	40/80					400	11	10			axial rod
7	30/60					400	11	10			axial rod

Figure 59.   17 October / 14 November Experimental Run Sheet

THIS PAGE INTENTIONALLY LEFT BLANK

APPENDIX B: PDE SOP

Test Cell #2
Standard Operating Procedures (S.O.P)
Engine Start UP
(last modification date 19 June 2007)

Prior to starting preparations
1. Notify all lab personnel of live test cell.
2. Turn ON control console
3. Turn ON warning lights
4. Notify the Golf Course (x2167, ext#1) (Only required if Hot Fire Test is conducted)

Preparing Test Cell
1. Push the Emergency Stop IN (secured)
2. Turn ON BNC Cabinet Power Strip.
3. On Control Computer, open LABVIEW and ensure that the execution target contains the PXI address. Open control panel and run the program.
    a. RT Target address: 172.20.120.118
    b. Control Program Path
        i. Open
        ii. Test Cell #2 Manual Control v20 (runs v19b)
        iii. Enter Run Path Name
            1. If this is not completed prior to running you will lose the data file that was created with the default name.
4. Turn ON 24 VDC in the control room cabinet
5. OPEN Main Air (HP Air Tank Valve) and High Pressure Air
    a. Blue hand valve should be opened slowly as not to shock the lines
    b. Node 4 air valve in test cell #1 open
6. OPEN H_2 & O_2 six packs
7. Enter Test Cell #2 and OPEN all the supply gas bottles that are going to be used
8. OPEN both JP-10 valves
9. Ensure that PXI Controllers, Kistlers, and Power strip in the black cabinet are ON.
10. Turn ON 24 VDC power supply for Test Cell #2 TESCOM Control Power.
11. OPEN Shop Air, Isolation Valve (High Pressure Air) and Main Air
12. If JP-10
    a. CLOSE 440 VAC knife switch for Oil Pump (ON)
13. TURN ON Cooling Water (If required)
14. TURN ON TPI (do not exceed 85 on heater control knob) – 30-60-85 (1 min intervals)
15. CONNECT Vitiator Spark Plug.
16. If required, set up any visual data recording equipment.

17. Evacuate all non-essential personnel to the control room
18. Check Shop Air Compressor in heater room– approx 120 psi min
19. RUN the control
20. Close Blast Door
21. Lock Gate

Running the Engine
1. Set Main Air, Secondary/Purge Air, and all other gases pressures (ER3000) ON RPL00
   a. Set Main Air and Purge Air (ER3000)
      i. 01 Main Air
      ii. 04 Secondary Air – Set to 220
   b. Supply Gases in Test Cell #2 TESCOM Node Address
      i. 20 Vit H_2O
      ii. 21 Vit O_2
      iii. 22 C_2H_4
2. **DISCONNECT CH 7 & 8**
3. Set All Engine Control Parameters (on BNC Pulse Generator)
   a. Send Engine Parameters to BNC
4. **RECONNECT CH 7 & 8**
5. Twist Emergency Stop Button clockwise (TEST CELL IS NOW LIVE)
6. ENABLE the Test Cell on the VI.
7. OPEN Open Vit, Torch, and C_2H_4 Ball Valves.
8. Verify Golf Course is clear
9. SOUND the Siren
10. START recording on VCRs
11. Fuel Pump On (If using JP-10)
12. TURN ON Data Recording Switch
13. Manually engage Main Air flow
14. START Vitiator

****************************WARNING*********************************
      The next step will result in the commencement of a run profile and ignition.
* Note: The 3-Way Ball Valve has a control in the Vitiator sequence. If the Vitiator is used then the 3-Way Ball will not divert through the engine until 375º F and will dump overboard at the end of the run at 175º F.

15. COMMENCE RUN
      a. High Speed DAQ will be triggered and the engine profile will commence
16. STOP RUN.
      a. Pulse generation will be stopped.
17. TURN OFF Data Recording Switch
18. Wait for main air to divert
19. STOP Main Air Flow
20. Ensure all Ball Valves are closed

21. Fuel pump OFF (If using JP-10)
22. DISABLE the Test Cell on the VI.
23. Push Emergency Stop Button IN

Test Cell #2
Standard Operating Procedures (S.O.P)
Engine Shut DOWN
(last modification date 19 June 2007)

1. SET all supply gases to ZERO, Nodes 1, 4, 20, 21 & 22
2. ClOSE all gas supply valves using LabView
3. STOP control code.
4. Push Emergency Stop Button IN
5. Turn OFF Power Strip in BNC Timing Cabinet
6. If Gas Turbine Igniter (Test Cell #1) used DISABLE BEFORE turning off 24 VDC
7. TURN OFF 24 VDC power supply (check with other test cells first)
8. CLOSE Jamesbury Valve (check with other test cells first)
9. REMOVE Vitiator Spark Plug head
10. SECURE TESCOM 24VDC power. (check with other test cells first)
11. CLOSE Shop Air, High Pressure Air, and Main Air
12. If using JP-10
    a. OPEN 440 VAC Knife switch (OFF)
13. TURN OFF Cooling Water
14. CLOSE Supply gases
15. CLOSE JP-10 supply valves
16. TURN OFF TPI
17. CLOSE H_2 & O_2 six packs
18. VENT H_2 & O_2 lines
19. STOW Cameras and other equipment used in testing.
20. CLOSE Test Cell #2.
21. TURN OFF Warning Lights.

THIS PAGE INTENTIONALLY LEFT BLANK
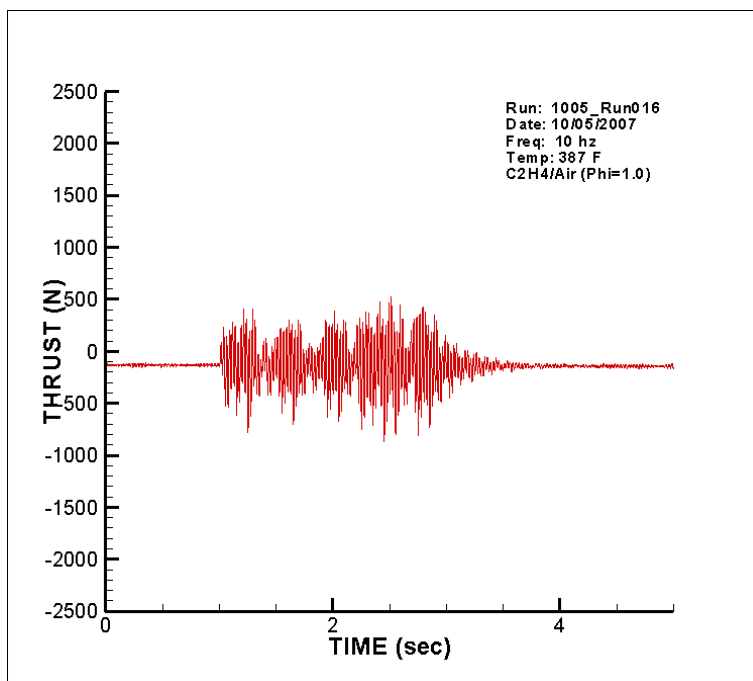
APPENDIX C: ADDITIONAL EXPERIMENTAL DATA

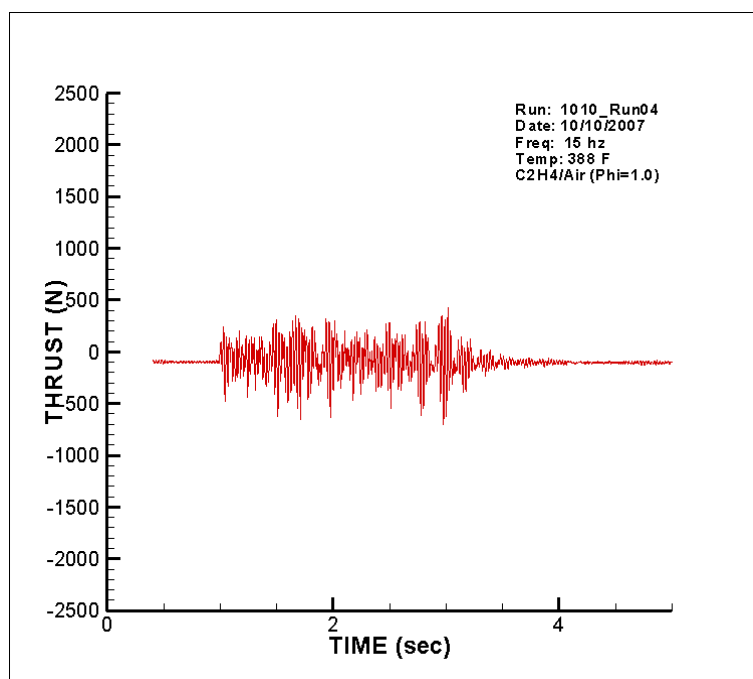Figure 60.   10 Hz Raw Data (Abs. Unc. +/-0.452%)

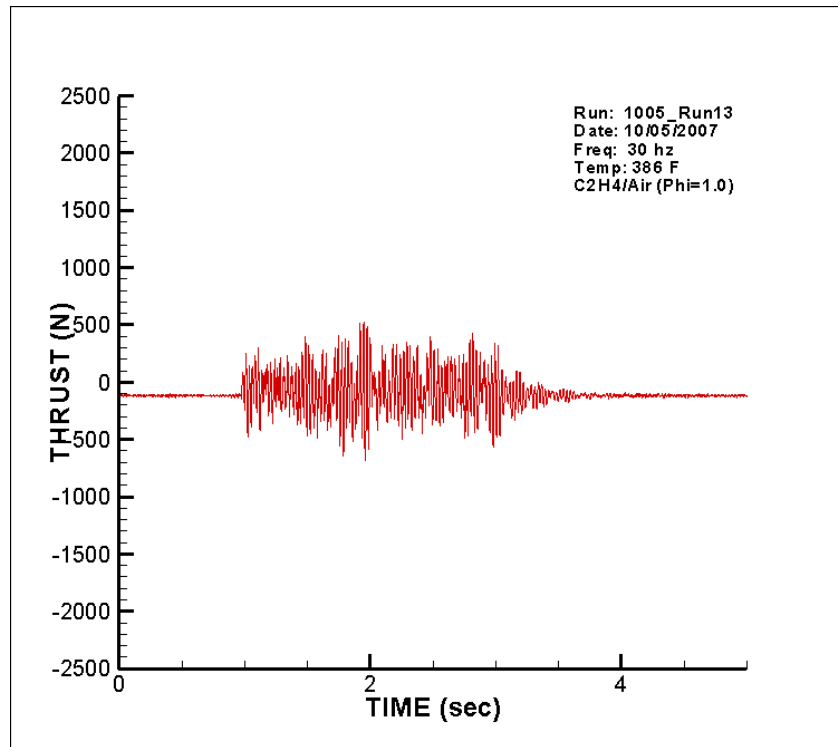Figure 61.   15 Hz Raw Data (Abs. Unc. +/-0.452%)

Figure 62.   30 Hz Raw Data (Abs. Unc. +/-0.452%)
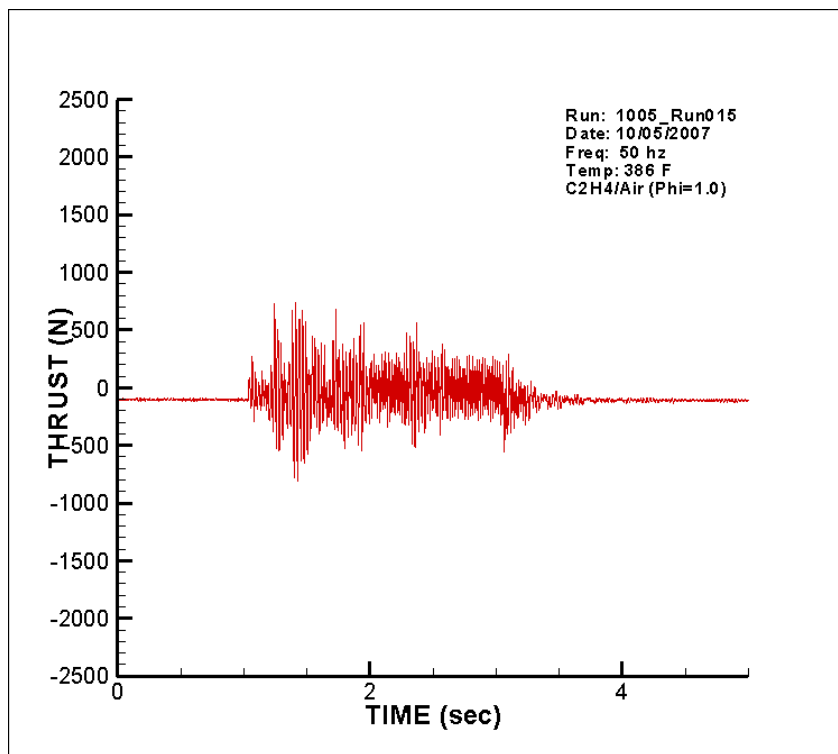

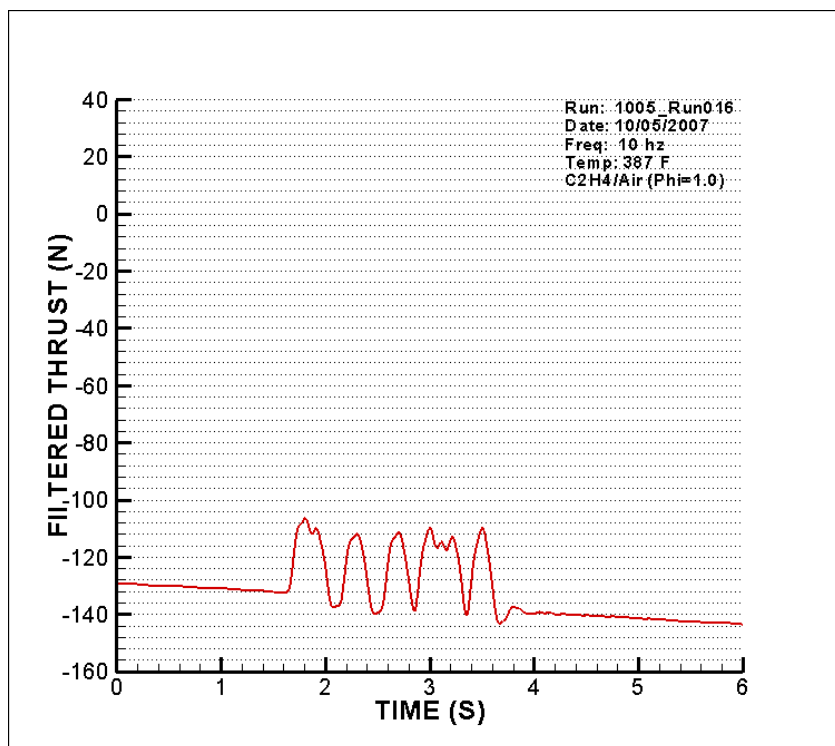Figure 63.   50 Hz Raw Data (Abs. Unc. +/-0.452%)

Figure 64.   10 Hz Filtered Data (Abs. Unc. +/-0.452%)
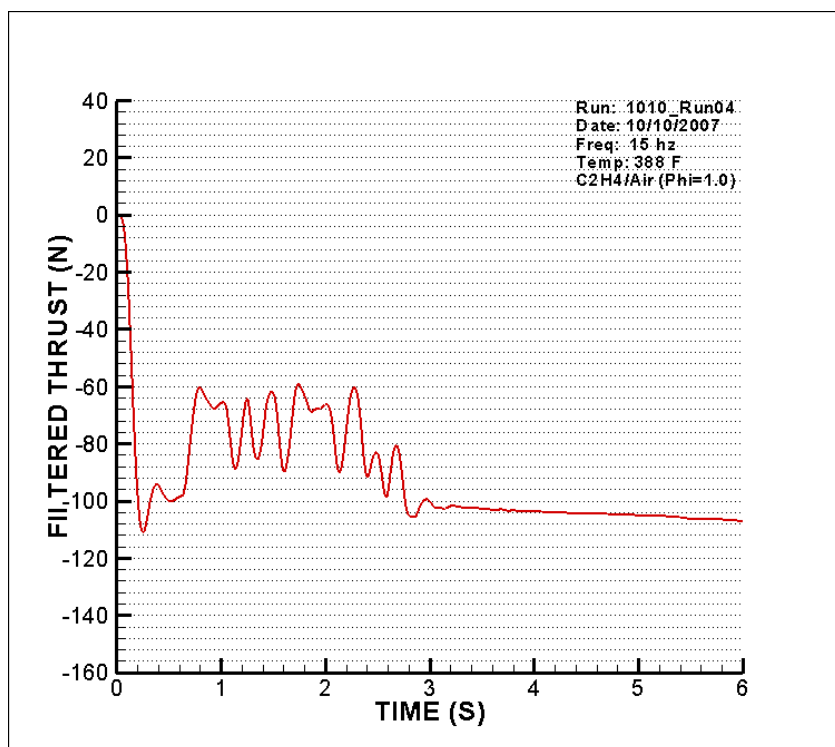

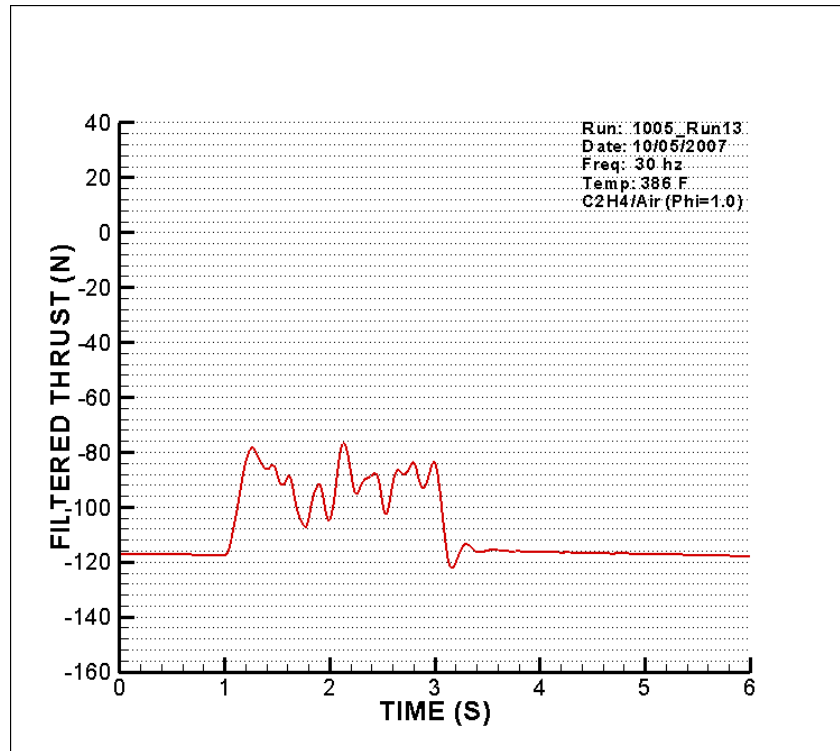Figure 65.   15 Hz Filtered Data (Abs. Unc. +/-0.452%)

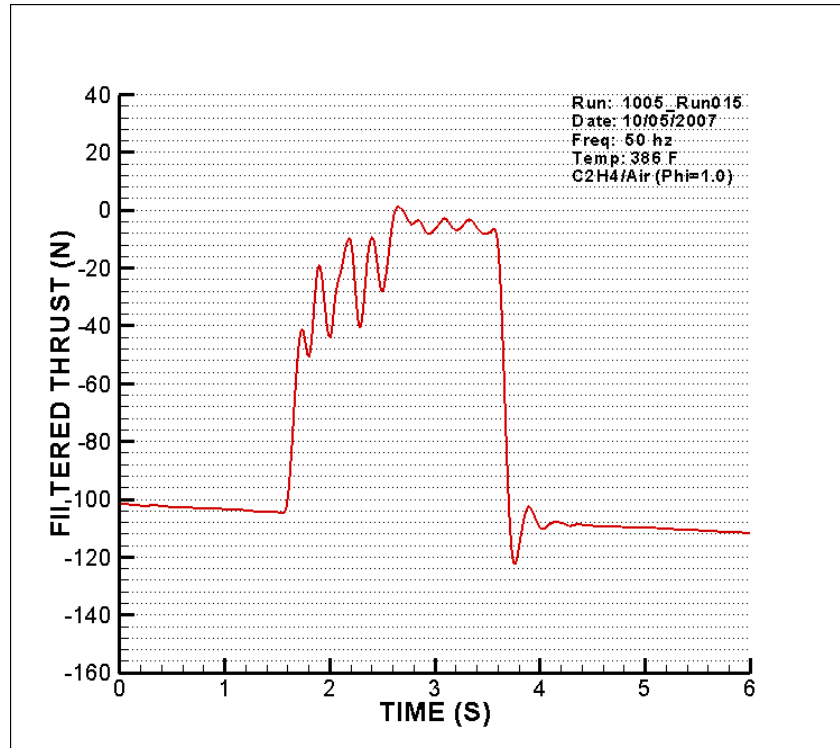Figure 66.   30 Hz Filtered Data (Abs. Unc. +/-0.452%)

Figure 67.   50 Hz Filtered Data (Abs. Unc. +/-0.452%)

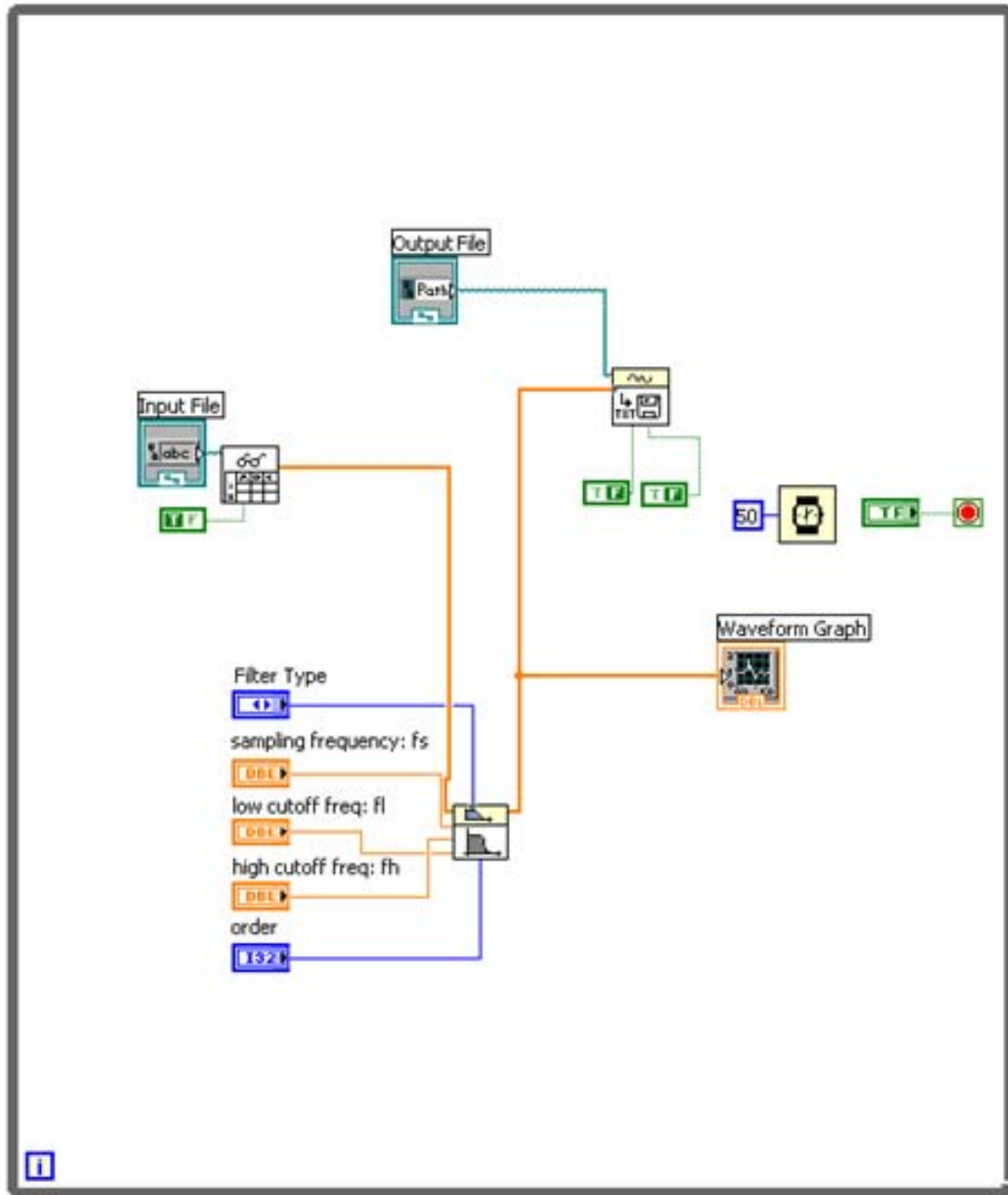# APPENDIX D: LABVIEW VI CODING

Figure 68.　　Labview Filtering Algorithm Coding
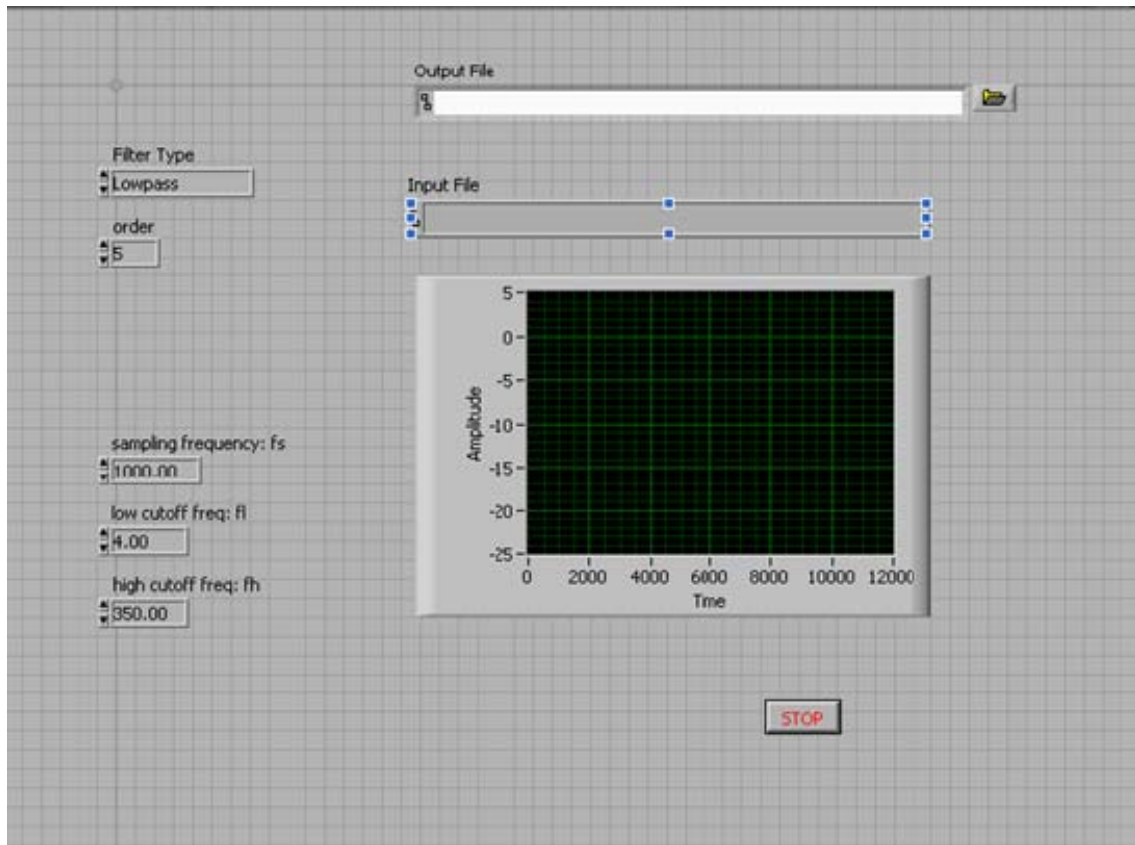
Figure 69.   Labview Filtering Algorithm GUI

LIST OF REFERENCES

[1]   H. Hoffmann, "Reaction-Propulsion Produced by Intermittent Detonative Combustion," German Research Institute for Gliding, Report ATI-52365, August 1940.

[2]   P.D. Hutcheson, "Design, Modeling And Performance Of A Split Path Jp-10/ Air Pulse Detonation Engine", Master's Thesis, Naval Postgraduate School, Monterey, California, December 2006.

[3]   P.G. Harris, S.M. Guzik, and R.A. Stowe, "Design Methodology for a Pulse Detonation Engine as a Ramjet Replacement," AIAA Paper 2004-3400, Joint Propulsion Conference and Exhibit, Ft. Lauderdale, Florida, 11-14 July 2004.

[4]   K.K. Kuo, *Principles of Combustion,* Second Edition, John Wiley and Sons, 2005.

[5]   W.H. Heiser, D.T. Pratt, "Thermodynamic Cycle Analysis of Pulse Detonation Engines," Journal of Propulsion and Power, Vol. 18, No. 5, 2002.

[6]   C.M Brophy, R. K. Hanson, "Fuel Distribution Effects on Pulse Detonation Engine Operation and Performance," Journal of Propulsion and Power, Vol. 22, No. 6, 2006.

[7]   *Cesium-based Velocimeter for Model Validation*, Retrieved October 10, 2007, from http://hanson.stanford.edu/research/propulsion/cesiumV.html.

[8]   Glassman, I., *Combustion*, Second Edition, Academic Press, Inc., 1987.

[9]   B.T. Channell, "Evaluation and Selection of an Efficient Fuel/Air Initiation Strategy for Pulse Detonation Engines", Master's Thesis, Naval Postgraduate School, Monterey, California, September 2005.

[10]   G. Roy, S. Frolov, D. Netzer, A. Borisov, *High-Speed Deflagration and Detonation*, ELEX-KM Publishing, 2001.

[11]   J.B. Liu, P. Ronney, and M. Gundersen, "Corona Discharge Ignition of Premixed Flames", http://carambola.usc.edu/research/coronaignition/coronaignition.html, September 2005.

[12]   E.J. Touse, "Transmission of a Detonation Wave Across a Sudden Expansion With Varying Mixture Composition," Master's Thesis, Naval Postgraduate School, Monterey, California, December 2003.

[13]   E. Schultz, "Detonation Diffraction Through an Abrupt Area Expansion," Doctoral Thesis, California Institute of Technology, Pasadena, California, April 2000.

[14]   C.N. Hackard, "Ignition Delay Characteristics for Transient Plasma Ignition of Ethylene/Air and JP-10/Air Mixtures in a Pulse Detonation Engine," Master's Thesis, Naval Postgraduate School, Monterey, California, December 2007.

[15]   Operations and Maintenance Manual, *Six Component, 500 Pound Pulse Detonation Measurement System,* Pacific Press Co., N00244-02-C-0060, Manual No. 110028, September, 2002.

[16]   W.T. Thomson, M.D. Dahleh, *Theory of Vibration with Applications*, Fifth Edition, Prentice Hall, Inc., 1998.

INITIAL DISTRIBUTION LIST

1.   Defense Technical Information Center
     Ft. Belvoir, VA

2.   Dudley Knox Library
     Naval Postgraduate School
     Monterey, CA

3.   Dr. Gabriel Roy
     Office of Naval Research
     Arlington, VA

4.   Professor Christopher Brophy
     Department of Mechanical and Astronautical Engineering
     Naval Postgraduate School
     Monterey, CA

5.   Professor Knox Millsaps
     Department of Mechanical and Astronautical Engineering
     Naval Postgraduate School
     Monterey, CA

6.   Professor Jose Sinibaldi
     Department of Mechanical and Astronautical Engineering
     Naval Postgraduate School
     Monterey, CA

7.   CDR Brady Bartosh
     Naval Postgraduate School
     Monterey, CA